12-31-2019

Perivascular waste metabolites clearance in central nervous system (cns)

Yiming Cheng
New Jersey Institute of Technology

Copyright Warning & Restrictions

The copyright law of the United States (Title 17, United States Code) governs the making of photocopies or other reproductions of copyrighted material.

Under certain conditions specified in the law, libraries and archives are authorized to furnish a photocopy or other reproduction. One of these specified conditions is that the photocopy or reproduction is not to be "used for any purpose other than private study, scholarship, or research." If a, user makes a request for, or later uses, a photocopy or reproduction for purposes in excess of "fair use" that user may be liable for copyright infringement,

This institution reserves the right to refuse to accept a copying order if, in its judgment, fulfillment of the order would involve violation of copyright law.

Please Note: The author retains the copyright while the New Jersey Institute of Technology reserves the right to distribute this thesis or dissertation

Printing note: If you do not wish to print this page, then select "Pages from: first page # to: last page #" on the print dialog screen

ABSTRACT

PERIVASCULAR WASTE METABOLITES CLEARANCE IN CENTRAL NERVOUS SYSTEM (CNS)

by
Yiming Cheng

Efficient clearance of interstitial waste metabolites is essential for normal brain homeostasis. Such effective clearance is hampered by the lack of a lymphatic system in the brain, and the cerebrospinal fluid (CSF) is unable to clear large size waste metabolites in the brain. Here, a novel idea that brain arterial endothelium and smooth muscle cells reactivity regulates the clearance of these water-insoluble large size waste metabolites through the perivascular dynamic exchange, and that low dose ethanol promotes this perivascular clearance is proposed.

In Aim 1, the biodistribution of a large size waste metabolite (Amyloid-β protein mimic) in rat perivascular space as a proof-of-concept is examined. Then the effects of low dose alcohol (ethanol) for promoting perivascular clearance path are evaluated. The result shows that ethanol increases perivascular clearance by enhancing the dilative reactivity of arterial endothelial cells (ECs) and alpha-smooth muscle cells (α-SMCs) via the activation of endothelial specific nitric oxide synthase (eNOS) and nitric oxide (NO) production. In Aim 2, the underlying molecular mechanisms of low dose ethanol on the perivascular clearance of waste metabolites is examined. The result shows that low dose ethanol specifically activates eNOS in arterial wall and generates physiological favorable level of NO without affecting the integrity of the Blood-Brain Barrier (BBB). This vasodilator NO stimulates the dilative reactivity of ECs- α-SMCs, which promotes

the diffusive movement of waste metabolites from interstitial space/CSF to perivascular-perivenous drainage path. Decrease in phosphorylation of myosin light chain in α-SMCs and increase in arterial vessel diameter validates α-SMCs reactivity and movement of waste metabolites towards perivascular space. In Aim 3, the contrast effects of chronic moderate alcohol intake on perivascular clearance of waste metabolites is assessed. The result reveals that chronic alcohol intake switches the induction of eNOS to inducible nitric oxide synthase (iNOS), thereby generating high level of NO. This continuous production of NO by iNOS in chronic alcohol exposure causes oxidative damage of the arterial endothelial-smooth muscle layers, and reduces dilative reactivity. Decrease in tight junction protein levels validates the BBB dysfunction, and increase in phosphorylation of myosin light chain in α-SMCs validates the impairment of α-SMCs reactivity, that are closely correlated with decrease in waste metabolites movement towards perivascular clearance path.

The current work affords huge clinical relevance since aggregation of large size waste metabolites like Ab protein around the perivascular space is a hallmark of Alzheimer's disease. As such, the findings suggest new strategies for prevention and treatment of neurological diseases that are associated with clearance of entangled proteins.

PERIVASCULAR WASTE METABOLITES CLEARANCE IN CENTRAL NERVOUS SYSTEM (CNS)

by
Yiming Cheng

A Dissertation
Submitted to the Faculty of
New Jersey Institute of Technology
and Rutgers University Biomedical and Health Sciences – Newark
in Partial Fulfillment of the Requirements for the Degree of
Doctor of Philosophy in Biomedical Engineering

Department of Biomedical Engineering

December 2019

.

APPROVAL PAGE

PERIVASCULAR WASTE METABOLITES CLEARANCE IN CENTRAL NERVOUS SYSTEM (CNS)

Yiming Cheng

Dr. James Haorah, Dissertation Advisor — Date
Associate Professor, Department of Biomedical Engineering, NJIT

Dr. Namas Chandra, Committee Member — Date
Distinguished Professor, Department of Biomedical Engineering, NJIT

Dr. Kevin D. Belfield, Committee Member — Date
Professor and Dean, College of Science and Liberal Arts, NJIT

Dr. Jiang-Hong Ye, Committee Member — Date
Professor, Department of Pharmacology and Physiology,
Rutgers University, New Jersey Medical School

Dr. Kevin Pang, Committee Member — Date
Professor, Department of Pharmacology, Physiology & Neuroscience,
Rutgers University, New Jersey Medical School

BIOGRAPHICAL SKETCH

Author: Yiming Cheng

Degree: Doctor of Philosophy

Date: December 2019

Undergraduate and Graduate Education:

- Ph.D. in Biomedical Engineering,
  New Jersey Institute of Technology, Newark, NJ, 2019

- Ph.D. in Biomedical Engineering,
  Rutgers University Biomedical and Health Sciences, Newark, NJ, 2019

- Master of Science in Biomedical Engineering,
  New Jersey Institute of Technology, Newark, NJ, 2014

- Bachelor of Science in Life Science,
  Tongji University, Shanghai, People's Republic of China, 2012

Major: Biomedical Engineering

Presentations and Publications:

Cheng Y, Liu X, Ma X, Garcia R, Belfield K, & Haorah J. (2019). Alcohol promotes waste clearance in the CNS via brain vascular reactivity. *Free Radical Biology and Medicine.*

Cheng Y and J. Haorah. (2019) How does the Brain remove its waste Metabolites from within? *International Journal of Physiology, Pathophysiology and Pharmacology*. (Accepted)

Xiaotang Ma, Yiming Cheng, Ricardo Garcia, and James Haorah. (2019) Hemorrhage Associated Mechanisms of Neuroinflammation in Experimental Traumatic Brain Injury. *Journal of Neuroimmune Pharmacology.*

This dissertation is dedicated to my wife, Xi Zhang and my kids, Chloe and Chris; it was their support that gave me the ability to complete this work.

ACKNOWLEDGMENT

I would like to thank my PhD advisor Dr. James Haorah for his great kindness and support.

I would also like to thank my committee members: Dr. Namas Chandra, Dr. Kevin Belfield, Dr. Jiang-Hong Ye and Dr. Kevin Pang for their suggestions.

I would like to thank Department of Biomedical Engineering for the financial support.

I express my heart-felt gratitude to my lab mates, Xiaotang and Agnieszka. I truly appreciate my colleagues from CIBM3 team, Dr. Rama, Matt, Danny, Aswati, Ningning and from Belfield research group, Xinglei. It would be significantly more difficult without their scientific inputs and personal helps to finish my experiments.

TABLE OF CONTENTS

TABLE OF CONTENTS
(Continued)

TABLE OF CONTENTS
(Continued)

Chapter **Page**

TABLE OF CONTENTS
(Continued)

Chapter **Page**

LIST OF TABLES

LIST OF FIGURES

LIST OF FIGURES
(Continued)

CHAPTER 1

INTRODUCTION

1.1 Objective

The objective of this dissertation is to present findings of large size waste metabolites clearance from brain and the underlying regulation mechanisms. Clinically, large size waste metabolites like tauopathy, prion-like proteinopathies, cerebral amyloid angiopathy, and Aβ proteins are accumulated around the perivascular space (PVS) in brain tissue from neurological diseases, including Alzheimer's disease [1-3]. However, how these entangled proteins that originate from brain interstitial space due to neuronal activities translocate towards PVS and what are the underlying regulation mechanisms are still unknown. Here, we hypothesize that a dynamic driving force that produces by arterial vessel contraction/dilation creates a "*pumping-like effect*" within PVS, pooling large metabolites towards PVS and promoting their clearance from inside brain to systematic circulation. To validate this idea, we use low dose alcohol as a proof-of-concept to stimulate dilative vascular reactivities. The rationale is that low dose alcohol, through a signaling molecule Nitric Oxide (NO), is known to induce vessel dilation [4]. Epidermological evidence reveal that different alcohol drinking patterns exihibit disctinctive corelations with onset and progression of neurological diseases that are associated with entangled proteins aggregation [5]. A detail discussion regarding the effects of alcohol will be expanded in Chapter 3-5.

As such, to address these questions, three specific aims are evaluated:

1) To determine the movement pattern of waste metabolites from cerebrospinal fluid (CSF) and interstitial spaces to perivascular spaces (PVS);

2) To examine that movement of waste metabolites at perivascular spaces is associated with vessel dilation that regulated by interaction of brain endothelium and smooth muscle cells;

3) To evaluate the contrast effect of low dose and chronic/moderate alcohol intake on perivascular clearance.

1.2 Summary of Literatures

The brain is the command center of the body that regulates the vital functions of circulation, respiration, motor function, metabolic activities, or autonomic outcomes. The brain coordinates these non-stop activities at the expense of huge energy utilization. This energy demand is achieved by active transport of nutrients across the endothelial blood-brain barrier (BBB). Trafficking of xenobiotics and inflammatory agents into the brain across the BBB or across the two other brain interfaces is harmful to brain cells, resulting in waste metabolites production in the interstitial space (IS). Clearance of these waste metabolites maintains the normal brain homeostatic functions, while aggregation leads to serious neurological disorders. In the absence of lymphatic system, the CSF flow serves as the clearance path in the CNS for water soluble peptides/solutes. The CSF disposal path is unable to clear large size waste metabolites, such as Aβ protein in AD. This section will first briefly discuss the existing entry routes of nutrients, immune cells or xenobiotics into the brain. Focus will be on the clearance paths and mechanisms of waste metabolites clearance in the CNS. This will include the mechanisms of waste metabolites movement from IS to perivascular clearance (PVC), from IS-CSF-PVC, and the exchanged from PVC to circulation. Therapeutic approach to improve the clearance mechanisms for ameliorating neurological diseases will be concluded finally.

1.2.1 Brain Barrier Interfaces

The brain is the command center of the body. It controls the many functions of cardiovascular and systemic circulation, respiratory center, motor activities, metabolic function, renal and gastrointestinal excretion, and autonomic nervous system. Coordination of these numerous activities is carried out by the release of endocrinal chemical messengers known as hormones. The brain does this by receiving signals from sensory nerve cells, integrating and processing the information in interneurons, and sending out the message to the effector tissue organs through the motor neurons. Relaying of the message from the brain central nervous system to different part of the body through peripheral nervous system is connected by brainstem via the spinal cord. Constant supply of nutrients/minerals/ions across the selectively permeable blood-brain interface known as the blood-brain barrier (BBB) meets the energy demand of the brain. The localization of the tight junction proteins, protein/nutrient/ion transporters, multidrug resistant efflux receptors, or enzymes at the BBB, selectively maintain the ionic/nutrients homeostasis in the brain by dumping toxic agents in the circulation [6], as illustrated in **Figure 1.1**. Thus, small size molecules like glucose, amino acid, essential minerals/ions are transported across the BBB by carrier-mediated transporters, whereas receptor mediated transporters translocated the large size peptides and proteins [6, 7].

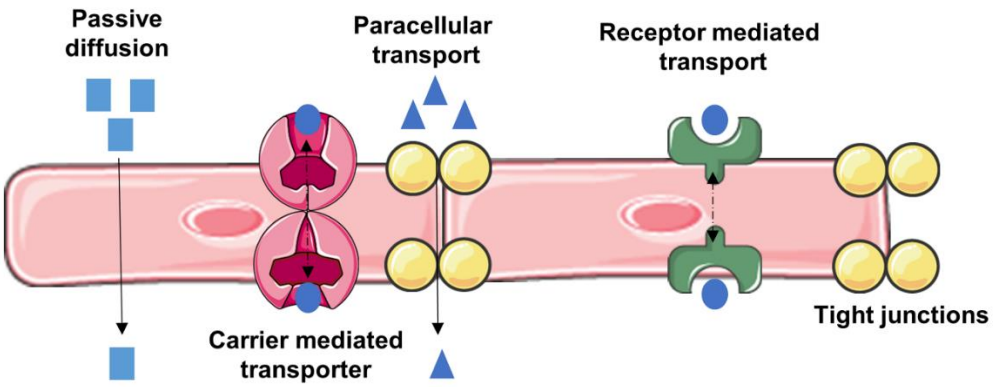

Figure 1.1 Routes of transport across the BBB. Passive diffusion favors lipophilic molecules; Carrier mediated transporters bi-directionally transport molecules influx and/or efflux through BBB endothelial cell layer; receptor mediated transport requires binding of ligand for transport of macromolecules such as glucose, peptides and proteins across BBB endothelium (transcytosis); paracellular pathway through tight junctions allows diffusion of for small molecules and cell trafficking.

In addition to endothelial BBB and blood-spinal cord barrier (BSCB) interfaces, there are two other epithelial barriers that can render entry of molecules into the brain. The interface between the blood and ventricular cerebrospinal fluid (CSF) is known as the epithelial choroid plexus (CP), and the interface between the blood and CSF subarachnoid is known as the epithelial arachnoid villi [8, 9]. The main function of CP is the secretory source of cerebrospinal fluid for maintaining the fluid volume and ionic balance in the CNS. The concept is essentially justified by the fact that CP serves as the drainage sink in the brain. Recent findings reveal that this epithelial barrier is also involved in immune cell trafficking [10] and pathogens entry interface [11, 12], as such CP is apparently involved in the development of neurological diseases [13]. Most recently, Uchida et al. (2019) showed the impairment of tight junction protein claudin-

11 expression at the BBB, at the blood-spinal cord barrier (BSCB), and at the epithelial arachnoid barrier in multiple sclerosis without affecting at the epithelial CP [14]. This finding indicates that CP barrier is unlikely involved in the development of neurological diseases. Choroid plexus is also implicated for supply of nutrients and signaling molecules to brain parenchyma, as such, it may play a role in brain development and aging [15]; however, this argument remains for open discussion. Another recent finding implicates CP as a potential BBB bypass route for drug delivery in the CNS [16]. This concept is based on the rationale that since carrier-mediated influx transporters or receptors are expressed in CP epithelium, these molecules can be designed for drug penetration across CP. The rationale uses the same principle that these molecules have been employed for drug delivery across BBB. The function of the second epithelial barrier known as the arachnoid villi interface between the blood and the CSF acts as the main drainage channels of water-soluble peptides/solutes from CSF subarachnoid to sagittal sinus for clearance. Intriguingly, micropinocytosis and vacuolization of endothelial cells present in the stromal central core of the villi seem to facilitate a bidirectional active transport across the arachnoid villi barrier [17].

Out of these two endothelial (BBB and BSCB) and two epithelial (CP and arachnoid villi) barrier interfaces in the brain, the BBB is the primary transport/trafficking route of nutrients, micro-organisms, immune cells, and xenobiotic substances into the brain. The myeloid cells in the brain response to inflammatory event in the form of phagocytosis, proteolytic degradation, and autophagy, which produces harmful waste metabolites. Such harmful metabolites include components of degenerating neurons and extracellular vesicles that are entrapped in the interstitial

space (IS). Proper clearance of these waste metabolites from interstitial fluid/CSF maintains the normal homeostasis function of the brain, while aggregation leads to neurological disorders. Here, we focus the clearance mechanisms of these waste metabolites from the brain with emphasis on perivascular clearance.

1.2.2 Interstitial Space Waste Metabolites

The main donor of fluid in the interstitial space is the blood circulation and cellular secretion. The total volume of the interstitial fluid (ISF) is believed to be contributed by passive diffusion of fluid from the circulation. The ISF contains cellular metabolites, cellular shedded microvesicles and exosomes under normal condition, but ISF will contain entangled proteins like amyloid-β in neuropathologic condition [18]. Therefore, understanding the mechanisms of these waste metabolites movement from ISF to terminal clearance path is exceedingly important for improving neurological diseases. The drainage of water-soluble metabolites from ISF to CP, and to CSF compartments is a major route for clearance of small-size and hydrophilic substances.

There are two school of thoughts on the mechanisms of ISF movement, the bulk flow and diffusive movement [19]. Cserr, et al. (1977 and 1981) showed that a bulk flow of the ISF independent of diffusion was responsible for clearance of waste metabolites in the CNS [20, 21]. Their conclusion was based on the findings that deposition of different molecular size tracers in rat brain interstitial space were drained at nearly identical half-life rates with varying diffusion coefficients. It was estimated that the rate of this bulk flow was 0.1–0.3 μL/g brain/min in rat brain [21, 22]. In recent time, the hypothesis of ISF bulk flow mechanisms has been challenged by other critiques. Sykova E and Nicholson C (2008) and Bakker EN et al. (2016) pointed out that the movement

of ISF in the interstitial spaces was attributed to diffusive movement rather than bulk flow mechanisms [23, 24]. Their argument was that first, the interstitial narrow spaces between cells are too limited to allow significant ISF bulk flow. Second, the extracellular matrix of the interstitial space contains repeated long chain polysaccharides like glycosaminoglycans, which are negatively charged, hydrophilic, and can easily trap water molecules and positive ions like sodium. These hindrance factors will not only deter the bulk flow of interstitial fluid, but also limit the movement of large size waste metabolites in the interstitial space. Thus, the question of whether the ISF move through bulk flow or passive diffusion mechanisms remains to be debated for further verification. Based on the emerging multiphoton imaging time-dependent interstitial bio-distribution of small, medium, and large size molecular weight fluorescent tracers, we will discuss my thought in glymphatic section below.

1.2.3 Clearance of Waste Metabolites in Cerebrospinal Fluid (CSF)

The cellular metabolites, extracellular vesicles, degraded peptides, and other degenerated cellular components contain in the interstitial fluid are mostly collected in the choroid plexuses (CP). The C3 compartment CP is localized in the cerebrum and C4 is localized in the cerebellum regions of the brain. The C3 and C4 are connected by an aqueduct. The interstitial fluid drainage sink (CP) and ventricular cerebrospinal fluid (CSF) is separated by the epithelial choroid plexus barrier, through which collected interstitial fluid is excreted into the CSF [25]. The CSF flow passes through the interventricular foramina of the third ventricle to the fourth ventricle via aqueduct. From the fourth ventricle, the fluid then enters the subarachnoid space (SAS) through a median and two lateral apertures [26, 27]. The CSF containing the water-soluble waste

metabolites, but not cells ultimately move through the subarachnoid space and it can also reach to perivascular space [28, 29]. The water-soluble metabolites in the CSF subarachnoid space is absorbed into sagittal venous sinuses through arachnoid granulations. The evident came from the work of Weed et al. (1914), who found that non-toxic tracers injected into CSF crossed arachnoid granulations along sagittal sinus and eventually penetrated into dura wall of the sinus [30, 31]. The absorption of CSF dye arachnoid granulations was further confirmed by electron microscopy studies, which showed that the presence of pressure-sensitive vacuolation cycle of pores indicate the one-way valves transcellular flow [32]. The CSF contents in the sagittal sinus, most likely at the confluence of sinus exits along the myelin sheath of olfactory bulbs through cribriform plate [33], which is then believed to deliver into the deep cervical lymph nodes through nasal lymphatics [34]. This drainage path from subarachnoid space to nasal lymphatic system was further confirmed in seven different species using microfils tracers [35]. Recently, these lymphatic vessels have been investigated in rodents by using specific antibodies [36, 37].

In summary, **Figure 1.2** schematic presentation illustrates the intracranial CSF flow. It is important to emphasize here that the exchange of waste metabolites from subarachnoid to superior sagittal venous sinus may account only the water-soluble small size metabolites. This is because the granulation at the arachnoid microvilli barrier restrict the clearance of large size waste metabolites. As such, the clearance mechanisms of large size waste metabolites Aβ proteins from the interstitial space or from the CSF remains to be investigated. To this end, emerging findings such as the glymphatic hypothesis and our most recent published article on perivascular clearance mechanisms

revealed the clearance mechanisms of large size waste metabolites from the interstitial space or from the CSF circulation.

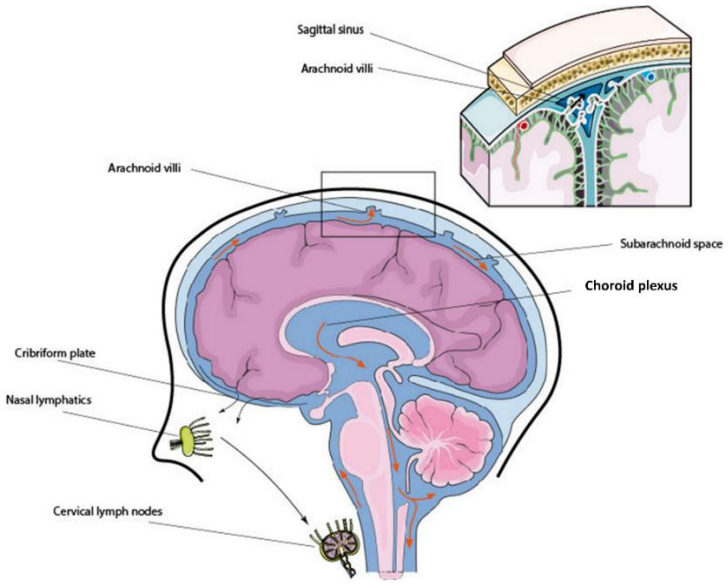

Figure 1.2 Schematic presentation of the intracranial CSF flow. CSF is produced by choroid plexus and flows from the third ventricle to the fourth ventricle through cerebral aqueduct. After circulating over hemispheres, CSF is absorbed into superior sagittal sinus, transverse sinus, and sigmoid sinuses via arachnoid villi, as well as efflux from the CNS along olfactory nerves through cribriform plate to nasal lymphatics and eventually to cervical lymph nodes.

1.2.4 Glymphatic System

Glymphatic hypothesis proposed by Iliff JJ, Nedergaard M, et al. (2012) revealed the continuously exchange of interstitial fluid (ISF) and cerebrospinal fluid (CSF) in the brain compartments [29]. According to this hypothesis, the exchange is facilitated by aquaporin-4 (AQP4) water channels that are expressed in highly-polarized astrocytic end feet. In that, CSF from subarachnoid spaces fluxed into deep brain tissues along pial and penetrating arterioles and into the brain parenchyma towards perivenous spaces, which is facilitated by the convective function of astrocytic AQP4 [29, 38]. **Figure 1.3**

illustrates the convective interstitial flow towards perivenous spaces surrounding deep veins. They showed that water-soluble waste metabolites in ISF were collected and carried towards perivenous space, from where metabolites were drained to lymph nodes and systemic circulation.

The evidence was shown by imaging the bio-distribution of small size (Texas Red: 3 kD), medium size (Ovalbumin, 647 kD), and large size (FITC-d2000 kD) molecular weight injection in mice through cisterna magna. It was observed that the tracers rapidly entered the cortical pial arteries, then fluxed into perivascular spaces along the penetrating arterioles, which was distinguished in Tie2-GFP:NG2-DsRed double reporter mice. The small size tracer was found to exit primarily along the central deep veins and lateral-ventral caudal rhinal veins, while the medium and large size tracers accumulated at perivascular and peri-arterial spaces respectively in time-dependent manner. Using AQP4 knockout mice, this same group of investigators validated the proof-of-concept that astrocytic AQP4 was in part responsible for the clearance of radiolabeled Aβ1-40 peptide because they observed 55% reduction of Aβ1-40 peptide clearance in AQP4 knockout mice compared with wildtype [29, 38-40]. This idea of glymphatic hypothesis is further embraced by the independent studies of other investigators [41]. However, on the basis of time-dependent movement of tracers as stated above, the movement of medium to large size metabolites in interstitial fluid favors diffusion rather than the bulk flow mechanism of glymphatic hypothesis.

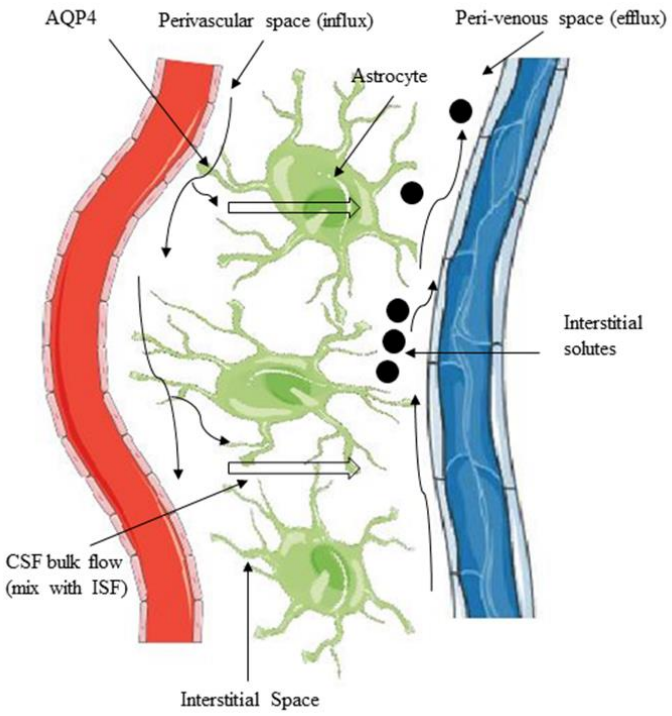

Figure 1.3 Movement of solutes in ISF and CSF through the glymphatic pathway. CSF from subarachnoid space fluxes into brain from perivascular spaces and exchanged with ISF. The exchange was facilitated by aquaporin-4 (AQP4) water channels that highly expressed in perivascular astrocyte end-foot. The bulk movement of CSF into brain drives the convective flow of ISF and interstitial solutes to perivenous route.

The reproducibility of bulk flow mechanism is questioned by several most recent publications. Some investigations argued that clearance of waste metabolites in interstitial fluid is a passive diffusion and not a bulk flow convective transport [42, 43]. This argument is based on the size of metabolites. A model of diffusive and convective transport in brain extracellular space was designed to illustrate the validation in support of this argument. Findings from this model stated that diffusion alone [44] or combined effects of diffusion and macroscopic fluid motion [45] is responsible for transport of waste metabolites in brain parenchyma rather than bulk flow. The combined effects appear to reconcile the conflicting transport mechanisms of solutes in ISF or in

perivascular space. This is in parallel with the findings that cyclic changes in arterial pressure produces mixing of flow in opposite directions in different spaces of the arterial wall [46]. It is likely that convection can assist the movement of solutes into and out of the ISF without producing the net flow of fluid as required by glymphatic system. The diffusive molecular flow along the peri-arterial sheaths into subarachnoid CSF [47], and the diffusive drainage of waste metabolites from brain parenchyma into the basement membrane of capillaries [28] also argued against the glymphatic hypothesis.

We discuss here that the transport of small size water-soluble waste metabolites could be mediated by glymphatic function. The missing piece is the accumulation of large size metabolites at the perivascular space, where glymphatic system does not account for the clearance mechanisms. This concept is clinically important because aggregation of entangled proteins at perivascular space is a hallmark of certain neurological diseases like Alzheimer's disease and cerebral amyloid angiopathy [1, 2, 48]. Unravelling the clearance mechanisms of these entangled proteins from perivascular to blood circulation would be novel for ameliorating the relevant neurological diseases. Our recent findings describe this novel clearance mechanisms at the perivascular space, which is discussed in perivascular clearance section.

1.2.5 Meningeal Lymphatic Vessels

Lymphatic system is critical for maintenance of physiological homeostasis and immune surveillance. It is a conventional believe that the central nervous system (CNS) lacks the lymphatic vessels. Recently, Aspelund et al., 2015 and Louveau et al., 2015, independently reported the existence of dura lymphatic vessels, known as the meningeal lymphatic vessels in the meninges of the brain [36, 37]. They showed this evidence by

positive stain of lymphatic endothelial cells marker hyaluronan receptor 1 (Lyve-1) and vascular endothelial growth factor receptor 3 (VEGFR3) marker along the superior sagittal and transverse sinuses.

Aspelund et al., 2015, concluded that dural lymphatic vessels absorb CSF from the adjacent subarachnoid space and from brain ISF through glymphatic system, in which CSF is then transported into deep cervical lymph nodes via foramina at the base of the skull [36]. They validated this drainage route by nearly complete absence of tracer accumulation in cervical lymph nodes in transgenic mice deficient of dural lymphatic vessels compared with wild-type after injection of tracer into the CSF. Louveau et al., 2015, found that the meningeal lymphatic cells were able to transport fluid and immune cells from the CSF and clear them to the deep cervical lymph nodes [37]. Their discovery of meningeal lymphatic function in the CNS becomes highly significant in the context of immune cell surveillance since the development of many neurological diseases involve inflammatory process. The findings of Aspelund et al. (2015) seems to connect with glymphatic hypothesis, but the CSF drainage route in meningeal lymphatic system appears to exit at the deep cervical lymph nodes, similar to conventional CSF exit. Here, we illustrate the possible connection of CSF flow, glymphatic and meningeal lymphatic system clearance route, **Figure 1.4**. Glymphatic system depicts the exchange of CSF/ISF waste metabolites at the perivascular space towards perivenous space, while meningeal lymphatic system accounts for cervical lymph nodes clearance route.

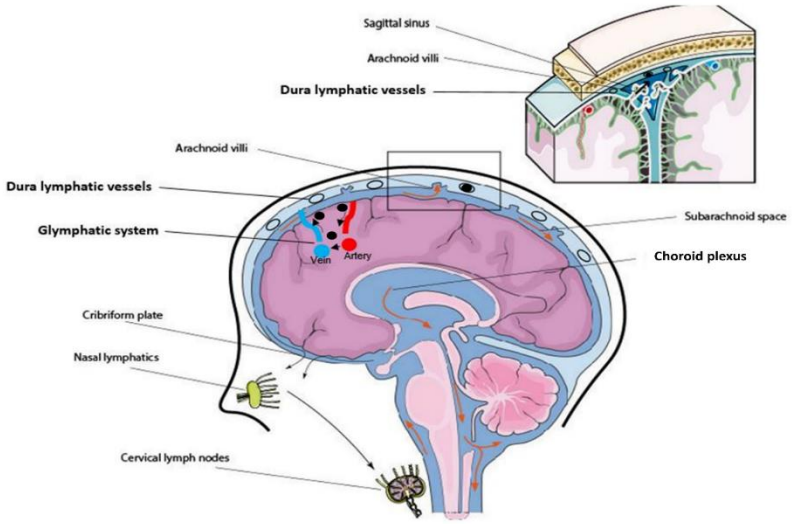

Figure 1.4 Connection of CSF circulation, glymphatic system and dura lymphatic vessels in terms of clearance. Glymphatic system (black arrow depicted flow direction) resided inside brain was responsible for small size water-soluble waste metabolites clearance (black dots). Lymphatic vessels (black circle) presented in dura was postulated to involve in waste metabolites clearance by granting access for waste metabolites that were drained by glymphatic system.

It is possible that waste metabolites from perivenous space may gain access to meningeal lymphatics through subarachnoid or along the drainage veins that can merge into dura sinus. It may be still too early to embrace the meningeal lymphatic vessel as clearance route of CNS waste metabolites because there is no direct evidence to strongly support this argument. In fact, multiple paths of CSF drainage in the CNS that are functionally and anatomically close to lymphatic vessels were known [49-51]. However, the exact connection between those routes and lymphatic vessels is largely unknown. This is because the precise location of lymphatic vessels, whether within subarachnoid, inside the dura or bathed between these two layers needs to be unraveled [52].

Since meningeal lymphatic vessels are not directly connected to CSF compartments, the primary route of CSF waste metabolites absorption from subarachnoid into sagittal sinus will be across the arachnoid villi. The arachnoid

microvilli barrier is permeable to small size water-soluble metabolites, as such the clearance mechanisms of large size waste metabolites remains to be investigated further. Thus, promoting the mechanisms of perivascular clearance becomes clinically significant since entangled proteins like A-β protein or neurofibrillary tau-phosphorylated protein are commonly aggregated at the perivascular space.

1.2.6 Perivascular Space Clearance Mechanisms

Perivascular space (PVS) is referred to the space surrounding the penetrating arterioles when diving down into deep brain tissues from pial arteries [53, 54]. The fine structure of PVS consists of vascular endothelial and glial cells. The glial layer of the astrocyte end-feet forms the outer wall, which becomes continuous with the vascular membrane and basal lamina as it penetrates into the deep brain [55, 56]. The PVS channels are known to involve in CSF/ISF waste metabolites movement, as indicated by distribution of horseradish peroxidase following lateral ventricle or subarachnoid space injection in cats and dogs [3]. Recently, a dynamic exchange of fluorescently labeled tracer between CSF/ISF and perivascular was shown in NG2-DS transgenic mice by using two-photon microscopy imaging [29]. In fact, in the 70's the PVS was implicated as a conduit of waste metabolites sink similar to the choroid plexuses because injection of horse radish peroxidase (HRP) tracer into striatum of rat was found to aggregate around the PVS [20].

The assumption of PVS serving as a conduit sink in the CNS is significantly in line with the accumulation of waste metabolites around vasculatures that are clinically observed in certain neurological diseases. The classic examples of such waste metabolites deposition around the perivascular space are the neuropathological

observations of phosphorylated tau protein in cerebral amyloid angiopathy (CAA) and aggregation of amyloid beta protein in Alzheimer's disease [1, 2, 5, 48]. These observations clearly suggest that PVS may be directly involved for the possible clearance of large size waste metabolites like phosphorylated tau protein and Aβ protein, which are transported by CSF, meningeal lymphatics and glymphatic function. Intriguingly, the ApoE family of molecules (ApoE2,E3) when mediated by low-density receptor protein (LRP1) seem to actively involved in the clearance of Aβ protein through BBB trans-vascular transcytosis [52, 57, 58]. In fact, experimental observations have shown that the trans-vascular clearance from brain to blood circulation across the BBB is believed to account for more than 80% of amyloid-beta clearance [59-61]. However, such findings are based on clearance of small Aβ peptide in normal physiological condition. In neuropathological condition, aggregation of phosphorylated tau protein and Aβ protein at the perivascular space still remains to be the hallmark of neurological diseases. The formation of this hallmark phenomenon needs further investigation to understand whether the aggregation of entangled proteins at the perivascular space is due to onsite formation or being translocated from the ISF. Since the aggregated proteins in AD are mostly originated from neuronal cell components, it is likely to translocate from the interstitial fluid rather than onsite formation. The rationale is that unlike the astrocyte end-feet, the location of neurons is not directly in contact with perivascular endothelial cells.

Thus, we posit here two fundamental questions for further investigation. What is the driving force that regulate the movement of these waste metabolites towards the perivascular space, and how to improve the clearance of these metabolites from

perivascular space into the circulation in a timely manner? Understanding the improved mechanisms of the intertwined processes will be significant to alleviate this neurological disease. To this end, my recent findings gain clinical significant in understanding the underlying cellular and molecular mechanisms of waste metabolites movement towards perivascular space. We have shown that large size waste metabolite injected into the CSF directly or into the cortical interstitial fluid diffused towards perivascular-perivenous space instead of clearing through the conventional CSF subarachnoid and sagittal sinus exchange [62]. We indicated that the hindrance for this exchange is due to the presence of arachnoid villi barrier between the two compartments which allows the absorption of mostly small size water-soluble metabolites/solutes. As a result, these stagnated waste metabolites are forced to move towards perivascular space, and we postulated that the driving force that regulate the movement appears to be the dilative reactivity of arterial endothelial cells and smooth muscle cells interactions.

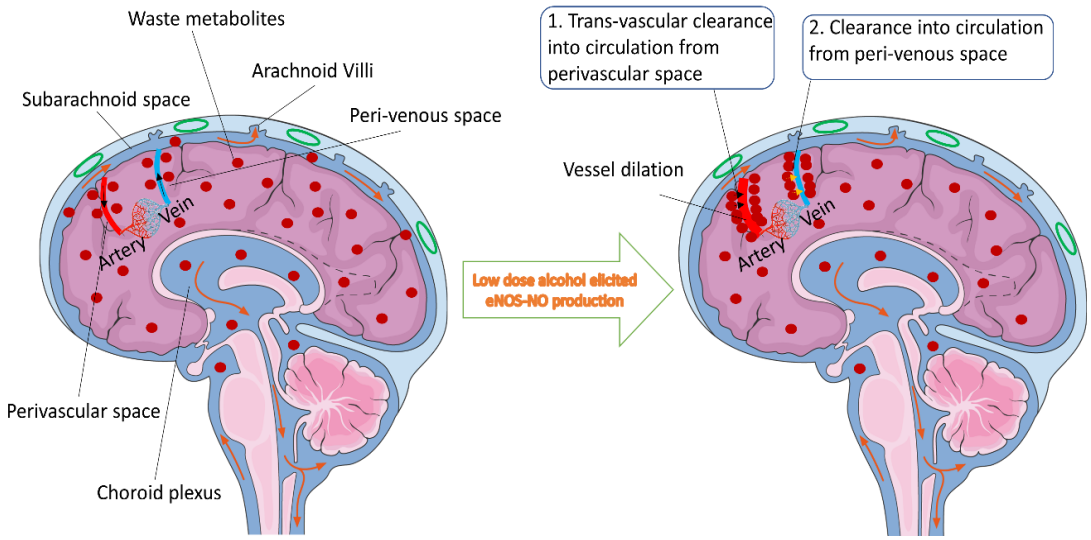

Figure 1.5 Schematic presentation of waste metabolites clearance at the perivascular-perivenous space. Arrows (orange) indicate the CSF subarachnoid flow and perivascular-perivenous clearance path (black) of large size waste metabolites (red dots) in neurodegenerative brain. Waste metabolites like β-amyloid proteins are aggregated more inside the interstitial space due to the lack of lymphatic system in the brain. Less metabolites are drained into the CSF flow due to less vessel dilative reactivity. In the presence of low dose alcohol (right), dilative arterial vessel reactivity promotes the dynamic movement of large size waste metabolites from interstitial fluid and interstitial-CSF subarachnoid to perivascular-perivenous route. Reactivity of endothelial and smooth muscle cells in arteries is mediated by alcohol-elicited eNOS activation and NO production. From perivascular and/or perivenous spaces, large size metabolites are exchanged into circulation through two postulated mechanisms: (1) trans-vascular clearance to circulation from perivascular space, and (2) diffusion into circulation from perivenous space.

The rationale is that reactivity of vascular smooth muscle cells was indicated to govern the cerebral arterial pulsation driven perivascular CSF flow locally [63]. This dynamic pulsatile pattern of neighboring blood vessels may exert significant attraction on fluid movement towards perivascular space. In this, the bioavailability of nitric oxide (NO), a potent vasodilator becomes essential to regulate dilative reactivity of cerebral arterial endothelial cells and smooth muscle cells interactions. Thus, we examined the

proof-of-concept that activation of brain endothelial specific nitric oxide synthase (eNOS) by low dose ethanol could produce favorable physiological levels of NO for increasing the cellular reactivity and increase diffusive movement of waste metabolites towards perivascular space. The rationale was that moderate level of ethanol has been shown to augment endothelial-SMCs dilative activity in placenta and pulmonary arterial vessels [4, 64, 65]. In deed my recent findings revealed that a very low dose ethanol (5.0 mM, equivalent of 0.02% blood alcohol level) significantly enhanced the diffusive movement of waste metabolites from ISF/CSF to perivascular-perivenous space [62]. We found that dilative reactivity of brain endothelial and smooth muscle cell was the underlying cellular and molecular mechanisms for this improved diffusive clearance of waste metabolites at the perivascular-perivenous space. **Figure 1.5** illustrates the underlying mechanisms of waste metabolites clearance at the perivascular-perivenous space.

My findings also validated the exchange between perivascular-perivenous and blood circulation by detecting fluorescent labeled large size waste metabolite in systemic blood plasma after CSF/parenchyma injection. The question of whether the maximum diffusion into the blood circulation takes place at the perivascular space or at the perivenous space, and/or both remains future studies. Other studies indicated that perivenous flow may gain access to meningeal lymphatic vessels or large caliber draining veins, which may then merge to form the dura sinus [29, 39], but it has no direct evidence. This rationale is unlikely because lymphatic vessels appear to localize in dura leaflets or inside surface of the dura that are separated from the CSF, as such it will not have access to waste metabolites. On the basis of tissue organ environmental

considerations, Rapper et al. (2016) concluded that unlike the function of the peripheral lymphatic system, the meningeal lymphatics may not involve in CSF waste metabolites drainage system [52]. In summary, the movement of Aβ protein from ISF/CSF subarachnoid to perivascular space is regulated by dilative reactivity of brain arterial smooth muscle and endothelial cells interactions. This clearance path can be significantly promoted by low dose ethanol via eNOS-induced NO production.

1.2.7 Conclusion

Efficient clearance of interstitial waste metabolites in CNS is essential for normal maintenance of brain homeostasis. We describe here the up-to-date emerging discoveries of various possible clearance systems operating in the brain apart from the conventional cerebrospinal fluid (CSF) clearance path. This includes glymphatic system, meningeal lymphatic vessels, diffusive movement of waste metabolites from ISF/CSF to perivascular space, and perivascular clearance of waste metabolites across the BBB trans-vascular vessels. Each of this individual discovery does carry significant impact on current scientific knowledge gap towards the understanding of waste metabolites clearance and immune cells surveillance function in the CNS. Apart from the focal finding of astrocytic aquaporin-4 mediated clearance path, the glymphatic system does reveal the movement of waste metabolites like amyloid-beta towards the perivascular space. Whether the movement of these waste metabolites from ISF/CSF to perivascular space is regulated by diffusion or a bulk flow mechanisms needs further verification. However, aggregation of waste metabolites at the perivascular space prompted the clearance path through the BBB trans-vascular or re-entry into the capillary basement membranes [66], which is relevant for eventual prevention of

neurological disease like Alzheimer's disease. Thus, improving the newly discovered CNS clearance path(s) in the absence of traditional lymphatic drainage system assumes great therapeutic relevance for many neurological diseases.

CHAPTER 2

MATERIALS AND METHODS

2.1 Materials and Reagents

Reagents: Primary antibodies rabbit anti-GFAP, iNOS, vWF, Glut-1, ZO-1, Occludin, Claudin-5, phospho-MLC; mouse anti-SMA, eNOS, 3-NT and anti-beta actin were purchased from Abcam (Cambridge, MA); anti-endomucin was purchased from Invitrogen (Carlsbad, CA). Rabbit anti- phosphor-MYL9, phospho-MYPT1/MYPT2 and phosphor-MYLK were purchased from Invitrogen (Carlsbad, CA). All secondary Alexa Fluor conjugated antibodies were purchased from Invitrogen (Carlsbad, CA). **Table 2.1** summarizes the details of the antibodies source, catalog numbers, and dilutions factors that were used for immunofluorescence staining and western blotting analyses.

A highly stable fixable dextran-conjugated Fluorescein, 2,000,000 MW (FITC-d2000) was purchased from Thermo Fisher Scientific (Waltham, MA), Nω-Nitro-l-arginine methyl ester (L-NAME, a NOS inhibitor) was purchased from Sigma-Aldrich (St. Louis, MO).

Table 2.1 Antibodies Source, Catalogue Numbers, and Dilutions Factors for Immunoflurescence Staining and Western Blotting Analyses

Antibody	Marker	Vendor	Catalogue #	Dilution for IHC	Dilution for WB
Anti-α-SMA	Alpha smooth muscle actin	Abcam	ab7817	1:250	1:1000
Anti-GFAP	Astrocyte	Abcam	ab7260	1:250	--
Anti-β-actin	Beta-actin	Abcam	ab8226	--	1:2000
Anti-Endomucin	Endomucin	Invitrogen	14-5851-82	1:200	--
Anti-iNOS	Inducible nitric oxide synthase	Abcam	ab15323	1:250	1:1000
Anti- 3-Nitrotyrosine	3-Nitrotyrosine	Abcam	ab110282	1:250	1:1000
Anti-Von Willebrand Factor	Von Willebrand Facto	Abcam	ab154193	1:250	1:1000
Anti-Glucose Transporter 1	Glucose Transporter 1	Abcam	ab652	1:250	1:1000
Anti-ZO1	ZO-1 tight junction protein	Abcam	ab96587	1:250	1:1000
Anti-Occludin	Occludin	Abcam	ab224526	1:250	1:1000
Anti-Claudin 5	Claudin-5	Abcam	ab15106	1:250	1:1000
Anti- Myosin light chain (phospho S20)	Myosin light chain (phospho S20)	Abcam	ab2480	1:250	1:1000
Anti-phospho-MYL9 (Thr18, Ser19)	pThr18/Ser19 of myosin light chain 2	Invitrogen	PA5-17727	1:200	1:1000
Anti-Phospho-MYPT1/MYPT2 (Ser668, Ser618)	MYPT1/2 (Phospho-Ser668/Ser618)	Invitrogen	PA5-64805	1:200	1:1000
Anti-Phospho-MYLK (Ser1760)	myosin light chain kinase (MLCK) that contains serine 1760	Invitogen	44-1085G	--	1:1000

2.2 Methods

2.2.1 Animals and Cell Culture

Eight-week old male Sprague-Dawley rats were purchased from Charles River

Laboratory (Wilmington, MA). Animals were maintained in sterile cages under pathogen-free conditions in accordance with institutional ethical guidelines for care of laboratory animals, National Institutes of Health guidelines, and the Institutional Animal Care Use Committee, Rutgers University.

For low dose/acute study: animals were randomly divided into 4 experimental groups (6 rats/group), 1) Control, 2) 5.0 mM ethanol, 3) 5.0 mM ethanol + L-NAME, and 4) L-NAME. A working concentration of 5.0 mM ethanol (EtOH, 0.230 g/kg body weight) was determined from a dose-dependent study of 0.046–0.460 g/kg body weight reconstituted in saline.

For chronic alcohol animal model: a pair-fed procedure was employed as previously described [67]. In brief, rats were initially acclimated to Lieber DeCarli control and 29 % calorie (5% vol/vol) ethanol (EtOH) liquid-diets from Dyets Inc for 1 week prior to weight-match pair feeding regimens for 10 – 12 weeks. Pair feeding of control animals (15 rats, 7 rats for acute/dose) was based on the amount of ethanol-liquid diets consumed by ethanol animals (8 rats). The macronutrient composition of control-liquid diets as percent of total calories is 47% carbohydrate, 35% fat, and 18% protein; and that of ethanol-liquid diets is 35% fat, 18% protein, 19% carbohydrate and 29% ethanol caloric intake. Daily food intake and weekly body weights were recorded.

2.2.2 Drug Concentration

Ethanol or the NOS inhibitor L-NAME (10 mg/kg body weight) constituted in saline was injected through tail vein using a 27 G needle. Detailed experimental conditions for control tracer dye bio-distribution through cisterna magna or intracortical route of injection is described below. For group 2, ethanol was administered 15 min prior to

tracer dye injection following anesthesia, while L-NAME was administered 5 min prior to ethanol and 20 min prior to tracer dye injection for group 3. For group 4, L-NAME was given 20 min prior to tracer dye injection.

2.2.3 Injection of Fluorescence Marker

All rats were anesthetized by intraperitoneal injection of 0.1 ml of ketamine (80–100 mg/kg) + xylazine (5–10 mg/kg) mixture using a 26-gauge needle as approved by the Panel on Euthanasia of the American Veterinary Medical Association (AVMA). Anesthetized rats were fixed in a stereotaxic frame. Then a total volume of 10 µl fluorescence tracers diluted in artificial CSF at a concentration of 5 mg/ml (0.5%) was injected via the cisterna magna at a rate of 2 µl/min over 5 min using 30-gauge needle syringe pump (Harvard Apparatus). The body temperature of animals was maintained at 37 °C with a temperature-controlled warming pad. Heart rate and respiratory rate were monitored through MouseSTAT® Pulse Oximeter & Heart Rate Monitor Module. To visualize the time-dependent movement of tracer from subarachnoid space into the brain parenchyma following cisterna magna injection, animals were perfusion fixed at 30 min, 1 h and 2 h before surgically removing the intact brain tissues. A thickness of 40 µm tissue slices were cut and mounted on a glass covered slides and tracer bio-distribution was imaged *ex-vivo* by epifluorescence microscopy.

2.2.4 Intracortical Tracer Injection

All rats were anesthetized as describes above. A total volume of 1.0 µl fluorescent labeled tracers were injected stereotactically into the brain parenchyma at a rate of 10 nl/s that controlled by a micro syringe pump (UMP3) from world precision instruments (Sarasota, FL). A 33-gauge needle was inserted via a small burr hole into

the brain at the following coordinates: right parietal skull, 2.0 mm lateral from the sagittal suture and 3.0 mm caudal from the coronal suture. After needle insertion, 30 min was given to allow the needle track to swell closed. To evaluate tracer bio-distribution, animals were perfusion-fixed between 1 – 4 h after injection and tissue slices (40 μm) were subsequently imaged as describe above.

2.2.5 *Ex-vivo* Fluorescence Imaging

Multi-channel whole-slice montages were acquired with Leica Aperio Versa 200 digital pathology grade slide scanner. This included separate DAPI, Green and Red emission channels. Exposure levels were determined based upon un-injected control slices, then maintained constant throughout the study. Fluorescent intensities were quantified using AreaQuant software specifically designed for this imaging application (Leica Biosystems) and expressed as average fluorescence intensity/unit area. This imaging technique allows for visualization of micro-structural details and digital scanning affords the ability to image large brain regions with no loss of resolution. In order to quantify fluorescence intensities, regions of interest were manually outlined in different brain section. For each channel (green 488 nm and red 594 nm), a minimum intensity threshold value was selected to exclude any background fluorescence from our calculation. The AreaQuant algorithm then determines if the intensity value of each pixel enclosed in the outlined region exceeds the minimum intensity threshold and outputs the total area of positive stain for each brain regions, the average intensity in each channel, and the expression profile of the tracers.

2.2.6 Surgery for Two-photon *in-vivo* Imaging

Rat surgery for two-photon imaging was as described by Eyo et al. [68]. Briefly, rats

were anesthetized and craniotomy (4.0 × 4.0 mm) was performed over the right parietal skull, 2.0 mm lateral from the sagittal suture and 3.0 mm caudal from the coronal suture, with the dura intact. A head plate was glued to the skull around the cranial window, and the plate was screwed into a customized stage and placed under the two-photon microscope. To visualize vasculatures, 1 ml BBB impermeable Texas Red-dextran 70 (MW 70 kDa; 1% in saline, Invitrogen) was injected through tail vein 30 min before imaging. Rats were maintained under anesthesia and body temperature was kept at 37 °C with a warming pad for the duration of imaging. Heart rate and respiratory rate were monitored as previous described.

2.2.7 *In-vivo* Imaging

Two-photon microscopy setting and operation were as described [69]. In brief, two-photon fluorescence microscopy (2PFM) was performed using a Bruker Ultima fluorescence microscope equipped with a Coherent Mira 900 laser source (200 fs, 76 MHz). The excitation wavelength was 860 nm for dextran-conjugated FITC and Texas Red, and the emission was collected using two external nondescanned PMT detectors (NDD) at 525–600 nm. A 20 ×, 1.0 N A. water immersion objective was employed for the 2PFM. A laser line-scan or ROI-based local excitation was used to better evaluate vessel diameter change and tracer movement over time.

2.2.8 Line Scan

To measure vessel diameters, 9000 ms X–Y line scan was conducted orthogonal to the vessel axis in penetrating arterioles 50–100 μm below the cortical surface. A customized Matlab code was developed to extract and calculate vessel diameter over time.

2.2.9 Immunofluorescent Staining

For tissues: Immunostaining was described in previously publications [67, 70]. In brief, frozen brain tissue sections (10 μm thickness) on glass slides were washed with PBS, fixed in acetone-methanol (1:1 v/v) fixative, blocked the cellular antigen with 3% bovine serum albumin at room temperature for 1 h in the presence of 0.4% Triton X-100 and incubated with respective primary antibodies such as rabbit anti-alpha smooth muscle actin(SMA) (1:250 dilution), rabbit anti-GFAP (1:250 dilution) and mouse anti-eNOS (1:250 dilution) for overnight at 4 °C. After washing with PBS, tissue sections were incubated for 1 h with secondary antibody: anti-rabbit-IgG Alexa fluor 594 (1:400 dilution) for GFAP and mouse-IgG Alexa fluor 594 (1:400 dilution) for SMA and eNOS. Cover slips were then mounted onto glass slides with mounting solutions containing DAPI (Invitrogen), and fluorescence microphotographs were captured by Leica Aperio Versa 200 digital pathology grade slide scanner.

For cells: Immunostaining procedure was described in previously publications [67, 70]. In brief, cells cultured on glass slides were washed with PBS, fixed in paraformaldehyde (4%) fixative, blocked the cellular antigen with 3% bovine serum albumin at room temperature for 1 hr in the presence of 0.4% Triton X-100 and incubated with respective primary antibodies for overnight at 4°C. After washing with PBS, cells were incubated for 1 hour with secondary antibody. Cover slips were then mounted onto glass slides with mounting solutions containing DAPI (Invitrogen), and fluorescence microphotographs were captured by Leica Aperio Versa 200 digital pathology grade slide scanner.

2.2.10 Western Blot

A cerebral blood vessel isolation was performed using mesh filtration to concentrate protein content that originated solely from vasculatures [71]. In brief, fresh brain tissue was homogenized on ice using pestle in HBSS solution with 1% HEPES. Whole brain homogenization was centrifuged at 2,000×g for 10 min and 4,400×g for 15 min (in 20% dextran) at 4 °C. Then, pellet containing vessels was re-suspended into ice-cold 1% bovine serum albumin (BSA) solution and proceed to mesh filter (20 um) for isolation. Western blot was performed as described by previous publication [72]. In brief, isolated brain vessels or cell lysis from respective experimental conditions were lysed with CellLytic-M (Sigma) for 30 min at 4 °C, and centrifuged at 14000×g. The concentrations of protein from tissue homogenates were estimated by bicinchoninic acid (BCA) method (Thermo Fisher Scientific, Rockford, IL). Protein load was 20 μg/lane in 4–15% SDS-PAGE gradient gels (Thermo Fisher Scientific). Molecular size separated proteins were then transferred onto nitrocellulose membranes, blocked with superblock (Thermo Fisher Scientific), and incubated overnight with respective primary antibody to alpha-SMA, eNOS and beta-actin (all diluted at 1:1000) at 4 °C, followed by washes and incubation with horse-radish peroxidase conjugated secondary antibodies (corresponding to primary, diluted at 1:12000) for 1 hr at room temperature. Immunoreactive bands were detected by West Pico chemiluminescence substrate (Thermo Fisher Scientific). Data was quantified as arbitrary densitometry intensity units using the ImageJ software package.

2.2.11 Real-time NO Detection

For tissues: Briefly, freshly isolated brain tissues was prepared in ice-cold oxygenated

(95% O2 and 5% CO2) artificial cerebrospinal fluid (aCSF). Coronal slice (1 mm) was prepared using brain matrices and transferred to a recovery chamber for 30 min with oxygenated aCSF at 37 °C temperature before experiment. NO was measured using free radical analyzer with a specific NO probe (TBR4100, World Precision Instruments, Sarasota, FL). The NO probe is able to polarographically measure the concentration of NO gas in solutions. The system was calibrated using different concentrations of NO donor S-Nitroso-N-acetyl-dl-penicillamine (SNAP, Cayman Chemical) to generate a standard curve. To block endogenous NO, oxygenated aCSF containing 1 mM L-NAME was added to tissue 30 min prior experiments. Probe was positioned ~1 mm above tissue surface using a micromanipulator (World Precision Instruments, Sarasota, FL) and baseline of NO release was recorded prior EtOH treatment. Tissue was then treated with 5 mM EtOH (in aCSF) and subsequently with 1 mM L-NAME (in aCSF). NO concentration was recorded using NO probe as described at the same time. Experiment was simultaneously performed with control from the same tissue source to exclude experimental drift in NO release unrelated to the study.

For cells: To block endogenous NO prior experiment, cells were firstly incubated with medium containing 50 µM L-NAME for 30 min. During experiment, probe was positioned ~ 1 mm above cell layer surface using a micromanipulator (World Precision Instruments, Sarasota, FL) and baseline of NO release was recorded prior EtOH treatment. Cells were then treated with 10 mM EtOH or 15 µM SNAP (in medium) and data was collected at 10, 20, 30, 60 and 120 min respectively. Experiment was simultaneously performed with control from the same cell source to exclude experimental drift in NO release unrelated to the study.

2.2.12 Plasma Fluorescence Intensity

Whole blood was collected from the tail vein before sacrificing and stored in citrate-treated blood tubes (Fisher) to avoid coagulate. To extract plasma, whole blood was centrifuged at 1000×g for 10 min (4 °C). Clear supernatant was carefully collected and aliquoted into small tubes. Arbitrary fluorescence intensity was determined in 96-well plate using plate reader (Molecular Devices) at 490 excitation and 525 emission wavelengths.

2.2.13 Endothelial and Smooth Muscle Cells Culture

Rat primary brain vascular endothelial cells and were purchased from ScienCell (Carlsbad, CA) and rat primary brain vascular smooth muscle cells were purchased from Cell Biologics (Chicago, IL). Briefly, cells were cultured on collagen-coated flash in complete medium with supplements provided by vendor.

2.2.14 Cell Toxicity Assay

Endothelial cells and smooth muscle cells (1×104/well, determined by cell number titration) were seeded into a 96-well plate respectively and incubated in at 37°C under a humidified atmosphere of 5% CO2 and 95% air for 24 hours prior experiment to allow fully attachment. Cells were then incubated with medium containing different concentration of alcohol (0, 2.5 mM, 5 mM, 10 mM and 20 mM) for 2 hours. Toxicity was subsequently measured by using MTT assay kit (Abcam). In brief, adding 50 μl of MTT reagent to each well, and then incubated the plate at 37°C for 3 h. After incubation, 150 μl of MTT solvent was added to each well and absorbance was measured at 590 nm using a multi-well spectrophotometer (Molecular Device).

2.2.15 Data Analysis

All results values are expressed as the mean ± SE, N = 6. Statistical analysis of the data was performed using SPSS 24 (IBM). In the present studies, wherever the numeric values of N are indicated, it represents the actual number of animals/samples used for that specific experiments or the actual number of experiments performed in cell culture setting, and not the number of replicates per experimental condition. Comparisons between samples were performed by ANOVA with Tukey's post-hoc tests. Differences were considered significant at $*p < 0.05$.

CHAPTER 3

ALCOHOL PROMOTES WASTE CLEARANCE IN THE CNS VIA BRAIN VASCULAR REACTIVITY

3.1 Summary

The efficient clearance of the interstitial waste metabolites is essential for the normal maintenance of brain homeostasis. The brain lacks the lymphatic clearance system. Thus, the drainage of waste metabolites in the brain is dependent on a slow flow of cerebrospinal fluid (CSF) system. Glymphatic system claims the direct bulk flow transport of small size water-soluble waste metabolites into to the perivenous space by aquaporin-4 water channels of the astrocyte end-feet, but it did not address the diffusive clearance of large size waste metabolites. In this chapter, we addressed the clearance mechanisms of large size waste metabolites from interstitial fluid to perivascular space as well as from CSF subarachnoid into perivascular space via the paravascular drainage. A low dose ethanol acting as a potent vasodilator promotes the dynamic clearance of waste metabolites through this perivascular-perivenous drainage path. We observed that ethanol-induced increased in vascular endothelial and smooth muscle cell reactivity regulated the enhanced clearance of metabolites. Here, we found that activation of endothelial specific nitric oxide synthase (eNOS) by ethanol and generation of vasodilator nitric oxide mediates the interactive reactivity of endothelial-smooth muscle cells and subsequent diffusion of the CNS waste metabolites towards perivascular space. By detection of tracer dye (waste metabolite) in the perivenous space and in the blood samples, I further confirmed the improved clearance of waste metabolites through this

unraveled interstitial-perivascular-perivenous clearance path. As such, we conclud that alcohol intake at low-dose levels may promote clearance of neurological disease associated entangled proteins.

3.2 Background

Efficient clearance of interstitial fluid (ISF) waste metabolites by cerebrospinal fluid (CSF) flow is essential for normal healthy maintenance of brain homeostasis, because unlike most tissue organs the brain lacks a lymphatic system. The classical view of the CNS clearance system is that the interstitial fluid (ISF) contains the extracellular and intracellular waste metabolites that are drained into choroid plexus [31], from here CSF flows into subarachnoid space (SA) through the median and lateral apertures. CSF is then exchanged into dural sagittal sinuses via a restricted granulation known as subarachnoid microvilli, then the sagittal sinuses, merged at the confluence of sinuses, are drained into nasal or cervical lymphatic vessels [26, 27, 30]. Johnston et al. (2010) showed this path by filling the subarachnoid compartment of seven different species, from small rodents to humans, with yellow microfil CSF tracer dyes to trace the drainage path of CSF into nasal lymphatics [35]. They found that microfil was observed primarily in the subarachnoid space around the olfactory bulbs and cribriform plate. The contrast agent followed the olfactory nerves and entered extensive lymphatic networks in the submucosa associated with the olfactory and respiratory epithelium.

Recently, Louveau et al. (2015) and Aspelund et al. (2015) have shown the existence of dura associated lymphatic vascular system in the brain's meninges whole-mount fixing the meninges still attached to the skull [36, 37]. They observed distinctive

expression of lymphatic endothelial cells including lymphatic vessel endothelial hyaluronan receptor 1 (Lyve-1) and vascular endothelial growth factor receptor 3 (VEGFR3) along the blood vessels of superior sagittal and transverse sinuses. The involvement of dural lymphatic vessels for the drainage of metabolites in dural venous sinus was shown by injecting tracers into the CSF of animals and by detecting the tracers in the lumen of Lyve-1-expressing vessels and in the deep cervical lymph nodes [37]. It was further confirmed that there was a significant reduction of tracers in Lyve-1-expressing vessels and a complete absence of tracers in the cervical lymph nodes of transgenic mice deprived of lymphatic vessels [36]. Since anatomical sites of lymphatic vessels were strictly localized in brain dura meninges [36, 37, 52], as such transport of soluble waste metabolites into lymphatic vessels would be dependent on CSF subarachnoid circulation. Notably, the exchange of waste metabolites from subarachnoid to superior sagittal venous sinus is valid only for water-soluble small size metabolites because of granulated subarachnoid microvilli barriers. Thus, dural lymphatic vessels, also known as meningeal lymphatic clearance system may not clear large size waste metabolites.

The recently discovered glymphatic system showed a molecular size dependent clearance profile of fluorescent dye tracers in the CNS, when tracers were injected through intracisterna magna [29]. The small size tracer (Texas Red, 3 kDa) directly entered the interstitial space and influx into the perivascular space along penetrating arterioles. The clearance of this small size tracer from perivascular space into central deep veins and lateral-ventral caudal rhinal veins is facilitated by aquaporin-4 (AQP4) water channel of a highly-polarized astrocytic end feet. Such an AQP4 facilitated

exchange between CSF and ISF is restricted to small size waste metabolites because the medium size tracer (Ovalbumin, 647 kDa) gets accumulated at perivascular space within 3 hours of injection. The tracer then slowly penetrated into the basement membranes of parenchymal capillaries and perivascular space of large caliber draining veins, suggesting a capillary-venous drainage route. In contrast, a large size tracer (FITC, 2000 kDa) was found to be aggregated at the perivascular space, lacking a distinct clearance path [29]. Injection of radiolabeled amyloid β1–40 (Aβ, a small peptide) into mouse striatum was rapidly cleared through the glymphatic pathway since the clearance was significantly diminished in AQP4 deficiency transgenic mice [29]. This further implicates the importance of glymphatic system clearance in neurological disease, like Alzheimer's disease [29, 38-40], even though glymphatic system did not account for the clearance of such large size waste metabolites in the CNS.

However, the reproducibility of the accredited bulk flow transport mechanism of glymphatic hypothesis has been questioned by a number of most recent verification studies. These investigations concluded that clearance of waste metabolites from the brain is more of a diffusion rather than bulk flow convective transport, based on the metabolites molecular size [42, 43]. In support of this argument, a model of diffusive and convective transport in brain extracellular space stated that diffusion alone size [44] or combined effects of diffusion and macroscopic fluid motion [45] is adequate to account for transport of waste metabolites in brain parenchyma rather than bulk flow alone. The later appears to be a more reconcile argument for such conflicting experimental observations, notably the transport of solutes in opposite directions in the perivascular space. This is in parallel with the findings that cyclic changes in arterial

pressure produces mixing or flow in opposite directions in different spaces of the arterial wall [46]. In this case, convection can assist the movement into and out of the cortex without necessarily producing the net flow of fluid into the cortex as required by glymphatic system. Furthermore, the diffusive molecular flow along the peri-arterial sheaths into subarachnoid CSF [47], and the diffusive drainage of waste metabolites from brain parenchyma into the basement membrane of capillaries [28] argued against the glymphatic hypothesis.

The fact is that large size waste metabolites like tauopathy, prion-like proteinopathies, cerebral amyloid angiopathy, and Aβ proteins are seen accumulated around the perivascular space in brain tissue from neurological diseases [1, 2, 48]. Such observations suggest that large size waste metabolites are not cleared by CSF, glymphatic, or meningeal lymphatic systems. Here, we address the fundamental questions of what dynamic force specifically drives the movement of these waste metabolites towards perivascular space, and can we strategize to enhance the clearance of these waste metabolites from perivascular space into the circulation? It has been shown that the blood-brain barrier (BBB) trans-vascular clearance from brain to blood provides functionally a major pathway for elimination of different waste metabolic products from brain into the circulation including amyloid-beta, which is believed to account for > 80% of amyloid-beta clearance under physiological conditions [59-61]. Thus, uncovering the mechanisms of moving the waste metabolites towards perivascular space and the clearance of waste metabolites from perivascular space into the circulation should have significant clinical impact for possible prevention of many neurological diseases. We hypothesize that increasing the reactivity of brain arterial endothelial and

smooth muscle cell function by low dose ethanol can enhance the dynamic diffusion of water-insoluble large size CSF/interstitial metabolites into perivascular space and subsequent clearance into the circulation. Here we test the idea that activation of brain endothelial specific nitric oxide synthase (eNOS) by low dose ethanol produces potent vasodilator nitric oxide that can diffuse readily into the underlying SMCs to cause arterial vessel dilation through intracellular calcium signaling. The rationale is that activation of eNOS by low concentration of ethanol elevates physiological NO levels and augments endothelial-SMCs interactive reactivity [4, 64, 65]. This eNOS derived NO acts as a potent protective brain vascular tone and vasodilation [70].

3.3 Results

In this study, we examined the idea that reactivity of endothelial and smooth muscle cells plays a critical role in the interstitial-perivascular-perivenous clearance of large size waste metabolites in the brain. Here we first focused on the dynamic bio-distribution of a 2000 kDa fluorescent dye representing large size waste metabolites following two different routes of injection, through cisterna magna and direct intracranial cortical injection. Cisterna magna route directly deposits the tracer into the C3 region of CSF-subarachnoid flow, while deposition of tracer dye into the intracranial cortical region move through the interstitial space. Stimulation of brain arterial endothelial and smooth muscle cells reactivity by low dose ethanol was correlated to increase clearance of waste metabolite through interstitial-perivascular-perivenous space. We observed that reactive vascular endothelial-smooth muscle cell dilation and contraction regulates the diffusion and clearance of waste metabolites via the interstitial-perivascular-perivenous path. The

clearance path is supported by the present findings.

3.3.1 Injection of FITC-d2000 into C3 Region of CSF Flow Accumulates in Perivascular Space via the Subarachnoid-paravascular Movement

To evaluate the movement pattern of large size waste metabolites in the brain, we first injected FITC-d2000 (MW: 2000 kDa) directly into the CSF flow via cisterna magna which bypass the interstitial movement. This large size fluorescence tracer represents large size waste metabolite like A-β proteins, which is validated in Appendix E (**Figures E1 and E2).** We then evaluated the bio-distribution of tracer in the brain at different time points. We observed that a direct deposition of tracer into the C3 region of CSF-subarachnoid flow and penetrated into the perivascular space via the paravascular route time-dependently. For example, in less than 30 min after intracistertna magna injection, the subarachnoid (SAS) was filled with fluorescence tracer, but very little tracer penetrated in less than 0.5 mm depth of paravascular area from SAS (**Figure 3.1A**). But after 60 min, more tracer was observed penetrating deep into brain perivascular space (**Figure 3.1B – C**). The magnified imaging data from **Figure 3.1D – F** showed the biodistribution of aggregated tracer along the different segmental branches of arterial vessel. These data suggest that waste metabolites from CSF flow can move into perivascular space through subarachnoid-paravascular drainage path.

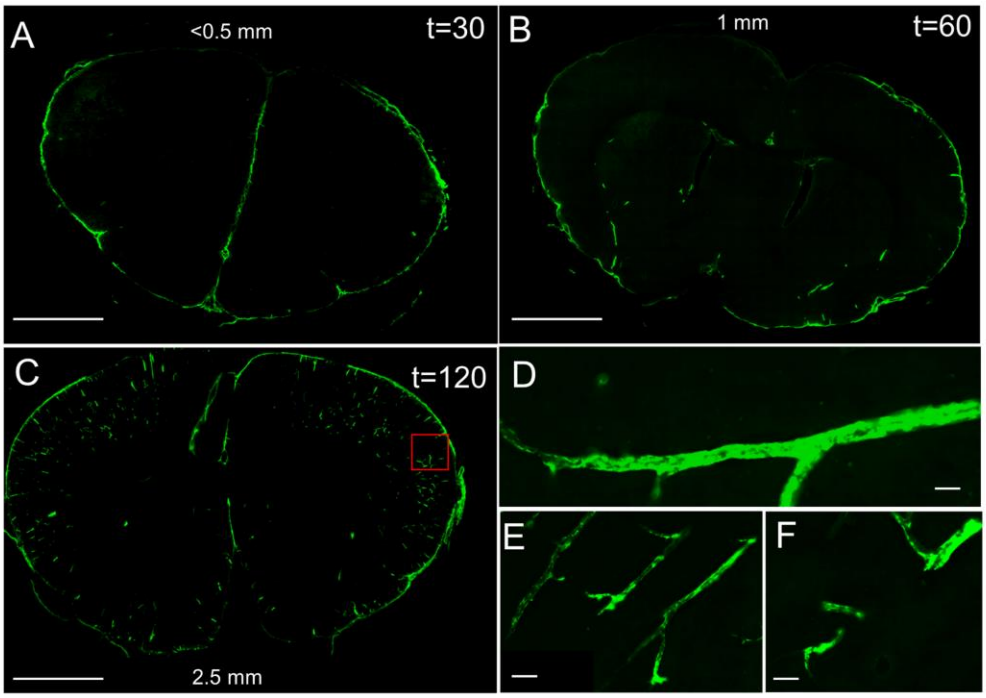

Figure 3.1 Tracer bio-distribution after cisterna magna injection at 30, 60, and 120 min. [A-C] data indicated that tracer was firstly filled in SAS (t<30min), and subsequently penetrated into brain along vasculatures. [D-F] details the magnified view of vasculatures in the boxed in C. Data are representative of N=6 animals. Scale bar: [A, B and C] 3 mm; [D, E and F]: 50 µm.

We then evaluated the exact location of the tracer in perivascular space. The arteriole perivascular space consists of endothelial cells, pericytes, and smooth muscle cells including basement membrane proteins that are ensheathed by astrocytic end-feet from the brain side. The capillary perivascular space will contain all cellular components like in arteriole but there is absence of smooth muscle cells. Co-localization of this tracer with immunostaining of perivascular cellular markers indicated that the waste metabolite tracer was found to be entrapped in between astrocytes (**Figure 3.2A**, GFAP) particularly at the astrocytic end-feet (**Figure 3.2 B & C**) and vascular smooth muscle cells (**Figure 3.2D – G**) as indicated by colocalization of alpha-SMA and tracer. I also observed that the waste metabolite tracer did not readily cross the blood vessel but

aggregated around perivasculature at early time point as shown in **Figure 3.2E – G**. These observations seen in immunostaining colocalization studies were further confirmed by multiphoton imaging techniques (**Figure 3.2 H, H1, H2 & H3**; Green: FITC-d2000, CSF tracers; Red: Texas red-d70, label vasculatures).

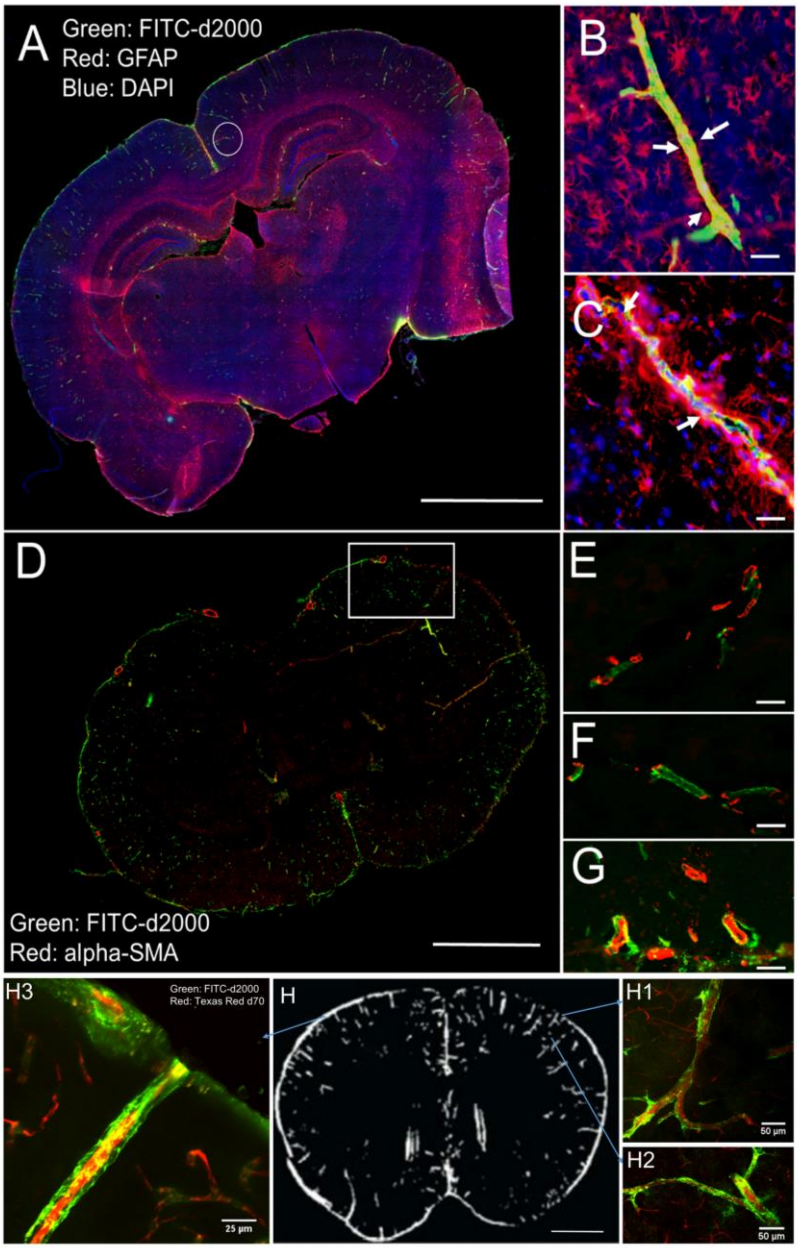

Figure 3.2 Co-localization of FITC-d2000 after cisterna magna injection with astrocyte marker (GFAP) and vascular smooth muscle marker (alpha-SMA) revealed location of tracers relative to vasculatures. [A]: Co-localization of tracer (FITC-d2000, 120 min after cisterna magna injection) and astrocytes (GFAP). [B and C]: Detail views revealed that tracers were wrapped by astrocytic end-feet (white arrows). [D] Co-localization of tracer (FITC-d2000, 120 min after cisterna magna injection) and smooth muscle cells (alpha-SMA). [E – G]: Detail views on right revealed that tracers were outside smooth muscle layer, not in vessel lumen. [H]: Two-photon scanning of tracer bio-distribution (Green: FITC-d2000; Red: Texas-Red d70). Animals were injected with two types of tracers: FITC (green) was delivered through cisterna magna; Texas-Red (red) was injected through tail vein to label vasculatures. 2 hours were allowed before sacrificing.

[H] indicated location of vessel segments that presented in H1, H2 and H3. Data suggested that after cisterna magna injection, tracers aggregated along vasculatures. Data was representation of N=6 animals. Scale bar: [A and D]: 3 mm; [B and C]: 100 μm; [E, F and G]; [H]: 3 mm; [H1 and H2]: 50 μm; [H3]: 25 μm.

3.3.2 Intracranial Cortical Injection of FITC-d2000 Reaches the Perivascular Space Prior to Subarachnoid Clearance Path

In contrast to deposition of waste metabolites directly into the CSF flow through cisterna magna injection, we also injected a FITC-d2000 tracer directly into brain interstitial space at the depth of 0.5 mm in the right cortical surface, 2.0 mm lateral to sagittal suture and 3.0 mm away from caudal coronal suture at different time points. The rationale was to determine if waste metabolites can diffuse directly into the perivascular space from site of production (parenchyma) or the route of translocation would follow the path of CSF flow via subarachnoid-paravascular clearance. We found that tracers started to diffuse directly into para-and peri-vascular space from interstitial space after 60 min of cortical injection, as indicated by Texas red-d70 labeled for vasculatures and FITC-d2000 Green representing large size waste metabolites (**Figure 3.3B – D**). At this time point, no tracers were detected at subarachnoid space through this route of injection (**Figure 3.3A**), indicating that waste metabolites can move directly into PVS via the interstitial diffusion. There was more accumulation of tracer in the perivascular space at longer time points of 240 min (**Figure 3.3E – F**). This cumulative aggregation of tracer in the PVS was from interstitial movement and dynamic translocation of CSF flow because subarachnoid space was also filled with tracer at this later time point. Co-localization of tracer and vascular smooth muscle marker (alpha-SMA) immunostaining revealed that most of the tracer was arterial and capillary structures (**Figure 3.3G – H**).

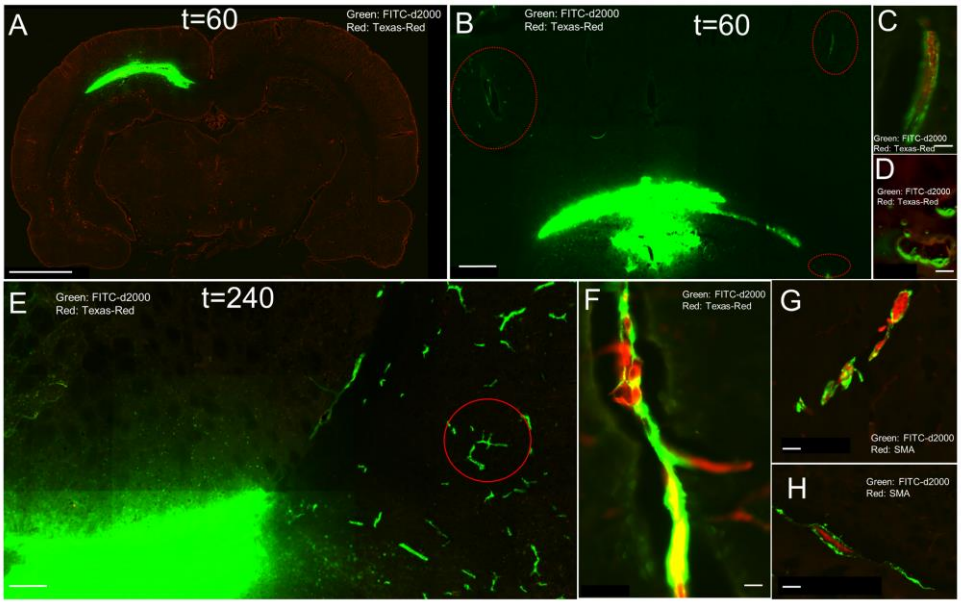

Figure 3.3 Intracortical deposition of FITC-d2000 (green) directly into cortex (0.5 mm below cortical surface) allow us to track the time-dependent diffusion of tracer along the perivascular space marked by vessel marker Texas-Red d70 injected through the tail vein. 45 µm brain slices on glass slides were subjected to fluorescence microscope. [A, B, and E] indicate the time-dependent location of tracer. Small traces of tracers were already translocated from site of injection to the perivascular space before reaching to CSF, indicated by the absence of fluorescence in SAS. More tracers were found to move at longer time (E). Detail view in [C, D, F] suggested that the accumulation of tracers at PVS. [G and H]: co-localization of tracer (green) with smooth muscle actin (red) indicated that these vessels were arterials due to the presence of smooth muscle cell. Data are representative of N=6 animals. Scale bar: A: 1 mm; B and E: 300 µm; C, D, F and G: 50 µm; H, I and J: 30 µm.

3.3.3 Evaluation of the Putative Mechanisms of Tracer Movement Towards Perivascular Space

We then evaluated the putative mechanism of dynamic waste metabolites movement towards PVS that could be associated with clearance path. Based on previous findings [23, 28, 66, 73], we rationalized that increase in arterial vessel dilative reactivity by low-dose alcohol may regulate the movement of waste metabolites towards PVS. The justification was that low dose alcohol was known to enhance vessel dilation through nitric oxide (NO) production in endothelial cells [74]. As such, we first established the

dose-response of ethanol concentrations from 2 – 10 mM on the tracer movement from CSF to perivascular space. We determined 5 mM ethanol gave the maximal biodistribution of tracer and this optimal working concentration is approximately equivalent of 0.02% blood alcohol level, which is about 4 – 5 times lower than the legal limit of 0.08 – 1.0% blood alcohol level. We observed that low dose of 5 mM ethanol injection into rat via the tail significantly ($p<0.05$) enhanced the movement of the 2000 kDa FITC tracer from CSF to PVS compared with control (**Figure 3.4A**). Three different regions of brain slices were selected according to rat brain atlas map (**Figure 3.4A**), and we observed a similar trend of increased distribution of tracer by ethanol in all the three different brain regions. However, this stimulating effect of ethanol was reversed by nitric oxide synthase inhibitor L-NAME, indicating that low dose ethanol increased the movement of tracer through NOS mediated NO production.

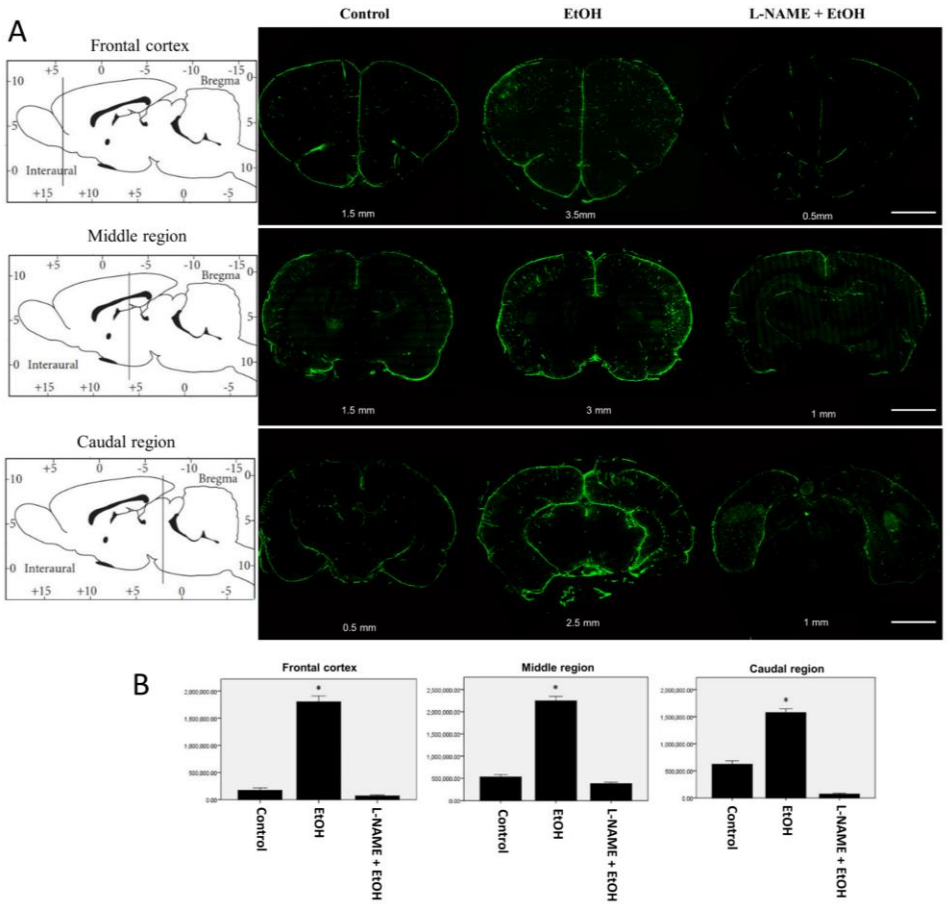

Figure 3.4 [A] Bio-distribution of tracer at 2 hours after cisterna magna injection in control, 5 mM EtOH, and L-NAME + 5 mM EtOH. Coordination of brain coronal tissue slices (45 μm) are shown according to rat brain map in three different locations, where bio-distribution of tracer was imaged in the whole brain section. Scale bar: 2 mm. [B] The quantity of tracer distribution in brain was calculated as mean fluorescence intensity on each slide (from N=6 animals, 10~15 slices were taken from each animal, +SEM). Data indicated that alcohol significantly increased the biodistribution of tracer and vascular reactivity, while NOS inhibitor L-NAME reversed the effect compared with control (*$p<0.05$).

Thus, among all isoforms of NOS, we evaluated the effects of 5.0 mM ethanol on qualitative and quantitative levels of endothelial specific eNOS, and subsequent production of NO levels in brain tissues. This biological marker was examined to validate the idea that low dose ethanol enhanced the movement of waste metabolites along the perivasculature through NO induced vessel dilative pathway. Interestingly,

immunostaining revealed a huge increase of eNOS induction by low dose alcohol group (**Figure 3.5A**), which was further validated by significant elevation of eNOS levels by ethanol compared with control ($p<0.05$), as determined by Western blot analysis (**Figure 3.5B**). To correlate the low dose ethanol-induced eNOS activation with NO generation, we analyzed the real-time NO production in live rat brain tissue by Free Radical Analyzer (World Precision Instruments, Sarasota, FL) using a micro-sensor detector. In line with eNOS activation, low dose alcohol exposure significantly elevated the production of NO in rat brain compared with baseline (**Figure 3.5C**). As expected, co-treatment of L-NAME not only inhibited the induction of eNOS but also the production NO level. These data collectively suggest that low dose alcohol can promote perivascular clearance of waste metabolites through eNOS-mediated NO production by increasing the cerebral arterial vessel dilations.

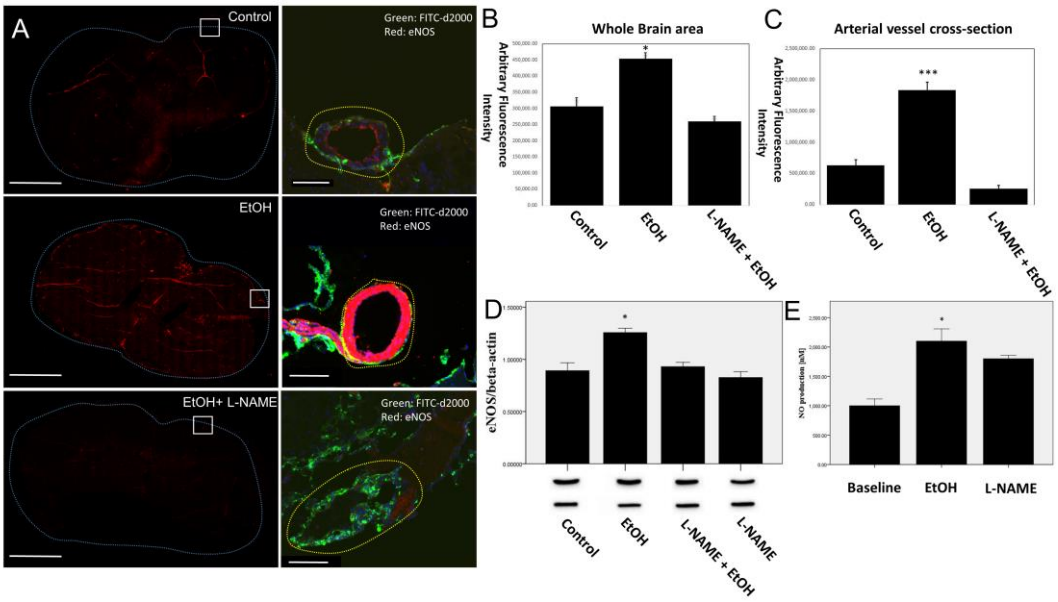

Figure 3.5 Induction of eNOS by low dose ethanol produces endothelial derived nitric oxide. [A] Left: Colocalization of eNOS (red) and tracer (green) in whole brain tissue slice. Right: detailed view in boxed area. Data indicated that eNOS was elevated by EtOH. (N=6 animals, 10~15 slices per animal). Scale bar: Left: 3mm; Right: 50 μm. [B and C] The quantity of tracer distribution in brain was calculated as mean fluorescence intensity on each slide (from N=6 animals, 10~15 slices were taken from each animal, +SEM). Fluorescence intensity quantification of eNOS was calculated as mean fluorescence intensity on each slide (from N=6 animals, 10~15 slices were taken from each animal, +SEM) and presented as bar graphs for both whole brain scanning [B] and arterial vessel cross-section [C]. Data indicated that both quantification showed statistically significance upregulation of eNOS by low dose EtOH. Magnitude of increase in eNOS levels in the whole brain area quantification is similar to that of Western blot analyses. Whereas, the fold increase in arterial vessel is much higher than that of whole brain or Western blot because localization of eNOS is specific to arterial endothelium. [D] Western blot analysis of eNOS levels in different experiment conditions. Data was analyzed using image J to obtain arbitrary densitometry intensity units. Three replicates were done for each animal sample from N=6 animals. Bar graphs data were quantified from the ratio of eNOS to that of β-actin bands, and expressed as mean ±SEM. [E] Real-time NO production in live rat brain tissue (1 mm) by Free Radical Analyzer, where NO production was simultaneously monitored. Bar graphs show the average NO concentration under each condition, and expressed as mean ±SEM. The asterisk indicates the statistical significance (*$p<0.05$) in EtOH compare with control.

3.3.4 Low Dose Alcohol Enhances Dynamic Vessel Dilation

To validate the proof-of-concept that ethanol-induced arterial vessel reactivity promotes the pool of waste metabolites along the PVS, we determined dynamic dilative vessel reactivity by multiphoton imaging in live animals. We found that low dose alcohol significantly increased tracer movement towards PVS within 15 min, where the flux of tracer could be detected easily in the depth of 50 – 100 μm below cortical surface (**Figure 3.6A**). This increase in tracer accumulation in the PVS in the presence of alcohol was further supported by a significant vessel dilation (**Figure 3.6B - C**) and a significant increase in arterial vessel diameter (**Figure 3.6D**) as revealed by two photon line scan. This alcohol-induced significant increase in arterial vessel dilation and contraction suggest the active interaction between brain endothelial cell and smooth muscle cell within the arterial cellular components via the signaling molecule eNOS-elicited NO production. Such a cross-talk between endothelial cell and smooth muscle cell is unlikely to occur in the capillary since smooth muscle cells are absent in the capillary.

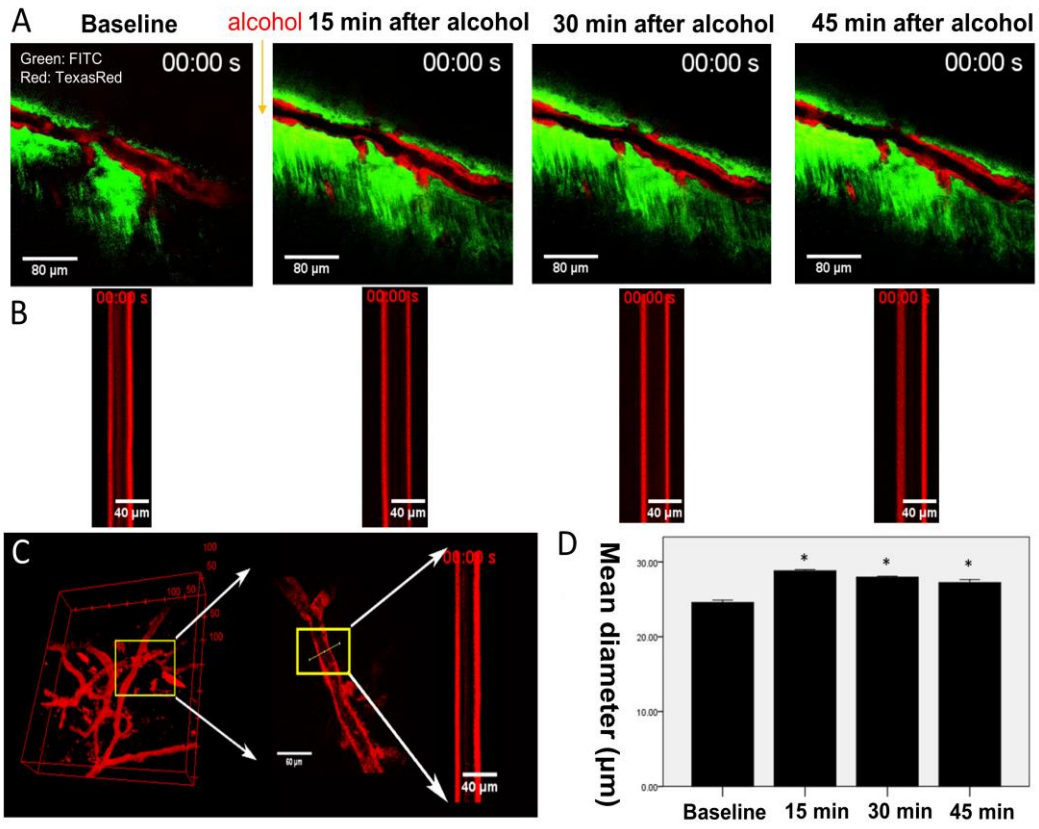

Figure 3.6 Low dose alcohol enhances dynamic vessel dilation: [A] Time-lapse *in-vivo* two-photon imaging of florescent tracer (green, injected via intracisterna) and vessel marker Texas-Red (injected via tail vein) showed the time-dependent aggregation of tracer in perivascular space in 50-100 μm below cortical surface. [B] Dynamic imaging of changes in vessel diameter over time (N=3) before and after exposure to 5 mM ethanol at different time lapse. [C] Left: Cerebral was visualization of cerebral vasculature by two-photon imaging after intravenous tail vein injection of Texas Red-d70 showing penetrating arteriole in box (25 μm in diameter). Right: Selected area for X-T line scan to examine the changes in vessel dimeter, which was analyzed by customized Matlab at different time lapse. [D] Calculated changes in vessel dimeter, wherein baseline was collected before alcohol exposure. A 9000 ms epoch line scan was applied every 15 minutes to determine the changes in vessel diameter, which is shown in bar graphs. Two-way ANOVA with tukey's post-hoc test show the statistical significance * $p<0.05$ compared with baseline, expressed as mean ±SEM, N=3.

We then examined the idea that generation of the alcohol-induced vasodilator NO from brain endothelial cells can readily diffuse into the underlining smooth muscle cells (SMCs) reactivity. The rationale is that elevation of physiological NO levels in

endothelial cell augments the endothelial-SMCs interaction to increase arterial vessel dilation. The qualitative data from immunostaining staining of α-SMCs showed an increase reactivity in low dose alcohol group compared with controls (**Figure 3.7A**), which was in agreement with alcohol-induced NO production by endothelial cells. In parallel with an increase α-SMCs expression, the quantitative assay by Western blot analysis validated the significant elevation of α-SMCs levels in alcohol condition compared with controls (**Figure 3.7B**). This data suggests an active interaction between vascular endothelial cells (ECs) and smooth muscle cells through a paracrine signaling pathway in which ECs derived nitric oxide acts as the key signaling molecular messenger for vessel dilation. The underlying mechanism of ECs-SMCs interaction through NO will be thoroughly discussed in next chapter.

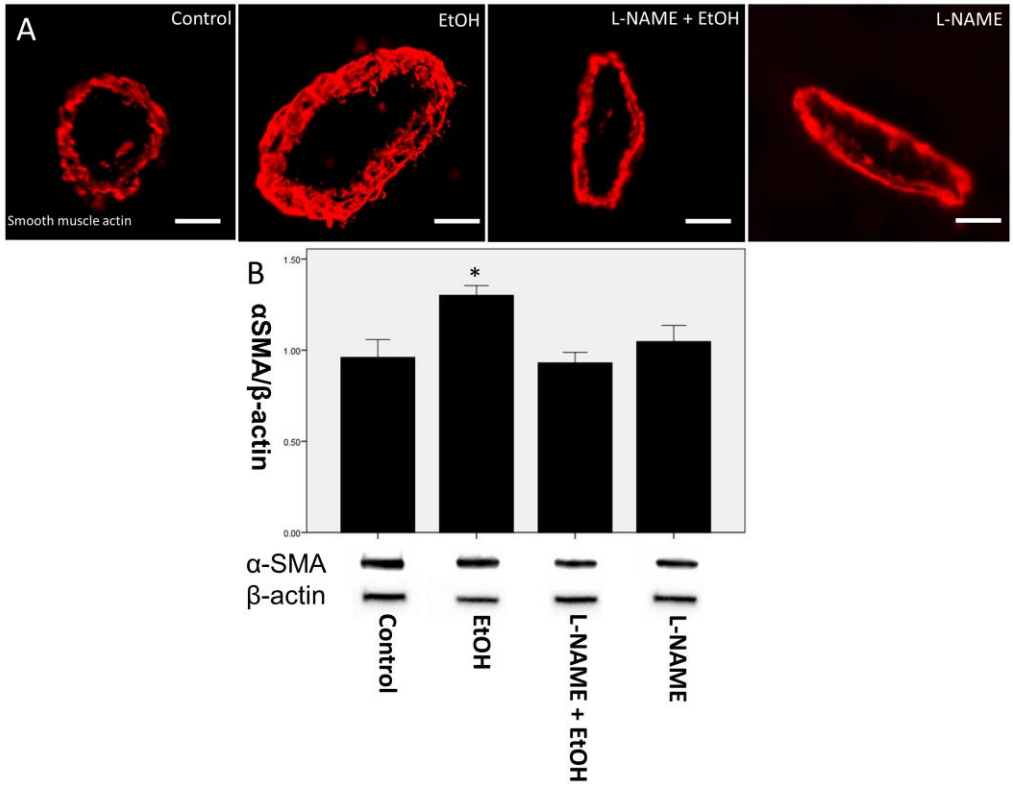

Figure 3.7 [A] Shows the representative expression of brain vascular α-smooth muscle actin (αSMA, red) in whole brain tissue sections (10 μm thick) in different experiment conditions with a significant increase by ethanol exposure (N=6 animals, 10~15 slices per animal). Scale bar: 30 μm. [B] Western blot analysis of αSMA levels in different experiment conditions. Data was analyzed by image J to obtain arbitrary densitometry intensity units. Three replicates were done for each animal per condition. Bar graphs show the quantified data that were expressed as ratio of αSMA immunoreactive bands to that of β-actin bands, with mean ±SEM. * indicates the statistical significance $p<0.05$ compared with control or L-NAME+EtOH/L-NAME alone.

3.3.5 Vessel Dilation Increases Waste Metabolite Clearance

So far, we have shown that large size waste metabolites that are not able to diffuse across the subarachnoid (SA)-superior interface (due to the presence of SA microvilli) in CSF flow get accumulated in perivascular space in the presence of low dose alcohol. This includes the interstitial-perivascular movement of waste metabolites. The diffusion of these metabolites towards the perivascular space appeared to be regulated by alcohol

mediated increase in arterial vessel contraction and dilation. We then examined whether these accumulated waste metabolites at the perivascular space will diffuse into the perivenous space across the bed of capillaries, and get exchange/efflux into the blood circulation as clearance mechanisms. The results clearly showed an increase colocalization of the 2000 kDa FITC tracer and venule marker (endomucin) in alcohol group (**Figure 3.8A – B**) compared with controls (**Figure 3.8C – D**), even though the tracer aggregation in perivenous space was not as high as in perivascular space. This data suggests a limited exchange of metabolites from perivascular space to perivenous space, which indicates efflux of metabolites from perivascular/perivenous space into the blood circulation.

This led us to examine validation of tracer in blood plasma samples from different experimental conditions as a proof-of-concept. Blood samples were collected at the time of sacrifice from different experimental groups with/without L-NAME injection, and separated the plasma. The 2000 kDa FITC tracer in blood plasma samples was detected by SpectraMax Multi-Mode fluorescence microplate reader at the specific excitation (490 nm) and emission (525 nm) wavelengths. We observed a significant increase of tracer fluorescence intensity in the plasma samples in low dose alcohol group compared with controls or the alcohol plus L-NAME group (**Figure 3.8E**), indicating that low dose alcohol promotes the waste metabolites clearance path from perivascular/perivenous space into the blood circulation. These findings suggest the existence of large size waste metabolites clearance path from perivascular or perivenous space into the blood circulation, which is regulated by alcohol-induced NO mediated cerebral vessel dilation.

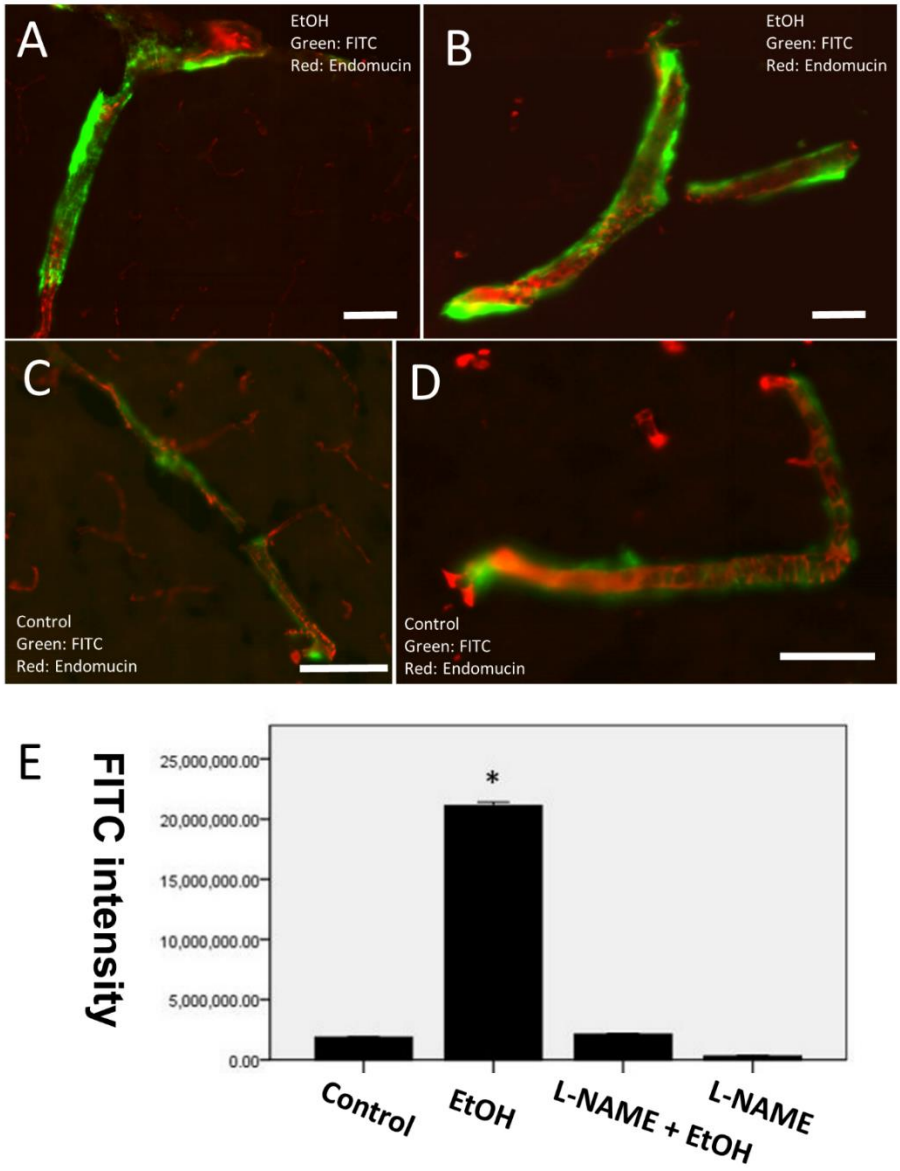

Figure 3.8 Validating the diffusive exchange of waste metabolite from perivascular to perivenous space (at the bed of capillaries). [A - D] Colocalization of FITC tracer (Green) and venule marker endomucin (red) in alcohol group (A&B) compared with control (C&D), indicating an exchange of large size metabolites from perivascular space to perivenous space. Scale bar: 30 μm. [E] Detection of FITC-d2000 in blood plasma collected after 120 min cisterna magna injection from different experiment conditions, (n=6/per group, + SEM). One-way ANOVA and post-hoc turkey test (* $p<0.05$, compared with control) was performed to compare difference between each group.

3.4 Discussion

We discuss the findings that large size waste metabolites in the brain that are unable to clear out by the conventional CSF clearance path get diffused towards perivascular-perivenous space from the interstitial fluid and from the CSF-subarachnoid flow. Thus, there is a dynamic movement of large size waste metabolites from interstitial space and subarachnoid towards perivascular space under normal physiological condition. To mimic those large size waste metabolites, we used a relative large molecular weight fluorescent tracer (2000 KD) and administered into brain. The rationale is that due to the molecular size limitation and also shown by other study [29], after injection into brain tracers tended to accumulate at perivascular space instead of being eliminated through typical clearance routes including BBB trans-vascular clearance, degradation and CSF/ISF diffusion as noted in publication [66]. This physiological behavior is comparable with what have been observed in certain neurological diseases including perivascular phosphorylated tau protein disposition in cerebral amyloid angiopathy (CAA) and aggregated amyloid beta protein in Alzheimer's disease [75, 76]. To validate the use of tracers, we also showed that the tracers used in the study revealed similar movement pattern as A-β proteins following differnet injection routes (**Figures D.1 and D.2**). Thus, though differed from chemical composition, given the physiology similarity of tracers and large size waste metabolites in brain as discussed, the movement pattern of tracer was considered informative towards current study purpose.

We firstly showed the perivascular disposition phenomenon by the bio-distribution of large size molecular weight fluorescent tracer injection from two different routes, a direct deposition of tracer into the CSF flow by intracisterna magna injection and a direct

deposit of tracer into interstitial space through intracranial cortical route. Even though the subarachnoid (SAS) was filled with fluorescence tracer within 30 min, the actual penetration of tracer into the perivascular space occurred after 60 minute in intracistertna magna injection (**Figure 3.1A-F**). In the interstitial cortical injection, the tracer diffused directly into perivascular space within 60 min (**Figure 3.3A-D**), while the CSF flow was filled with tracer at the much later time points (**Figure 3.3E-F**), indicating the slow clearance of large size waste metabolite from interstitial fluid to C3 choroid flexus. These data suggest that waste metabolites can diffuse directly into PVS time-dependently from interstitial fluid and from CSF-subarachnoid flow, which is regulated by endothelial-smooth muscle cell dilation. Similar alternative clearance mechanisms of direct translocation of interstitial solutes to perivascular space have been proposed in mouse model [28].

Intriguingly, the data showed that a very low level of 5.0 mM ethanol, equivalent of 0.02% blood alcohol level can enhance the dynamic movement pattern of these waste metabolites towards perivascular-perivenous space. This concentration is far below the legal limit of 0.08 % blood alcohol level. In spite of alcohol being an addictive substance, the low-dose of this legalized substance is likely to improve the clearance of waste metabolites in the brain. Thereby, one drink of alcohol a day may ameliorate the progression of many neurological diseases that are originated from toxicity of non-clearance waste metabolites. Interestingly, a number of recent population-based cohort studies concluded that heavy alcohol use in chronic condition is associated with development dementia and progression of Alzheimer's disease and cerebral amyloid angiopathy [77-84], the hallmark of these neurological diseases happen to be the

deposition of waste metabolites like A-β protein, or protein prion-like proteinopathies around the perivascular space [1, 2, 48]. These cohort studies also unequivocally noted the protective effects of low dose alcohol use against the progression of dementia and AD/CAA, with unknown mechanisms. It is apparent that beneficial or destructive effects of alcohol is dependent on the duration and concentration use. In the present studies, we use low level of alcohol to understand the protective mechanisms for promoting perivascular clearance because low-moderate alcohol use is protective of vascular and cardiovascular function [4, 64, 65, 85-87]. We also showed that use of alcohol concentrations that are between 2.5 mM - 20 mM (~ 0.08%) revealed comparable effects in terms of PVS clearance (**Figure E.1).** The likely reason can be attributed to the findings that these alchol concentrations are adequately to stimulate eNOS expression and NO release (**Figure E.2**), which regulated the PVS clearance efficiency. In addition, repetitive intake of low dose alcohol (5 mM) showed similar effect (**Figure E.3**), which lined up with the beneficial effect of low dose alcohol intake.

We noted here that the contrast effects of low dose alcohol intake and chronic use of high dose alcohol (equivalent of alcohol dependent subjects) in the context of blood-brain barrier permeability and perivascular clearance path will be discussed in the following chapters.

We then addressed the underlying clearance mechanisms of the accumulated waste metabolites from perivascular or perivenous space into the blood circulation by two approaches. The exchange of waste metabolites from perivascular space to perivenous space across the bed of capillaries, and detection of waste metabolite in blood samples collected from jugular vein. Colocalization of tracer with venule marker clearly showed

a significant accumulation of tracer in perivenous space of alcohol group compared with controls (**Figure 3.8A-D**), however the tracer intensity was less than that of perivascular space (**Figure 3.6A**). These results indicated the movement of metabolites from perivascular to perivenous space across the bed of capillary. The exchange of waste metabolites from perivascular/perivenous space into the blood circulation as the clearance path was examined by the presence of fluorescent tracer in blood plasma samples from various experimental conditions. A significant detection of tracer in the plasma samples in low dose alcohol group was markedly higher than controls or alcohol plus NOS inhibitor L-NAME groups (**Figure 3.8E**). These data suggest that the tracer was leaked into the circulation from perivascular/perivenous exchange because this large size waste metabolite was not permeable from subarachnoid to sagittal sinuses due to blockade by subarachnoid microvilli. The significantly low level of tracer present in NOS inhibitor plus alcohol group also suggested the direct role of alcohol-induced NO elicited perivascular/perivenous-blood circulation clearance path.

We then validated the underlying mechanisms that alcohol-elicited eNOS specific NO production promoted the cerebral arterial vessel dilation and clearance. The rationale was that NO production augmented the endothelial-smooth muscle cell reactive interactions and arterial vessel dilation. This is because low dose alcohol consumption led to an increase eNOS activity and NO production [4, 64, 65], whereas high dose chronic alcohol consumption led to detrimental consequences on vascular function [67, 88, 89]. In support of our hypothesis, we observed an increase reactivity of α-SMCs in low dose alcohol qualitatively and quantitative compared with controls or in the presence of NOS inhibitor **(Figure 3.7A-B)**. The observations were in line with

the findings that NO-mediated endothelial-smooth muscle cells interaction was key to arterial vessel reactive dilation [90, 91], and perhaps the movement of tracer along PVS [73]. The rationale is that endothelial-derived NO generation can diffuse readily into the underlying SMCs and cause vessel dilation through a cascade of paracrine-mediated biochemical signaling events [90, 91], wherein NO serves as the key signaling molecule for vessel dilation.

Apart from local level regulation of vessel dilation including response to mechanical forces (e.g., shear stress) and chemical stimuli (e.g., NO) as discussed above, it was also known that vessel contraction/dilation was neural activity dependent and increased vessel dilation was coupled sensory stimulus. For example, using whisker stimulation and cortical spreading depolarization, researchers observed microvascular diameter changes in smooth muscle covered microvessels in brain [63]. However, due to the study scope limitation, the current research focus was primarily on the local level regulation of regional blood vessel dilation that exerted by low dose alcohol. Brain activity dependent regulation was not discussed in this dissertation.

In conclusion, the diffusive movement of large size waste metabolites from interstitial fluid and from CSF-subarachnoid flow into perivascular-perivenous drainage path is regulated by reactive dilation of endothelial-smooth muscle cells. We found that low dose alcohol can significantly promote these waste metabolites movement towards the perivascular-perivenous space and its clearance into the circulation. We confirmed that alcohol-elicited eNOS specific NO production regulated the cerebral arterial vessel dilation through endothelial-smooth muscle cell reactive interactions (**Figure 3.9**). The present findings are expected to have far-reaching translational significance, particularly

the timely clearance of entangled proteins in neurological diseases.

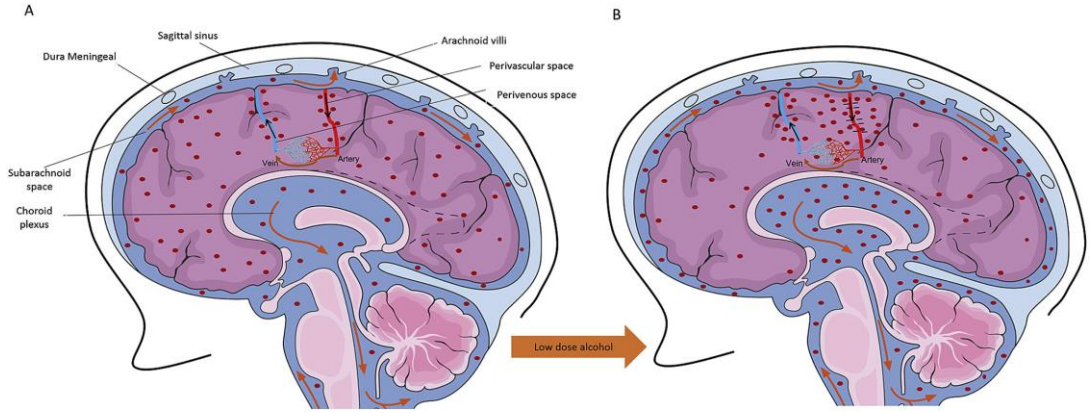

Figure 3.9 Illustration of alcohol promotes waste metabolites clearance. (A) Arrows (orange) indicate the CSF subarachnoid flow and perivascular-perivenous clearance path (black) of large size waste metabolites (red dots) in neurodegenerative brain. Waste metabolites like β-amyloid proteins are aggregated more inside the interstitial space due to the lack of lymphatic system in the brain. Less metabolite are drained into the CSF flows due to less vessel dilative reactivity. (B) Neurodegenerative brain in the presence of low dose alcohol. Dilative arterial vessel reactivity promotes the dynamic movement of large size waste metabolites from interstitial fluid to perivascular space and from interstitial-CSF subarachnoid to perivascular space. Reactivity of endothelial and smooth muscle cells in arteries is mediated by alcohol-elicited eNOS activation and NO production.

CHAPTER 4

MECHANISM OF ALCOHOL MEDIATED SMCs-ECs INTERACTION

4.1 Summary

We have shown that alcohol-mediated vasodilation can exert beneficial effects towards brain waste metabolites clearance through induction of endothelial function and enhancement of neighboring smooth muscle reactivity from previous chpater. Here in this chapter, we further investigated the underlying mechanism of ECs-SMCs interaction by addressing the response of endothelial cells to low dose alcohol and examining level of NO releasing and corresponding enzymes expression. We determined the activities of surrounding smooth muscle cells by evaluating the phosphorylation status of myosin light chain (MLC) and activities of corresponding regulatory subunits. Results indicated that low level alcohol promotes NO release from endothelial cells through eNOS. NO induced smooth muscle relaxation occured through myosin light chain dephosphorylation. Regulation of NO-mediated MLC dephosphorylation was done via the paradigm shift from myosin light chain kinase to myosin phosphatase activities. We validated such observations by qualitative immunostaining and quantitative Western blot analyses. Collectively, we showed that alcohol induced arterial vessel dilation was via eNOS mediated NO generation in ECs, which rapidly diffused into neighboring SMCs and caused MLC dephosphorylation through interplay of myosin light chain kinase and myosin phosphatase activities.

4.2 Background

Low-to-moderate consumption of alcohol is known to exert protective effect towards biological vascular system. Intriguingly, consistent epidemiologic evidence has pointed to an inversely association between moderate alcohol consumption and vascular disease [86, 87, 92]. For example, human studies revealed a 20 – 40 % reduction of cardiovascular disease among drinkers of alcoholic beverages compared with non-drinkers [93]. However, the underlying mechanism of such effect is still under debate.

Some researchers claimed that beverage choice among wine, beer and liquor may bear more relevance and they supported a preferential red wine protective effect that partly attributes to the polyphenolic antioxidant content [94]. This hypothesis was initiated by a report known as the 'French Paradox' that describes the low vascular disease and mortality ratio of the French population despite their high dietary intake of saturated fats, a phenomenon accredited to consumption of red wine due to its active composites, including resveratrol and other polyphenolic agents [95-97]. To support this point of view, several animal studies have focused on polyphenol vascular effects and revealed that wine polyphenols showed antioxidant, anti-inflammatory, hypotensive and anti-platelet aggregation actions [98-101]. In a human study, researchers showed that intaking of dealcoholized red wine at 1-week intervals significantly increased plasma antioxidants, indicating the strong antioxidant potential of wine polyphenols [102].

On the contrary, other studies showed that equal effects of alcohol beverage were observed on vascular disease risk and the content of ethanol and its subsequent metabolites acted as active protective agents [103]. For example, alcohol is known to

elicit nitic oxide (NO) generation in vivo through vascular endothelial function [74]. Researchers found that low dose alcohol improved vascular endothelial function through increasing endothelial nitric oxide synthase (eNOS) expression and nitric oxide (NO) production [74]. Loading low dose alcohol to certain cell types (e.g., human umbilical vein endothelial cells, bovine aortic endothelial cells) promoted NO production, eNOS protein expression [64, 104, 105] and corresponding mRNAs expression [65]. Similar phenomenon was observed in animal studies in which low dose ethanol consumption in rats increased nitric oxide production and eNOS expression in the aortic vascular wall [106]. Taken that NO can serve as a signaling molecule that regulates vascular dilative activity, studies have shown that low dose alcohol exertes a protective effect towards vasculatures through NO mediated vessels dilation. In vivo, animal studies have shown that acute low dose EtOH increases release of NO, augments endothelium-mediated vasodilatation [106-108] and decreases mean blood pressure [106]. In a human multiethnic study, drinkers (between 1 drink/month and 2 drinks/day) were more likely to have a higher flow-mediated dilation (FMD) than non-drinkers and those who drank >2 drinks/day, independently of the type of alcoholic beverage consumed [109].

In a previous study [62], we showed that low dose alcohol-elicited NO production promoted large size brain waste metabolites clearance by enhancing interaction of vascular endothelial cells (EC) and smooth muscle cells (SMC). But the mechanism underlying ECs-SMCs interactive cross-talk was not yet fully understood yet. Here, we investigated the idea that alcohol-elicited NO from ECs can immediately diffuse into neighboring SMCs, subsequently cause relaxation of myosin light chain (MLC) in SMC, and ultimately induce vasodilation. The rationale is that the contractility of smooth

muscle cell is controlled by a cellular component known as myosin light chain (MLC) and NO has been shown to actively engage in regulation of MLC regulatory subunits [110].

4.3 Results

In this chapter, we examined the idea that low dose alcohol mediated arterial vessel dilation was done through interaction of vascular ECs and SMCs whereby NO generated from ECs rapidly diffused into neighboring SMCs and subsequently caused SMC relaxation. To verify this idea, we firstly determined the response of ECs to low dose alcohol by examining NO generation and enzyme expression. Then we investigated how SMCs react to NO focusing on myosin light chain phosphorylation level and corresponding enzymes activities. The underlying mechanism of alcohol mediated arterial vessel dilation was supported by these findings.

4.3.1 Alcohol below 20 mM Has no Toxic Effect on ECs and SMCs

We first focused on the toxicity effect of different alcohol concentration on the co-culture system of two cell types: ECs and SMCs. The two cell types were mixed at 1:1 ratio and directly in contact with each other to mimic in vivo vascular structures. Corresponding cellular protein markers (vWF for ECs and SMA for SMCs) were evaluated to verify the co-existence (**Figure 4.1A and B**). A Serial concentration of alcohol was used to determine the toxicity as shown in the graph. Noted that the highest dose I used was 20 mM, which is approximately equivalent to the legalized blood alcohol level (~0.08%). I found that after incubating with alcohol at given concentrations for 2 hrs, no significant cell survival difference was observed among alcohol treatments compared with control (**Figure 4.1C**), indicating that alcohol concentration less than 20

mM have no toxic effect on ECs and SMCs, which is consistent with previous report [72].

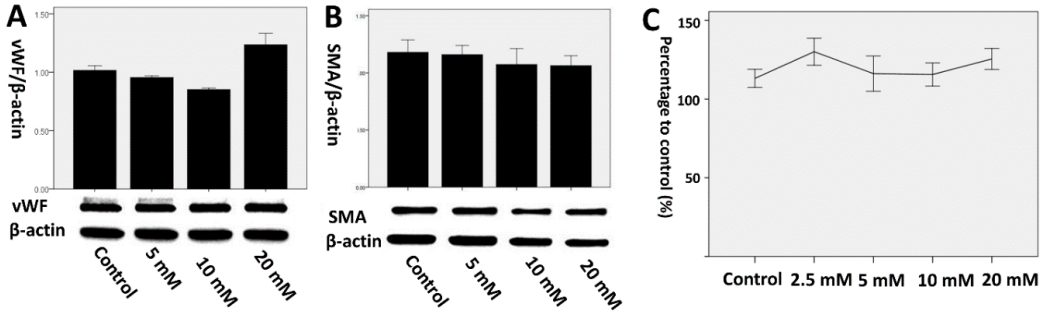

Figure 4.1 Cell toxicity evaluation. Various doses of alcohol were loaded to endothelial – smooth muscle cells co-culture system. Two hours were given before proceeding to MTT assay. [A and B]. Immunoreactive bands of vWF (endothelial cell markers), SMA (smooth muscle cell markers) and β-actin, and quantitative corresponding protein content in different experimental groups. Results were expressed as the ratio of protein of interest to that of actin bands and presented as mean values (± SEM). [C]. Cell toxicity assay by MTT showed viability with variable concentrations of alcohol represented by plot. Results were expressed as the ratio of OD value of each experimental condition to that of control and presented as mean values (± SEM). *Statistically significant ($p < 0.05$) compared with controls. Three replicates were done for each sample from at least N=3 cultures.

4.3.2 Alcohol Promotes NO Release from ECs through eNOS not iNOS

Next, we proceeded to investigate the response of ECs to alcohol (10 mM). The optimal alcohol concentration was determined from a dose-dependent study. We analyzed the real-time NO production in ECs by Free Radical Analyzer using a micro-sensor detector and found that alcohol exposure significantly elevated release of NO in ECs compared with baseline (**Figure 4.2A and B**). Moreover, we observed a time-dependent increase of NO production by checking different time intervals. This can be justified by the fact

that NO generation depends on corresponding enzymes induction.

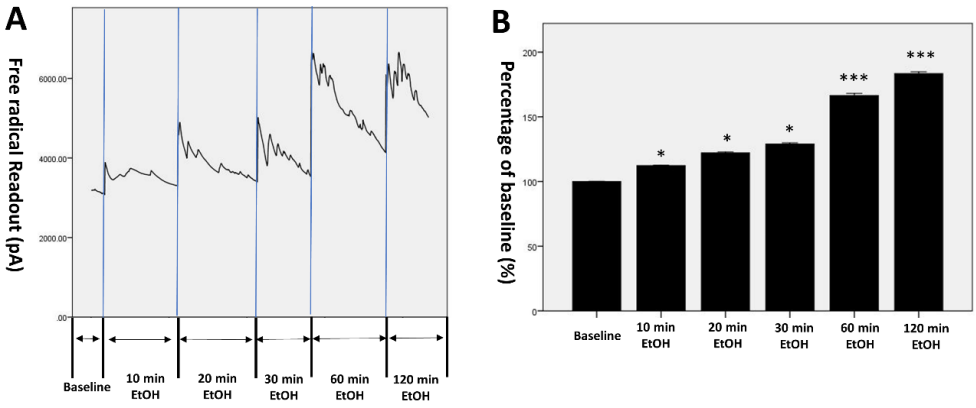

Figure 4.2 Real-time NO production in cultured endothelial cells in the presence of 10 mM EtOH. 50 µM L-NAME pre-treated tissue for 30 min as baseline. Medium containing 10 mM EtOH was supplied subsequently. [A]. Functional output from free radical analyzer. Graph denotes the current signal (pA) change (proportional to NO concentration) captured by the NO sensor during each data collection interval, which was marked by blue vertical lines. [B]. Bar graph was plotted as the ratio of signal readout of each acquisition interval to that of baseline and presented as mean values (± SEM). Statistically significant (*$p < 0.05$, ***$p<0.001$) compared with controls. Three replicates were done for each sample from at least N=3 cultures.

We then evaluated the induction of NO generation enzymes, eNOS and iNOS to correlate with NO release. Interestingly, immunostaining revealed a huge increase of eNOS induced by alcohol and not surprisingly the effect was neutralized by inhibitor (L-NAME) (**Figure 4.3A**), which was further validated by significant elevation of eNOS levels by ethanol compared with control ($p<0.05$), as determined by Western blot analyses (**Figure 4.3B**). On the contrary, no significant change of iNOS was found in

alcohol group compared with control by both immunostaining and western blot (**Figure 4.4A and B**), indicating that NO release can be mainly accredited to eNOS but not iNOS. This can be explained by the idea that elevation of physiological NO levels in endothelial cells through eNOS augments vascular function whereas iNOS mediates massive NO production associated with free radical generation, which exerts detrimental effect towards surrounding tissues [72, 111]. Further examination of nitrosative stress marker, 3-nitrotyrosine (3-NT) expression across groups showed no significant difference (**Figure 4.5A and B**), supporting this justification.

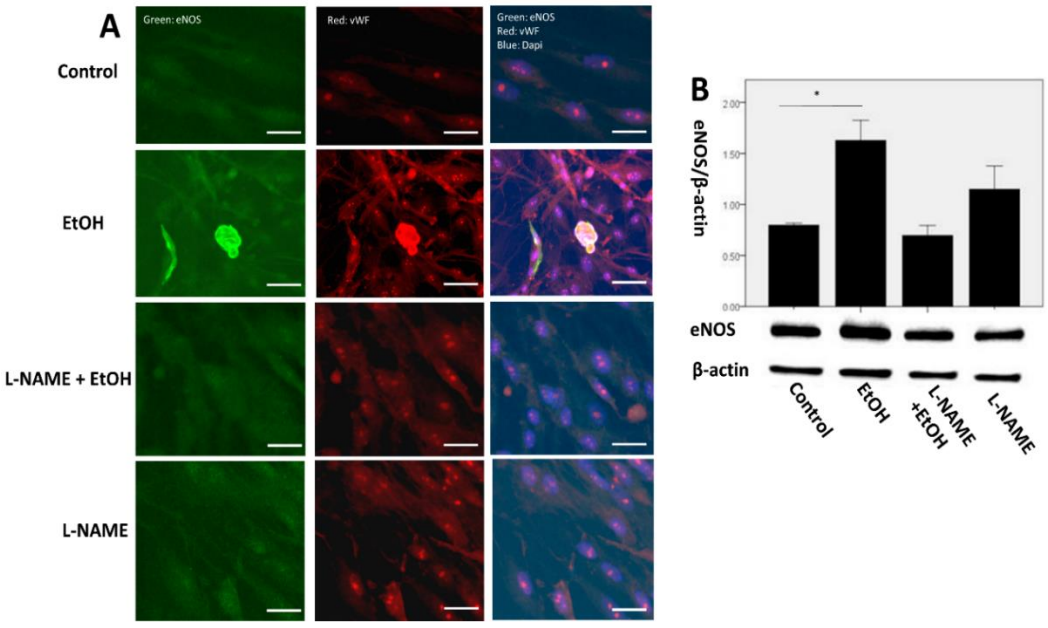

Figure 4.3 EtOH induces eNOS protein expression in endothelial cells. [A]. Immunostaining of eNOS (green) and vWF (red) protein in control, EtOH (10 mM), L-NAME + EtOH and L-NAME. eNOS and vWF were used as primary antibodies (information in Table 2.1). Alexa Fluor 488/594 were used as corresponding secondary antibodies. Data representats at least N=3 cultures per each group. Scale bar: 30 μm. [B]. Immunoreactive bands of eNOS and β-actin, and quantitative corresponding protein content among experimental groups. Results were expressed as the ratio of protein of interest to that of actin bands and presented as mean values (± SEM). *Statistically significant ($p < 0.05$) compared with controls. Three replicates were done for each

sample from at least N=3 cultures.

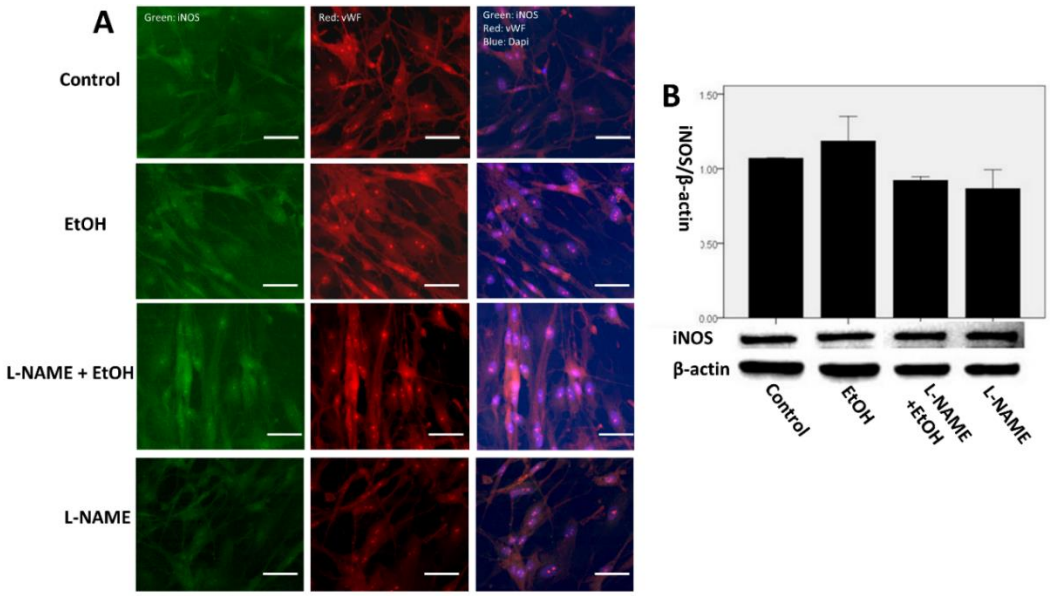

Figure 4.4 No difference of iNOS protein expression in endothelial cells under different experimental conditions. [A]. Immunostaining of iNOS (green) and vWF (red) protein in control, EtOH (10 mM), L-NAME + EtOH and L-NAME. iNOS and vWF were used as primary antibodies (information in Table 2.1). Alexa Fluor 488/594 were used as corresponding secondary antibodies. Data represents at least N=3 cultures per each group. Scale bar: 30 μm. [B]. Immunoreactive bands of iNOS and β-actin, and quantitative corresponding protein content among experimental groups. Results were expressed as the ratio of protein of interest to that of actin bands and presented as mean values (± SEM). No statistically significant ($p < 0.05$) difference compared with controls. Three replicates were done for each sample from at least N=3 cultures.

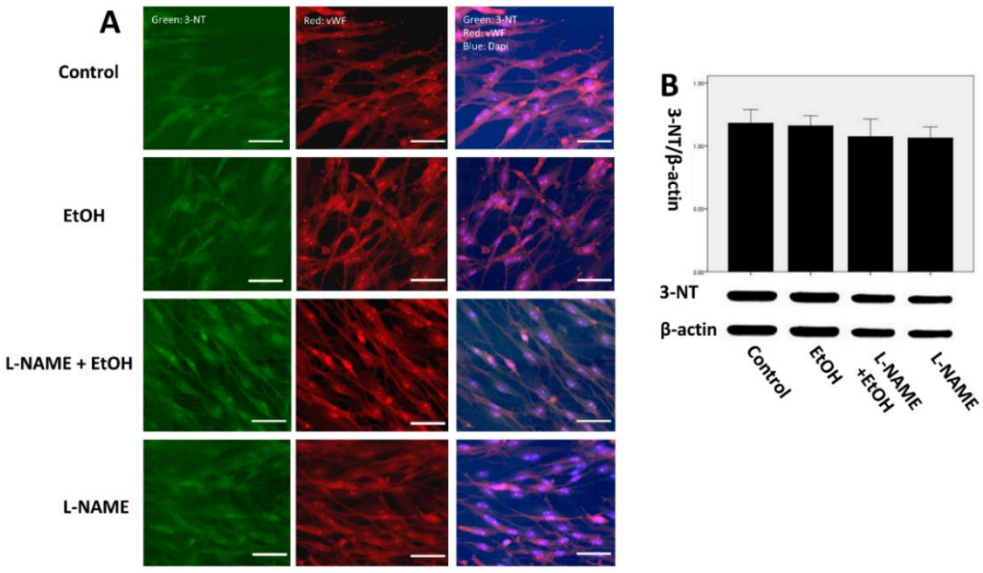

Figure 4.5 No difference of nitrosative marker, 3-nitrotyrosine expression in endothelial cells under different experimental conditions. [A]. Immunostaining of 3-NT (green) and vWF (red) protein in control, EtOH (10 mM), L-NAME + EtOH and L-NAME. 3-NT and vWF were used as primary antibodies (information in Table 2.1). Alexa Fluor 488/594 were used as corresponding secondary antibodies. Data was representation of at least N=3 cultures per each group. Scale bar: 30 μm. [B]. Immunoreactive bands of 3-NT and β-actin, and quantitative corresponding protein content among experimental groups. Results were expressed as the ratio of protein of interest to that of actin bands and presented as mean values (± SEM). No statistically significant ($p < 0.05$) difference compared with controls. Three replicates were done for each sample from at least N=3 cultures.

4.3.3 NO by Donor SNAP (15 μM) Not Induces Free Radical Damage in SMCs

To precisely investigate the effect of NO on SMCs, we also exposed cells directly to NO through the NO donor, SNAP (S-nitroso-N-acetylpenicillamine). NO is a highly active molecule that in the presence of O2, can react with O2− to form peroxynitrite (ONOO−), a potent oxidizing agent that can lead to cytotoxicity by nitrating and hydroxylating aromatic compounds, including guanosine and tyrosine (nitrotyrosine) [74, 112]. To avoid such deleterious effects, we tried to limit the amount of NO using but still adequately for experimental purposes. Therefore, we conducted a dose-dependent assay

(10 – 100 µM) and found that concentrations less than 20 µM did not induce noticeable nitrosative stress on SMCs, which agrees with a previous paper [72]. Among all concentrations, we found that 15 µM yielded best results for NO supply (**Figure 4.6A and B**) without significant free radicals damage (**Figure 4.7A and B**) and thus, was determined as the working dose.

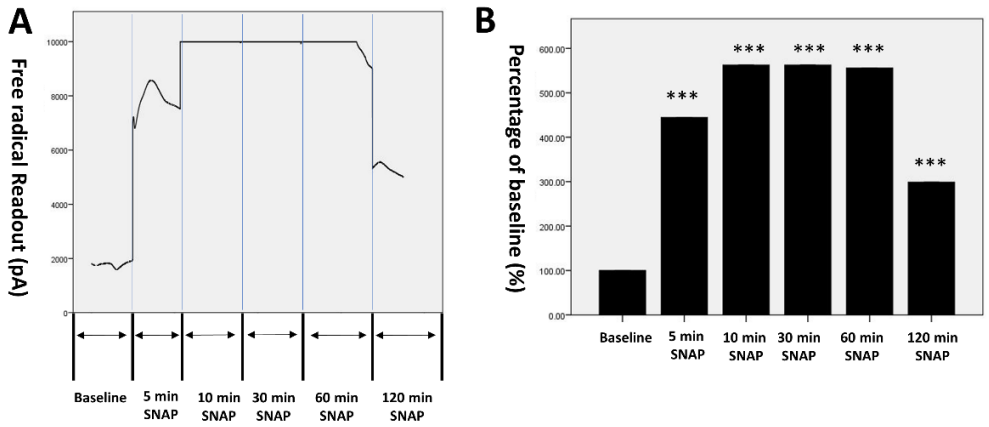

Figure 4.6 Real-time NO level in cultured SMCs in the presence of 15 µM SNAP. Cells were pre-treated with 50 µM L-NAME for 30 min as baseline. Medium containing 15 µM SNAP was supplied subsequently. [A]. Functional output from free radical analyzer. Graph denotes the current signal (pA) change (proportional to NO concentration) captured by the NO sensor during each data collection interval, which was marked by blue vertical lines. [B]. Bar graph was plotted as the ratio of signal readout of each acquisition interval to that of baseline and presented as mean values (± SEM). Statistically significant (*$p < 0.05$, ***$p<0.001$) compared with controls. Three replicates were done for each sample from at least N=3 cultures.

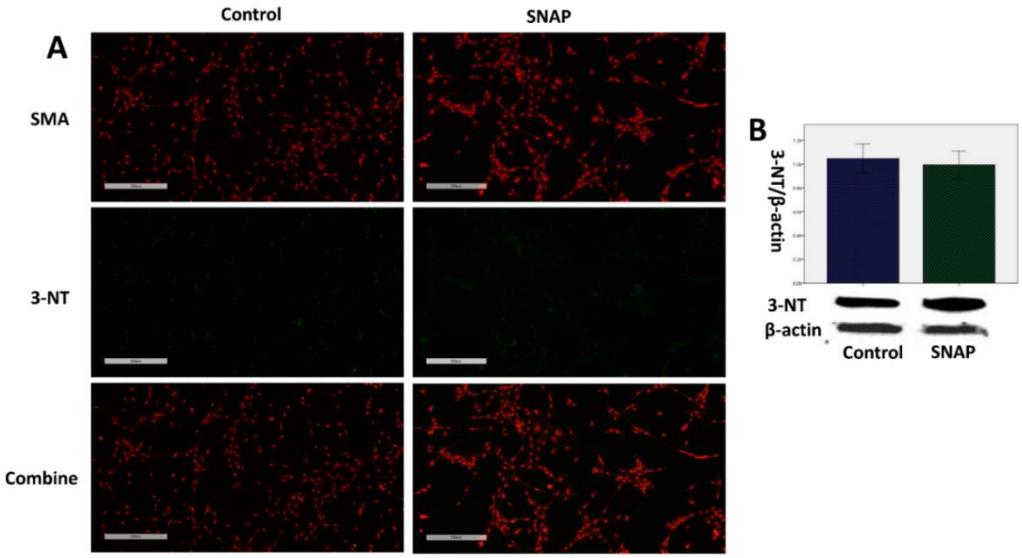

Figure 4.7 Nitrosative marker, 3-nitrotyrosine expression in cultured SMCs in the presence of 15 µM SNAP. [A]. Immunostaining of 3-NT (green) and SMA (red) protein in control and SNAP (15 µM SNAP). 3-NT and SMA were used as primary antibodies (information in Table 2.1). Alexa Fluor 488/594 were used as corresponding secondary antibodies. Data represents at least N=3 cultures per each group. Scale bar: 300 µm. [B]. Immunoreactive bands of 3-NT and β-actin, and quantitative corresponding protein content among experimental groups. Results were expressed as the ratio of protein of interest to that of actin bands and presented as mean values (± SEM). Statistically significant ($p < 0.05$) compared with controls showed no difference. Three replicates were done for each sample from at least N=3 cultures.

4.3.4 Alcohol Induced Smooth Muscle Relaxation Was through Myosin Light Chain Dephosphorylation

Next, we evaluated the mechanism of alcohol-elicited-NO from ECs induced smooth muscle relaxation by checking phosphorylation levels of myosin light chain (MLC). The phosphorylation of the 20-kDa myosin regulatory light chains (MLC) is the primary determinant of cross-bridge attachment and cycling during contraction and relaxation in smooth muscle [113]. In brief, phosphorylation of MLC leads to SMC contraction while dephosphorylation yields relaxation. Using specific antibodies that can detect

phosphorylation of MLC at Ser19/20 in smooth muscle cells, we found that compared with control, alcohol-induced-NO from ECs significantly diminished phosphorylation levels of MLC at Ser19/20 in SMCs and, in parallel quantitative assay western blot validated this finding (**Figure 4.8A and B**). The positive control from NO (SNAP) supported this finding. Since dephosphorylation of MLC suggests relaxation of SMC, the data indicates that alcohol-induced-NO-caused SMC relaxation was through dephosphorylation of MLC at Ser19/20.

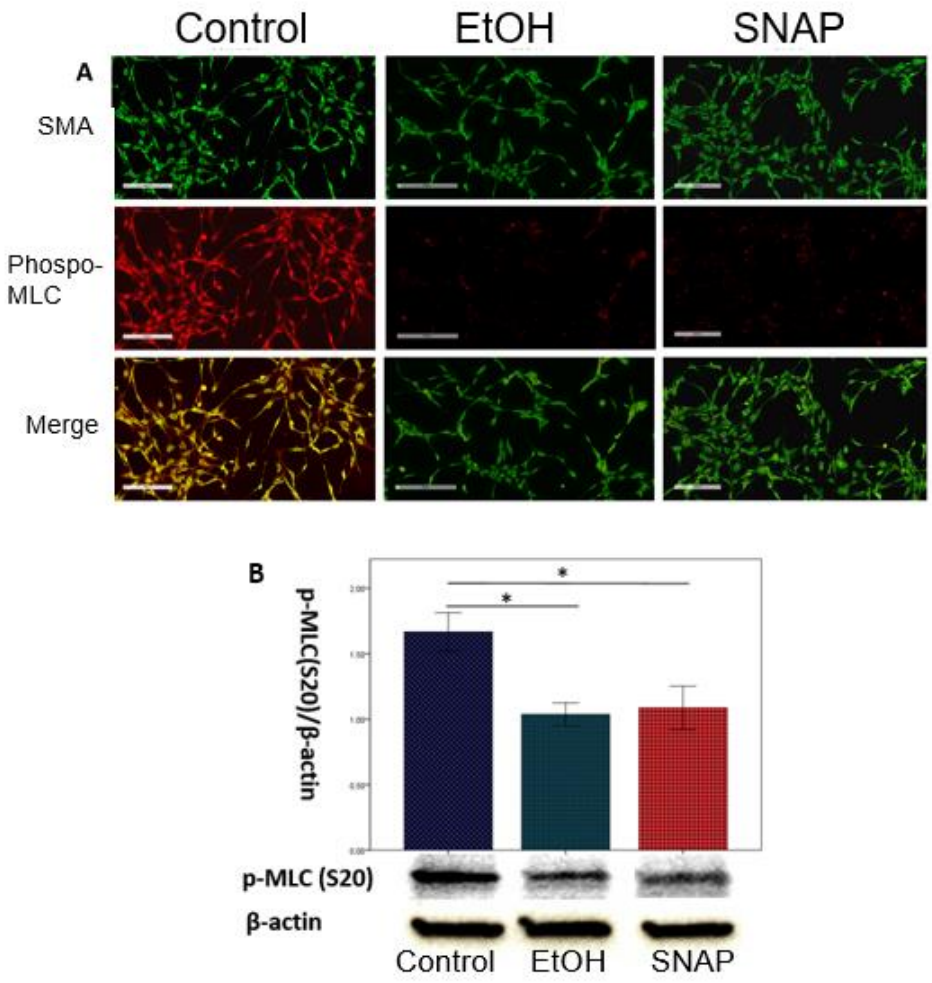

Figure 4.8 Phospho-myosin light chain (Ser19/20) level in cultured ECs-SMCs in the presence of 10 mM EtOH and15 µM SNAP. [A and B]. Immunostaining of SMA (green) and phosphor-MLC protein in control, low dose alcohol and SNAP (15 µM; NO donor as positive control). SMA and smooth muscle specific phosphor-MLC(Ser19/20) were used as primary antibodies (information in Table 2.1). Alexa Fluor 488/594 were used as corresponding secondary antibodies. Data represents at least N=3 cultures per each group. Scale bar: 200 µm. [B]. Immunoreactive bands of phosphor-MLC (Ser20) and β-actin, and quantitative corresponding protein content among experimental groups. Results were expressed as the ratio of protein of interest to that of actin bands and presented as mean values (± SEM). *Statistically significant ($p < 0.05$) compared with controls. Three replicates were done for each sample from at least N=3 cultures.

4.3.5 Alcohol Induced MLC Dephosphorylation Was via Myosin Phosphatase Activities

Further, we proceeded to investigate the underlying mechanism of alcohol-elicited-NO mediated MLC dephosphorylation in the co-culture system. MLC phosphorylation level was determined by the balance of the Ca2+ dependent myosin light chain kinase (MLCK) and myosin light chain phosphatase (MLCP) activities. When MLCK was activated by Ca2+ -calmodulin complex, it underwent posttranslational change, phosphorylation to become active [114]. Whereas its counterpart, MLCP activity was similarly regulated by phosphorylation mediated events but in a more complex way. According to recent publications, phosphorylation of the MLCP regulation subunit, myosin phosphatase target subunit 1 (MYPT1) at Ser618/668/692/695 residues can increase MLCP activities while at Thr696/853 residues, led to inhibitory effects [110, 115, 116]. Thus, by employing antibodies that target specific phosphorylation residues pertinent to each protein, we examined the activities of MLCK and MLCP in SMCs under control, alcohol and SNAP (positive control) treatment. Interestingly, we found that the phosphorylation level of MYPT1 at Ser618/668 in SMCs was significantly increased by alcohol and NO (positive control) through immunostaining and western blot (**Figure 4.9A and B**) assays, indicating that MLCP activities in SMCs were up-regulated by alcohol-induced-NO from ECs. Meanwhile, the level of phospho-MLCK at Ser 1760 was decreased under alcohol and NO treatment compared with control (**Figure 4.9C**), suggesting a reduction of MLCK activities by alcohol-induced-NO from ECs. Postitive control validated the role of NO in this process.

Collectively, the information that this data conveys is that alcohol-elicited-NO

release from ECs is strongly correlated with MLCP/MLCK activities in SMCs: NO led to elevation of MLCP activity but inhibition MLCK. When the entire system favored more MLCP, MLC turned to be dephosphorylated and SMC manifested relaxation.

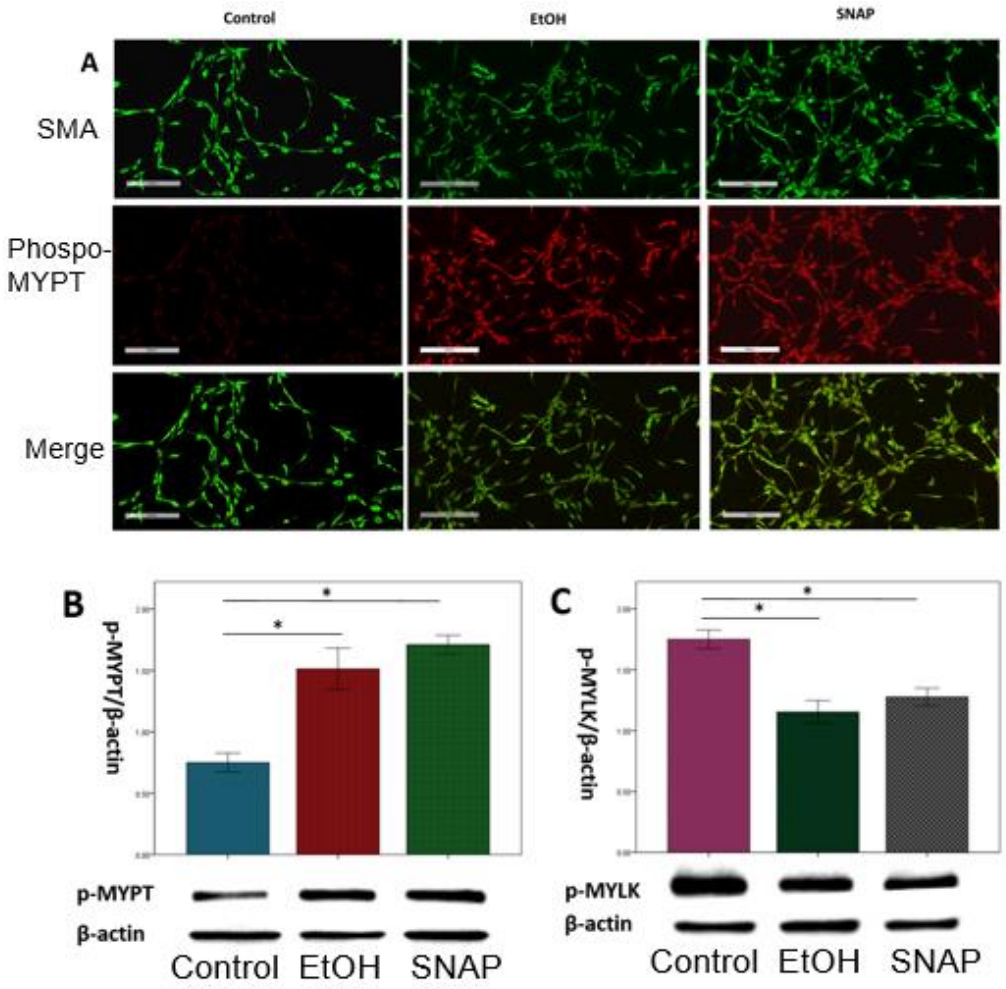

Figure 4.9 Phospho-MYPT1/2 (Ser618/688) and phosphor-MYLK (Ser1760) level in cultured ECs-SMCs in the presence of 10 mM EtOH and 15 μM SNAP. [A]. Immunostaining of SMA (green) and phospho-MYPT1/2 (Ser618/688) (red) protein in control, EtOH and SNAP (15 μM SNAP). SMA and phospho-MYPT1/2 (Ser618/688) were used as primary antibodies (information in Table 2.1). Alexa Fluor 488/594 were used as corresponding secondary antibodies. Data was representation of at least N=3 cultures per each group. Scale bar: 200 μm. [B and C]. Immunoreactive bands of [B]: phospho-MYPT1/2 (Ser618/688), [C]: phosphor-MYLK (Ser1760) and β-actin, and quantitative corresponding protein content among experimental groups. Results were

expressed as the ratio of protein of interest to that of actin bands and presented as mean values (± SEM). *Statistically significant ($p < 0.05$) compared with controls. Three replicates were done for each sample from at least N=3 cultures.

4.4 Discussion

In the present study, we discuss the finding that alcohol, especially at low dose ingestion, can promote arterial vessel dilation through enhancing interaction of vascular endothelial cells and smooth muscle cells. Firstly, we evaluated the response of ECs when exposed to low dose alcohol (10 mM) with focus on nitric oxide (NO) generation and corresponding enzymes expression. We showed that alcohol, at given doses, can increase NO releasing, which is mediated by elevation of eNOS expression instead of iNOS. This phenomenon was consistent with previous observation in animal studies [62] and can be justified by the difference between those two isomers in terms of NO generation: eNOS augments physiological NO levels in endothelial cells that regulate normal vascular function while iNOS is typically associated with free radical generation like peroxynitrite, inducing surrounding tissue damage [72, 111]. Further evidence of no over-expression of the nitrosative stress marker among groups (**Figures 4.5A and B**) validates this explanation.

We then investigated the underlying mechanism of alcohol-elicited NO-mediated relaxation of SMCs. Researches have shown that NO, known as an endothelium-mediated vessel dilator, can regulate neighboring smooth muscle contractility [106-108]. Smooth muscle cells, unlike skeletal and cardiac muscles, relied on phosphorylation of the 20 KDa regulatory myosin light chain (MLC) at the Ser19 residue to exert contractile activities [110]. The regulation of phosphorylation extent

was determined by the balance of the activities of two protein enzymes: myosin light chain kinase (MLCK) and myosin light chain phosphatase (MLCP) [115]. We showed that by treating cultured ECs-SMCs with alcohol and NO (positive control), the phosphorylation level of MLC was significantly diminished compared with control and that MLCP activities line up with MLC dephosphorylation levels whereas MLCK activities are adversely correlated (**Figures 4.8 and 4.9**), indicating that alcohol-elicited NO-caused SMCs relaxation was regulated by MLCP/MLCK mediated MLC phosphorylation.

NO can activate soluble guanylate cyclase, thus augmenting cGMP. Elevated cGMP presumably activates cGMP-dependent protein kinase (PKG) and hence induces a variety of phosphorylation events. For instance, the phosphorylation of several intracellular mechanisms by PKG results in a reduction in myoplasmic calcium [114, 117], which reduces engagement of calcium with calmodulin. Since formation of the Calcium-Calmodulin complex is essential for MLCK activation, a reduction of proper engagement will inevitably lead to decreasing MLCK activities and therefore dephosphorylate MLC. Also, cGMP-PKG was found to directly involve in MLCP regulation in several studies. For example, phosphorylation of Ser-695 at myosin phosphatase target subunit 1 (MYPT1) by cGMP mediated PKG was found to activate MLCP [110] and inhibition of NO mediated cGMP-PKG by NOS inhibitor (L-NAME) showed a reduction of phosphorylation at S695/S668, which correlated with decreasing MLCP activities [116].

Intriguingly, previously we reported that a very low level of 5.0 mM ethanol, equivalent of 0.02% blood alcohol level, can enhance the dynamic movement pattern of

large size waste metabolites towards the perivascular-perivenous space and the underling mechanism was that alcohol-elicited eNOS specific NO production regulated the cerebral arterial vessel dilation through endothelial-smooth muscle cell reactive interactions [62]. The current research further addressed the mechanism we proposed previously: alcohol induced arterial vessel dilation is via eNOS mediated NO generation in ECs, which rapidly diffuse into neighboring SMCs and cause MLC dephosphorylation through an interplay of myosin light chain kinase and myosin phosphatase activity (**Figure 4.10)**

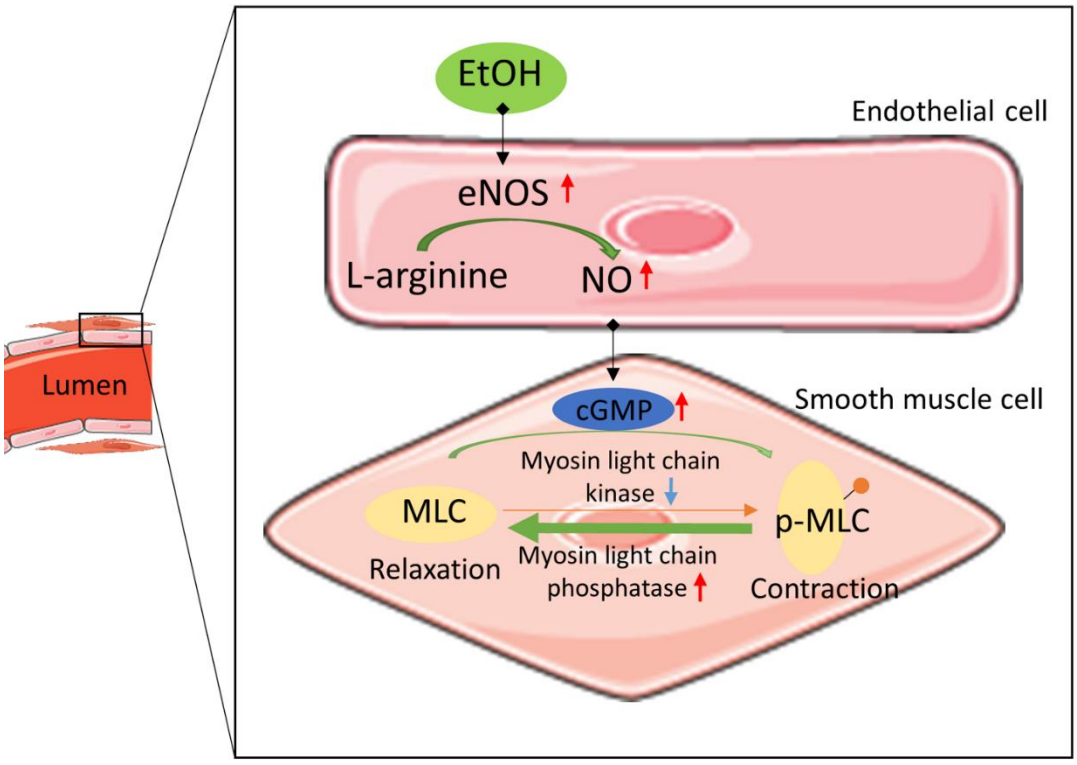

Figure 4.10 Schematic representation of alcohol mediated endothelial cells and smooth muscle cells interaction. Alcohol can elicit eNOS expression and NO production in endothelial cells. NO from endothelial cells rapidly diffuses into surrounding SMCs, causing elevation of cGMP. cGMP mediated PKG pathway leads to myosin light chain relax (de-phosphorylation) through: 1). up-regulation of myosin light chain phosphatase

activities; 2) down-regulation of myosin light chain kinase activities.

CHAPTER 5

CONTRAST EFFECTS OF LOW/ACUTE AND MODERATE/CHRONIC ALCOHOL ON CNS WASTE METABOLITES CLEARANCE

In previous chapters, we have shown that low dose alcohol promotes perivascular clearance of waste metabolites in the brain, which is regulated by dilative reactivity of arterial smooth muscle cells and endothelial cells via the signaling molecule, NO. These findings clearly indicate the importance of blood-brain barrier (BBB) transvascular clearance of large size metabolites in the CNS, where the lymphatic clearance system is absent. In this chapter, we examined the contrast effects of acute low dose and chronic moderate alcohol intake on perivascular clearance of waste metabolites in the brain.

5.1 Summary

To evaluate the contrast effects of acute low dose and chronic moderate alcohol intake on waste metabolites clearance in the brain, we injected a large size fluorescent dye representing waste metabolites like A-β protein into the cerebrospinal fluid (CSF). Then, we examined the bio-distribution of tracer towards perivascular space in different brain regions by whole brain tissue section scanning. We found that the underlying molecular and cellular mechanisms that drive the increase or decrease movement of tracer to perivascular space by acute/chronic alcohol exposure correlated to BBB integrity and arterial vessel reactivity. Accordingly, the contrast effects of alcohol appear to be regulated by the switch mechanisms of endothelial specific nitric oxide synthase (eNOS) activation by low dose and inducible NOS (iNOS) by moderately high alcohol exposure in chronic conditions. We validated these observations by qualitative and quantitative

data. As such, my conlusion is that low dose alcohol promotes the diffusive movement of waste metabolites to perivascular clearance through eNOS-derived NO-regulated arterial endothelial-smooth muscle cells dilative reactivity without affecting the integrity of BBB. Whereas, continuous induction of iNOS in chronic alcohol exposure causes oxidative damage of the arterial endothelial-smooth muscle layers that led to BBB dysfunction, reducing dilative reactivity, and decreasing movement of waste metabolites from interstitial space/CSF to the perivascular-perivenous drainage path.

5.2 Background

Effect of alcohol consumption and metabolism on vascular tissues yields biphasic consequences that depend on drinking patterns: low alcohol intake leads to beneficial effects while high amount of ingestion delivers detrimental results. Researchers found that low dose alcohol improved vascular endothelial function through increased endothelial nitric oxide synthase (eNOS) expression and nitric oxide (NO) production [74]. For example, loading low dose alcohol to various cell types (e.g., human umbilical vein endothelial cells, bovine aortic endothelial cells) elicited NO production, eNOS protein expression [64, 104, 105] and corresponding mRNA expression [65]. A similar phenomenon was observed in animal studies: low dose ethanol consumption in rats increased nitric oxide production and eNOS expression in the aortic vascular wall [106]. Given that NO is known as an endothelium-mediated vessel dilator that regulates vascular contractility, investigators found that low dose alcohol can exert a protective effect towards vasculatures due to NO mediated vessels dilation. In vivo animal studies showed that acute low dose EtOH intake increased release of NO, augmented

endothelium-mediated vasodilatation [106-108] and decreased mean blood pressure [106]. In a human multiethnic study, drinkers (between 1 drink/month and 2 drinks/day) were more likely to have a higher flow-mediated dilation (FMD) than non-drinkers and those who drank >2 drinks/day, independent of the type of alcoholic beverage consumed [109], indicating beneficial vascular effects gained from low dose alcohol.

On the contrary, moderate/chronic alcohol consumption assumed an opposite effect. For example, in a thoracic aorta isolated from chronic ethanol-fed rats, eNOS expression and NO levels were down-regulated, leading to diminished vasorelaxation [118]. In other studies, researchers observed that dilatation of rat basilar arteries or pial arterioles was less in alcohol fed rats compared with non-alcohol-fed rats; while superoxide dismutase and NAD(P)H oxidase inhibitor apocynin were able to ameliorate the loss of function, suggesting that ROS induced by chronic alcohol may lead to impaired eNOS-mediated vasodilation [119, 120]. In addition to what was described above, alcohol-induced oxidative/nitrosative stress was known to cause vascular damage. Alcohol-induced tissue injury was mediated via metabolism of ethanol by alcohol dehydrogenase and cytochrome P450 2E1 that produced acetaldehyde and reactive oxygen species/reactive nitrogen species (ROS/RNS) [111, 121]. Thus, tissue injury was supposed to occur in cell types that expressed ethanol metabolizing or radical generating enzymes, like inducible nitric oxide synthase (iNOS) [72, 122]. For example, it is widely known that the blood-brain barrier (brain microvessels) is vulnerable to alcohol-induced free radical damage. Haorah et al. revealed that alcohol metabolizing enzymes have been shown to localize in the brain microvessel endothelium [111, 123, 124] and metabolism of alcohol in brain endothelium generates oxidative and nitrosative

products that cause free radical damage to brain microvessels including the BBB [72, 111].

In previous findings [62], we described that alcohol promotes waste clearance in the CNS via brain vascular reactivity. It is known that waste metabolites can be drained out of the brain through various clearance systems, including enzymatic degradation, cellular uptake, transport across the blood–brain barrier (BBB), and interstitial fluid (ISF)/cerebrospinal fluid (CSF) absorption into the circulatory and lymphatic systems. Out of those clearance routes, BBB trans-vascular clearance from brain to blood provides functionally a major pathway for elimination of different waste metabolic products from brain and accounts for > 80% of clearance of amyloid-beta physiological conditions [59-61, 66]. However, large size waste metabolites like tauopathy, prion-like proteinopathies, cerebral amyloid angiopathy, and Aβ proteins are seen accumulated around the perivascular space in brain tissue from neurological diseases [1, 2, 48], suggesting that large size waste metabolites are not cleared by CSF, glymphatic, or meningeal lymphatic systems. We found that dynamic movement of large size waste metabolites from interstitial space and subarachnoid towards perivascular space is enhanced when interaction of brain vascular endothelial cells (ECs) and smooth muscle cells (SMCs) is prompted [62]. Interestingly, low dose alcohol (5 mM) can facilitate this process through up-regulation of NO since alcohol especially low dose was known to increase eNOS expression [64, 65, 74, 104]. We showed that clearance of large size waste metabolites was increased by low dose alcohol while NOS inhibitor neutralized this effect, indicating the underlying mechanism of alcohol-elicited eNOS activation and NO production [62].

However, the pendulum shifts when it comes to chronic alcohol intake. Epidemiological population-based cohort studies revealed that heavy alcohol use in chronic condition was associated with development dementia and progression of Alzheimer's disease and cerebral amyloid angiopathy [5, 77, 80, 81, 83, 84, 125, 126], the hallmark of these neurological diseases happen to be the deposition of waste metabolites like Aβ protein, or protein prion-like proteinopathies around the perivascular space [1, 2, 48]. These cohort studies also unequivocally noted the protective effects of low dose alcohol use against the progression of dementia and AD/CAA, with unknown mechanisms. Thus, it is apparent that the beneficial or destructive effects of alcohol depend on the duration and concentration used.

In conclusion, we hypothesize the contrast effect of low dose and chronic/moderate alcohol on brain waste metabolites clearance: low dose facilitates clearance by acting as a vasodilator through activating eNOS and enhancing brain vascular endothelial cells (ECs)-smooth muscle cells (SMCs) interaction, while chronic/moderate condition hampers the clearance due to iNOS/free radicals mediated impairment of ECs-SMCs interaction. The rationale is that activation of eNOS by low concentrations of ethanol elevates physiological NO levels and augments ECs-SMCs interactive reactivity whereas chronic/moderate causes free radical damage to microvessels and leads to BBB dysfunction, reducing vascular dilative reactivities and decreasing perivascular clearance.

5.3 Results

We investigated the contrast effects of low/acute and moderate/chronic alcohol on brain

waste metabolites clearance in this study. Here, we first focused on bio-distribution of 2000 kDa fluorescent dye representing large size waste metabolites in three different experimental conditions: control, low/acute alcohol (5 mM) and moderate/chronic alcohol. Low dose was found to promote dynamic movement of tracers along the perivascular space (PVS) while moderate/chronic showed an opposite effect. Further examination revealed that low dose alcohol elicited eNOS activation and improved ECs-SMCs interactive reactivity whereas chronic/moderate alcohol induced iNOS expression that led to tissue damage at brain vasculatures including endothelium, smooth muscle cells and blood-brain barrier (BBB) tight junction proteins, indicating that chronic/moderate alcohol decreased vascular dilative reactivities and exerted detrimental effect towards brain PVS clearance.

5.3.1 Animal Model of Liquid-Diet Alcohol Intake

To determine success of the pair-feeding procedure, we weighed and recorded rats' weight on a weekly basis. At the time of sacrifice (12 weeks), the average body weight was 428 ± 11.1 for pair-fed control and 451 ± 10.2 for pair-fed alcohol. This was consistent with previous reports that pair-fed alcohol revealed overall higher body weight distribution at the end of the feeding cycle compared with control [16]. Weekly body weight record showed that at early feeding cycles, alcohol feeding showed lower weight-gaining compared with control. That was because by nature animals required enough time to acclimate to the taste of alcohol. Once accustomed (after week 4), weight-gaining rate of alcohol rats exceeded that of control and weight of alcohol rats started to approach and preceded control (after week 6).

Table 5.1 Pair-feeding Rat Body Weight and Blood Alcohol Concentration Statistics before Sacrifice (12 weeks after feeding)

	Body weight (g) after 12 weeks pair-fed (n=15 pairs)					Blood alcohol concentration (mM)	
Group	**Mean**	**Standard Deviation**	**Median**	**Min**	**Max**	**Mean**	**Range**
Control	428	11.1	429	399	449	0.002	0 – 0.005
EtOH	451	10.2	451	437	468	15.6	9.1 – 28.8

Prior to sacrificing, blood alcohol concentrations for all rats was determined to be 9.1 – 28.8 mmol/L in alcohol diet ingested animals (**Table 5.1**), which was consistent with our previous results [127]. The huge variation in blood alcohol levels is common in animal studies due to nocturnal feeding habits of rats and variation in ethanol metabolic and clearance rate.

5.3.2 Injection of FITC-d2000 into C3 Region of CSF Flow under Control, Low Dose Alcohol and Chronic Alcohol Conditions

To evaluate the contrast effects of low/acute and moderate/chronic alcohol on dynamic movement and clearance of large size waste metabolites in the brain, we injected FITC-d2000 (MW: 2000 KD) directly into the CSF flow via cisterna magna. We then evaluated the bio-distribution of tracer in the brain two hours after injection under different experimental conditions. We observed that low/acute alcohol enhanced tracer movement along vasculatures whereas moderate/chronic hampered this process. For example, in the low/acute study, more tracers were found at the perivascular spaces (PVS) compared with control, which was in accordance with previous finding [62].

However, opposite effect revealed under the moderate/chronic treatment. We barely found any tracers at PVS two hours after injection in moderate/chronic condition, suggesting that dynamic movement of tracers was decreased (**Figure 5.1 Top A-I**). This qualitative data was further validated by quantification of arbitrary fluorescence intensity at PVS (**Figure 5.1 Bottom A,** *** $p<0.001$).

In addition, to evaluate the clearance efficiency, we also examined fluorescence intensity in systematic blood plasma collected from the jugular vein 2 hours after injection. Data (**Figure 5.1 Bottom B**) suggested that clearance from inside the brain to circulation was significantly (*** $p<0.001$) decreased in the chronic alcohol group compare with control, which was in parrel with the PVS tracer movement results.

Top:

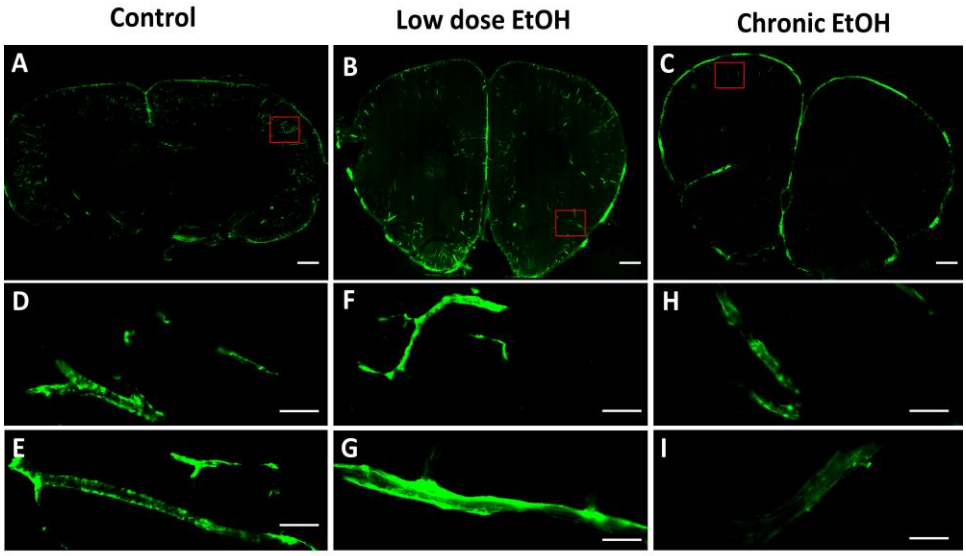

Figure 5.1 Tracer bio-distribution in the rat brain under different experiment conditions. Tracers were injected into the rats brain through cisterna magna and 2 hours were given before sacrificing. Coronary brain slices (45 µm) mounted with Dapi on glass slides were used for imaging. Top: [A, B and C]. Bio-distribution of CSF tracer (FITC-d2000, green) in control, EtOH (low dose alcohol) and chronic alcohol groups. Scale bar: 1 mm. [D-I]: Detail of corresponding boxed areas from A, B and C. Scale bar: 25 µm. Data was representation of at least N=6 animals per each group.

Bottom:

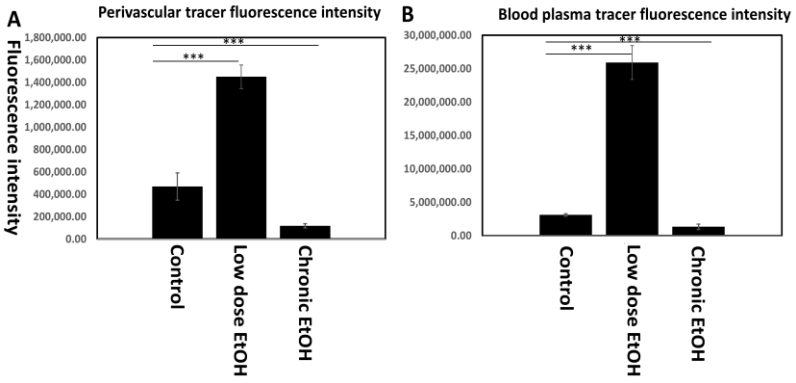

Figure 5.1 Bottom: [A]. Fluorescence intensity quantification of tracer biodistribution at the PVS was calculated as mean fluorescence intensity on each slide (from N=6 animals, 10~15 slices were taken from each animal, +SEM) and presented as bar graphs. Statistically significant (***$p < 0.001$) compared with controls. Three replicates were done for each animal sample from at least N=6 animals. [B]. Blood plasma tracer fluorescence intensity quantification. Samples were from N=6 animal per each group. Statistically significant (***$p < 0.001$) compared with controls.

5.3.3 Contrast Effects of Low Dose and Moderate/Chronic Alcohol on Vascular Smooth Muscles

To find out the reasons why chronic alcohol diminished PVS clearance efficiency, we studied two vascular components: smooth muscles and endothelium. The ratioale was that according to previous findings, PVS clearance was mediated by dilative vascular reactivities, which were regulated by endothelium and smooth muscles interaction.

Firstly, we investigated vascular smooth muscles. Immunostaining of α-SMCs (smooth muscel actin, red) showed increasing expression in the low/acute alcohol group compared with control whereas expression of α-SMCs in the chronic condition was decreased (**Figure 5.2A**). The observation was validated by quantitative assay western blot (**Figure 5.2B**), collectively suggesting that chronic alcohol intake impaired smooth

muscle actins, which respresents the architectural structure of smooth muscle cells.

We further examined the phosphorylation level of myosin light chain (MLC), which represents the contraction (phosphorylation) or relaxation (de-phosphorylation) status of smooth muscles. Immunostaining (smooth muscle specific p-MLC, green) showed that phosphorylation level of MLC was decreased by low dose (**Figure 5.2 A)**, indicating enhanced dilative vascular reactivities. Whereas in the chronic condition, p-MLC level was increased, suggesting that the vascular dilative reactivities were diminished. The observation was validated by quantitative assay western blot (**Figure 5.2 B**). As such, the summary is that chronic alcohol intake impaired vascular smooth muscles and decreased dilative vascular reactivities.

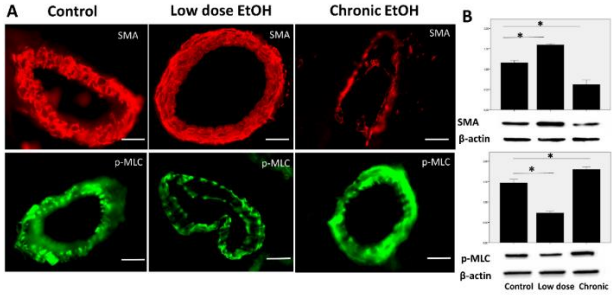

Figure 5.2 Effect of low dose and chronic alcohol intake on vascular smooth muscle reactivity. [A].Immunostaining of SMA (red) and smooth muscle specific phospho-MLC (green) protein at brain microvessels (indicated by structures) in control, low dose EtOH and chronic EtOH treatment. SMA and p-MLC were used as primary antibodies. Data was representation of at least N=6 animals per each group. Scale bar: 30 μm. [B]. Immunoreactive bands of SMA, p-MLC and β-actin, and quantitative corresponding protein content in three experimental groups. Results were expressed as the ratio of protein of interest to that of actin bands and presented as mean values (± SEM). Statistically significant (*$p<0.05$) compared with controls. Three replicates were done for each animal sample from at least N=6 animals.

5.3.4 Contrast Effect of Low Dose and Moderate/chronic Alcohol on Brain Vascular Endothelial cells and the Blood-Brain Barrier (BBB)

To investigate the effect of alcohol on brain vascular endothelial cells, we evaluated the

immunoreactivity of endothelial cell markers, von willebrand factor (vWF) and glucose transporter 1 (Glut-1). Immunostaining revealed that chronic alcohol intake diminished aimed proteins' (vWF and Glut-1) expressions while there was no change for low/acute exposure, which was further validated by western blot analyses (*$p<0.05$) (**Figure 5.3**). These results indicated that chronic alcohol impaired brain vascular endothelial cells compared with control and low dose.

Next, we procceded to investigate the integrity of blood-brain barriers (BBB), which were localized on the endothelium. We examined changes in expression of BBB tight junction (TJ) proteins: occludin, claudin-5 and zonula occluden 1 (ZO-1) by immunostaining and western blot since reduction in TJ protein levels or disruption of the architectural structure of any TJ protein was expected to impair BBB integrity. Immunostaining revealed that moderate/chronic alcohol exposure diminished expression of TJ proteins at brain microvessels compared with control (**Figure 5.4A**) while no significant change was observed in low/acute alcohol. These alcohol dosing-induced changes in TJ protein expressions were validated by western blot, and quantification of the TJ protein immunoreactive bands ($p<0.05$) (**Figure 5.4B**). This data was in agreement with previous findings that chronic alcohol abuse leads to breaking of the BBB [88, 89, 111].

In summary, we concluded that moderate/chronic alcohol intake impaired brain vascular endoethelial cells and compromised BBB integrities.

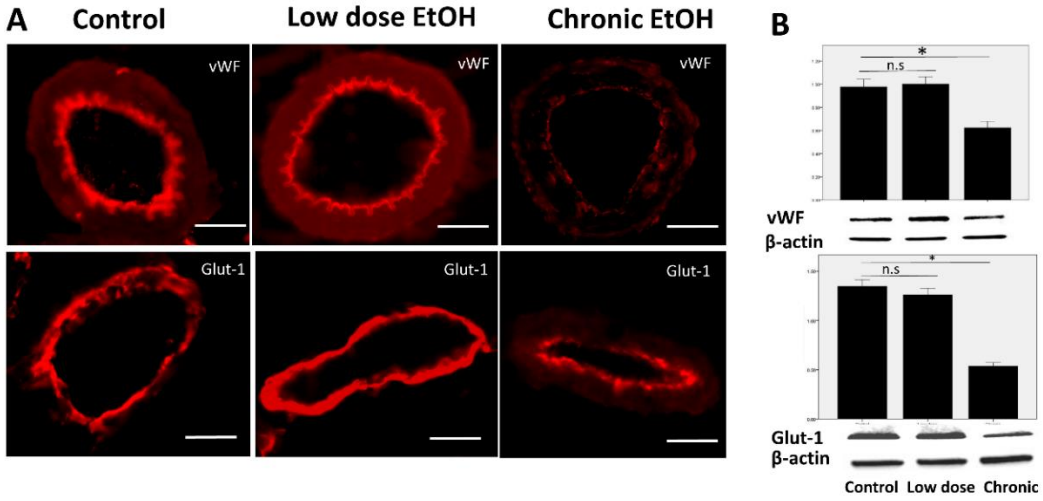

Figure 5.3 Effect of low dose and chronic alcohol intake on vascular endothelial cells. Coronal tissue sections (10 ~ 15 μm) were analyzed for endothelial cell markers (vWF and Glut-1: red) subcellular distribution while protein extracts from brain were analyzed for alterations in corresponding protein content. [A]. Immunostaining of vWF (red) and Glut-1 (red) protein around brain microvessels (indicated by circular structures) in control, low dose EtOH and chronic EtOH treatment. vWF and Glut-1 were used as primary antibodies (information in Table 2.1). Scale bar: 30 μm. Data was representation of at least N=6 animals per each group. [B]. Immunoreactive bands of vWF, Glut-1 and β-actin, and quantitative corresponding protein content in three experimental groups. Results are expressed as the ratio of protein of interest to that of actin bands and presented as mean values (± SEM). Statistically significant (*$p < 0.05$) compared with controls. Three replicates were done for each animal sample from at least N=6 animals.

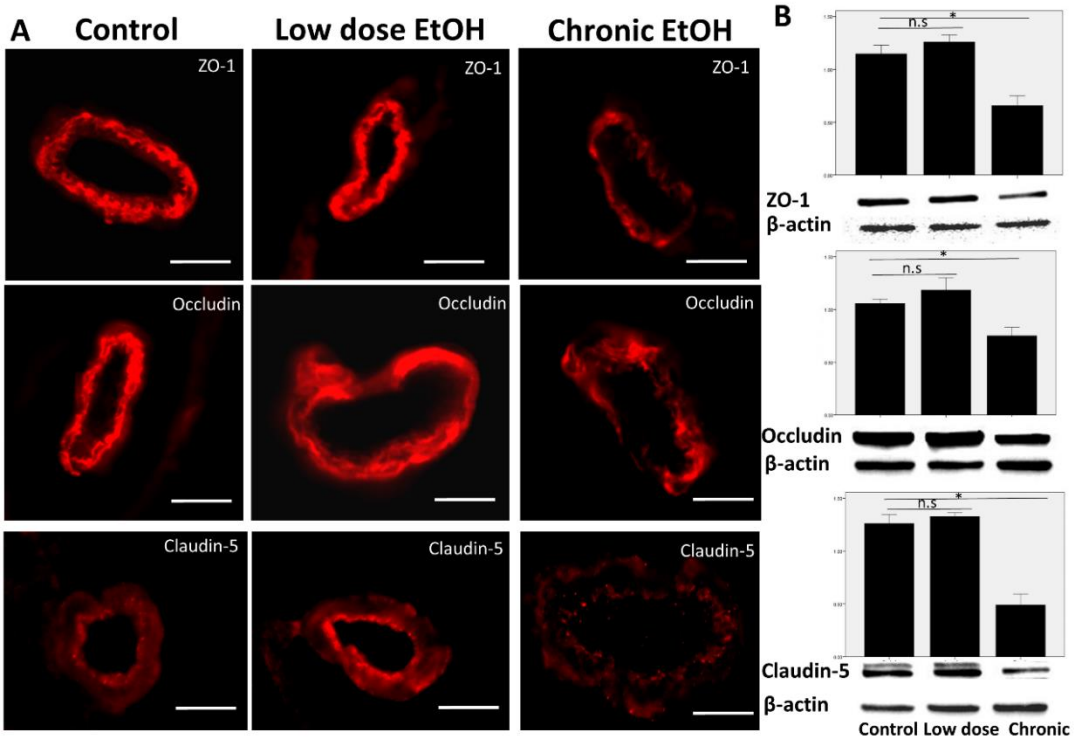

Figure 5.4 Effect of low dose and chronic alcohol intake on BBB tight junction proteins. [A]. Immunostaining of tight junction proteins: ZO-1, Occludin and Claudin-5 (red) in brain microvessels from coronal slices (10 ~ 15 μm) of control, low dose EtOH and chronic EtOH. ZO-1, Occludin and Claudin-5 were used as primary antibodies (information in Table 2.1). Scale bar: 30 μm. Data was representation of at least N=6 animals per each group. [B]. Western blot analysis of ZO-1, Occludin, Claudin-5 and β-actin in the whole brain tissue homogenates of rats at different experimental conditions. Results are expressed as the ratio of protein of interest to that of actin bands and presented as mean values (± SEM). Statistically significant (*$p < 0.05$) compared with controls. Three replicates were done for each animal sample from at least N=6 animals.

5.3.5 Induction of Free Radicals by Alcohol Causes Vasculature Damage

From previous data, it was shown that smooth muscles, endothelium and BBB integrities were impaired under chronic alcohol exposure. To find out the likely reasons that caused these observations, we focused on free radical generation - particularly the iNOS mediated nitrosative stress on brain vasculatures. Level of 3-nitrotyrosine (3-NT) was

the indicator of nitrosative stress, as it leads to formation of nitrated proteins. Immunostaining of 3-NT revealed that protein level was increased in the chronic condition while no change in the low/acute when compared with control (**Figure 5.5A**). Using the western blot assay, we detected three nitrotyrosine proteins (molecular weights of 210, 97, and 68 kDa). The 210-kDa protein was the major nitrated protein as compared with 97 kDa or 68 kDa nitrated proteins. Quantitative data validated our finding that chronic exposure significantly increased 3-NT expression (**Figure 5.5B**) (*$p<0.05$). The extent of nitrosative damage marker 3NT paralleled induction of iNOS, indicating that free radical damage was correlated with iNOS over-expression. eNOS expression was elevated under low dose condition, which lined-up with previous observations.

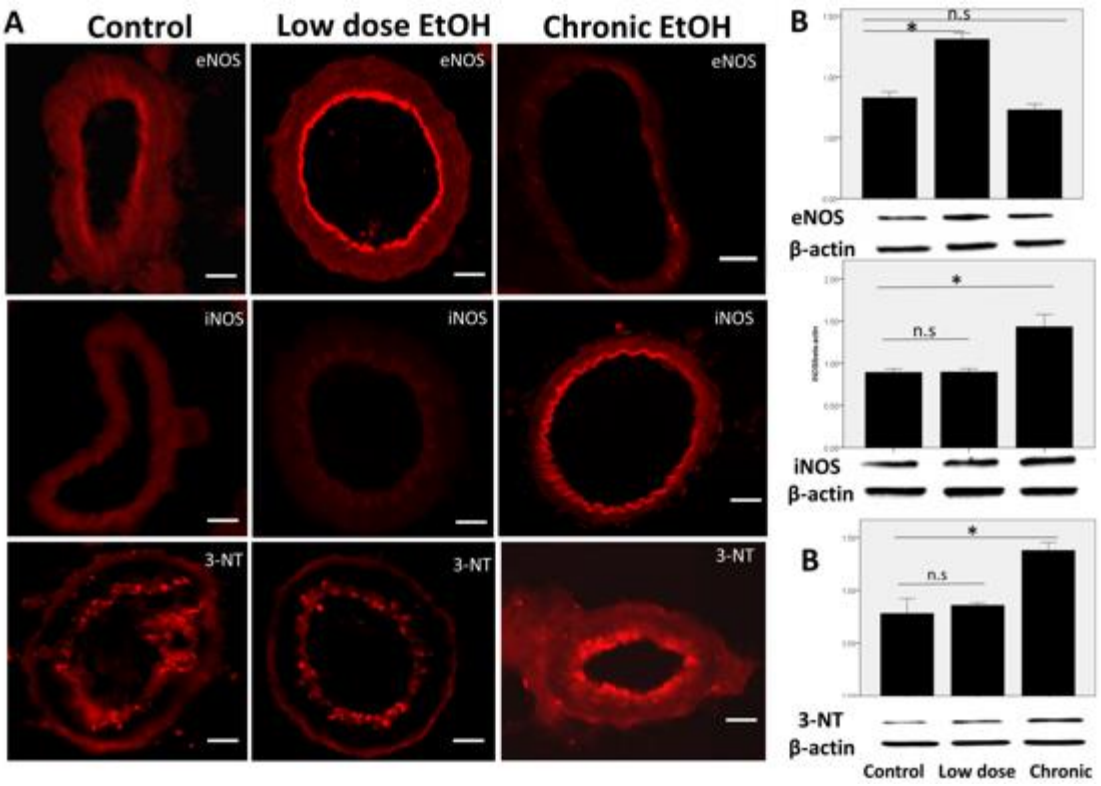

Figure 5.5 Effect of low dose and chronic alcohol intake on free radical generation. Coronal tissue sections (10 ~ 15 μm) were analyzed for eNOS, iNOS and 3-NT (nitrosative stress markers) subcellular distribution while protein extracts from brain were analyzed for alterations in corresponding protein content. [A]. Immunostaining of eNOS (red), iNOS (red) and 3-NT (red) protein at brain microvessels (indicated by structures) in control, low dose EtOH and chronic EtOH. eNOS, iNOS and 3-NT were used as primary antibodies (information in Table 2.1). Scale bar: 30 μm. Data was representation of at least N=6 animals per each group. [B]. Immunoreactive bands of eNOS, iNOS, 3-NT and β-actin, and quantitative corresponding protein content in three experimental groups. Results were expressed as the ratio of protein of interest to that of actin bands and presented as mean values (± SEM). Statistically significant (*$p < 0.05$) compared with controls. Three replicates were done for each animal sample from at least N=6 animals.

Thus, these data above collectively suggested that iNOS mediated nitrosative stress leads to free radical damage at brain vasculatures when exposed to the moderate/chronic alcohol whereas no such effect was found on the low/acute.

5.4 Discussion

We discuss the finding of contrast effects of alcohol (acute/low and moderate/chronic) on brain PVS waste metabolites clearance. In a previous study [62], we used low levels of alcohol to understand the protective mechanisms of promoting perivascular clearance because low alcohol use was protective of vascular and cardiovascular function [4, 64, 65, 85-87]. We found that low dose alcohol intake (5 mM) can increase interaction of brain vascular ECs-SMCs. Large size waste metabolites clearance in the brain that cannot be efficiently done through CSF, glymphatic, or meningeal lymphatic systems were able to be facilitated by alcohol through this mechanism. In fact, Lundgaard et al. (2018) showed the beneficial effects of low dose alcohol and the adverse effects of high dose alcohol on glymphatic function [85]. We noted here that the contrast effects of low dose alcohol intake and chronic use of moderate-to-high dose alcohol (equivalent of alcohol dependent subjects) were examined in the context of vascular reactivity, blood-brain barrier permeability and perivascular clearance since epidemiological evidence showed distinctive consequences on brain clearance and associated neurological diseases (e.g., Alzheimer's disease and cerebral amyloid angiopathy) under different alcohol drinking patterns as discussed previously [5, 77, 80, 81, 83, 84, 125, 126]. The data indicated that chronic alcohol hampered perivascular waste metabolites clearance, impaired dilative vascular reactivities and compromised BBB integrity, due to: 1) paradigm shift to iNOS in chronic conditions and 2) free radical damage induced by alcohol impaired brain microvessels during moderate/chronic alcohol exposure.

To mimic the large size waste metabolites, we injected a large molecular weight fluorescent tracer (2000 KD) as proof-of-concept. We showed the contrast phenomenon

by examining the bio-distribution of large size molecular weight fluorescent tracer through cisterna magna injection under low/acute and moderate/chronic conditions (**Figure 5.1**). We found that low/acute alcohol enhanced dynamic tracer movement and clearance while moderate/chronic hampered this process. Further evidence showed that vascular smooth muscles and endothelium were impaired and BBB intergrites were compromised under chronic alcohol conditons (**Figures 5.2 – 5.4**), indicating that the vascular dilative reactivities that are regulated by endothelial-smooth muscle interaction were diminished.

We also examined the expression of iNOS (**Figure 5.5**), which mediated free radical generating due to elevation of high amounts of NO compared with that of eNOS. Interestingly, iNOS showed an opposite expression pattern compared with eNOS. We then showed that free radical damages (3-NT) (**Figure 5.5**) that induced by chronic alcohol exposure impaired brain microvessels, which were in parallel with iNOS expression.

Collectively, the contrast effects of acute/low and chronic/moderate alcohol intake were examined in this chapeter. It was found that unlike low dose, moderate/chronic alcohol intake diminished PVS clearance compared with control. The contrast effects were due to that moderate/chronic alcohol induced free radical generation, which led to impairement of vascular endothelium and smooth muscles, dysfunction of BBB and decreased vascular dilative reactivities. The significance of this work is the discovery that mis-use/chronic alcohol abuse impairs the brain clearance system, which may lead to onset/progression of neurodeneration diseases, like Alzheimer's disease, supporting by epidemiological studies that discussed previously.

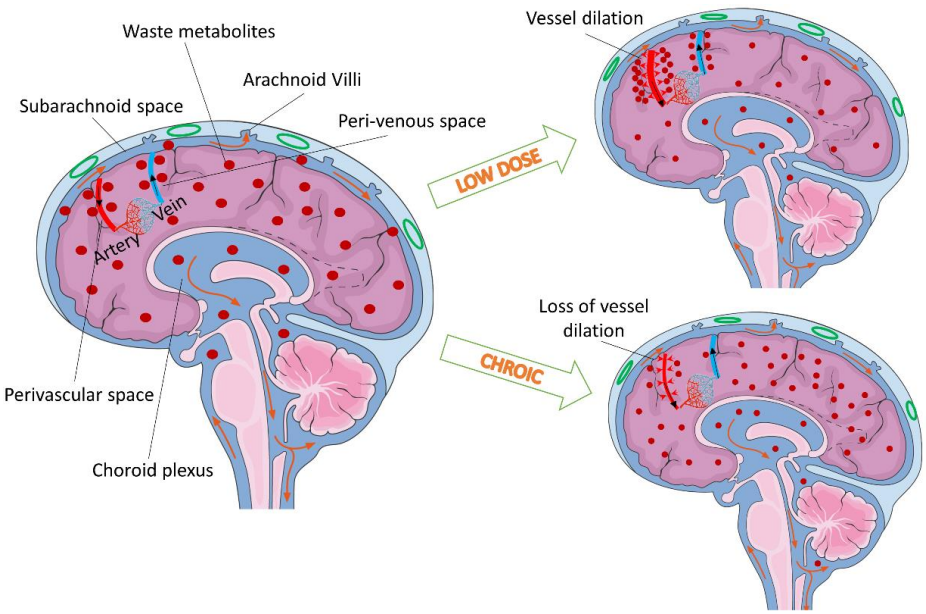

Figure 5.6 Illustration of Chapter 5. Left: Arrows (orange) indicate the CSF subarachnoid flow and perivascular-perivenous clearance path (black) of large size waste metabolites (red dots) in the neurodegenerative brain. Waste metabolites like beta-amyloid proteins are aggregated more inside the interstitial space due to the lack of a lymphatic system in the brain. Less metabolites drain into the CSF flows due to less vessel dilative reactivity. Right top: The neurodegenerative brain in the presence of low dose alcohol. Dilative arterial vessel reactivity promotes the dynamic movement of large size waste metabolites from interstitial fluid to perivascular space and from interstitial-CSF subarachnoid to perivascular space. Reactivity of endothelial and smooth muscle cells in arteries is mediated by alcohol-initiated eNOS activation and NO production. Right bottom: The neurodegenerative brain exposed to chronic/moderate alcohol intake. Loss of dilative arterial vessel reactivity due to free radical damage towards vasculatures hampers the dynamic movement of waste metabolites to the perivascular – peri-venous route. Paradigm shift from eNOS to iNOS initiates free radical generation and causes diminishing reactivity of endothelial and smooth muscle cells in arterial vasculatures with chronic/moderate alcohol exposure.

CHAPTER 6

SUMMARY CONCLUSION

Efficient clearance of the interstitial waste metabolites is essential for normal maintenance of brain homeostasis. The brain lacks the lymphatic clearance system – thus clearance of waste metabolites in the brain is dependent on cerebrospinal fluid (CSF) system. The recent discovery glymphatic system claims that the direct bulk flow transports small size water-soluble waste metabolites into to the perivenous space by aquaporin-4 water channels of the astrocyte end-feet, but it does not account for the clearance of large size waste metabolites, like peptide and/or protein aggregations.

Here, the clearance mechanisms of large size waste metabolites from interstitial fluid to the perivascular space as well as from the CSF subarachnoid into perivascular space via the paravascular drainage is investigated. A low dose ethanol (5 mM) is found to promote the dynamic clearance of waste metabolites through this perivascular-perivenous drainage path. This ethanol-induced effect can be explained by the findings that activation of endothelial specific nitric oxide synthase (eNOS) by ethanol and generation of vasodilator nitric oxide (NO) mediate the interactive reactivity of endothelial-smooth muscle cells. Futher evidence reveals that NO mediated ECs and SMCs interaction is regulated by myosin light chain activities, which depend on the balance between two opposite enzymatic acitivies: myosin light chain kinase and myosin light chain phosphatase.

In addition to that, the contrast effects of acute low dose and chronic moderate alcohol intake on BBB associated perivascular clearance of waste metabolites in the

brain is also examined. The underlying molecular and cellular mechanisms that drive the increase or decrease movement of tracer to perivascular space by acute/chronic alcohol exposure are correlated to BBB integrity and arterial vessel reactivity. Evidently, the contrast effects of alcohol appear to be regulated by the switch mechanisms of endothelial specific nitric oxide synthase (eNOS) activation by low dose and inducible NOS (iNOS) by moderately high alcohol exposure in chronic conditions. As such, it is concluded that low dose alcohol promotes the diffusive movement of waste metabolites to perivascular clearance through eNOS-derived NO regulated arterial endothelial-smooth muscle cell dilative reactivity without affecting the integrity of the BBB. Whereas, continuous induction of iNOS in chronic alcohol exposure causes oxidative damage of the arterial endothelial-smooth muscle layers that led to BBB dysfunction, reduced dilative reactivity, and decreased movement of waste metabolites from interstitial space/CSF to perivascular-perivenous drainage path.

Given the fact that large size waste metabolites like tauopathy, prion-like proteinopathies, cerebral amyloid angiopathy, and Aβ proteins are seen accumulated around the perivascular space in brain tissue from neurological diseases, the significance of this current work affords new therapeutical strategies for neurological diseases, particarly the timely clearance of entangled proteins.

APPENDIX A

MATLAB CODE FOR COMPUTING VESSEL DIAMETER CHANGE

This code is used to calculate vessel diameters that present in Chapter 3.

```
%%
folderContents = dir;
nFiles = length(dir);

arteryFiles = cell(nFiles,1);
nVids = 0;
for i = 1:nFiles
filename = folderContents(i).name;
if length(filename) > 3 && strcmpi(filename(1:2),'T=') && strcmpi(filename(end-3:end),'.avi')
nVids = nVids + 1;
arteryFiles{nVids} = filename;
end
end

arteryFiles = arteryFiles(1:nVids);
exposureTimes = zeros(nVids,1);
for i = 1 :nVids
exposureTimes(i) = str2double(arteryFiles{i}(3:end-4));
end

%%
nDivisions = 5;
peakQuantile = .9;
pixelLength = 40/38;
vesselDiameterYLim = [15,35];
interpFactor = 8;

frameRate = 4;
borderFraction = .1;

vesselDiameters = cell(nVids,1);


for i = 1:nVids
vw = VideoWriter(['T',num2str(exposureTimes(i)),'_vessel_diameters']); %#ok<TNMLP>
vw.FrameRate = frameRate;
open(vw);

cf = figure('units','normalized','outerposition',[0 0 1 1]);

%     set(cf,'visible','off')
exposureTimes(i) = str2double(arteryFiles{i}(3:end-3));
currentVideo = importdata(arteryFiles{i});

nX = size(currentVideo(1).cdata,2);
nY = size(currentVideo(1).cdata,1);
nFrames = length(currentVideo);

vesselDiameters{i} = zeros(nFrames,nDivisions);
```

```
for j = 1:nFrames;
iRed = currentVideo(j).cdata(:,:,1);
iFilt = double(iRed);
iFilt = filter2(eye(3)/9,iFilt);
iFilt = medfilt2(iFilt,[1,3]);


clf
subplot(1,3,1)
imshow(currentVideo(j).cdata)


for k = 1:nDivisions



y = round(k/(nDivisions+1)*(nY*(1-2*borderFraction)) + nY*borderFraction); %divide up only the
middle half to avoid text at head and foot of video
interpX = linspace(1,nX,nX*interpFactor);

lineVals = interp1((1:nX),iFilt(y,:),interpX);
mpp = 2*median(lineVals);
[~, peaks] = findpeaks(lineVals,'MinPeakProminence',mpp);

if numel(peaks) > 1
leftPeak = min(peaks);
rightPeak = max(peaks);
vesselDiameters{i}(j,k) = range(interpX(peaks))*pixelLength;
%               vesselDiameters{i}(j,k) = min(diff(sort((interpX(peaks))*pixelLength)));
else
vesselDiameters{i}(j,k) = 0;
end




subplot(1,3,1)
hold on
plot([1,nX],[y,y],'b','linewidth',2)
if ~isempty(peaks)
plot(interpX(peaks),y,'w.','markersize',12)
end

subplot(nDivisions,3,2+(k-1)*3)
hold on
plot(interpX,lineVals,'linewidth',2)
plot(interpX(peaks),lineVals(peaks),'k.','markersize',12);


if k == 1
title(arteryFiles{i}(1:end-4))
end

if k == nDivisions
xlabel('distance (\mum)')
```

```
end
ylabel('relative intensity')

subplot(nDivisions,3,3+(k-1)*3)
hold on
plot((0:j-1)/frameRate,vesselDiameters{i}(1:j,k),'.')
xlim([0,nFrames]/frameRate)
ylim(vesselDiameterYLim)

if k == nDivisions
xlabel('time (s)')
end
ylabel('distance (\mum)')



end

set(cf,'color','w')
vw.writeVideo(getframe(cf));
%       pause(.01)
end
close(vw)


end
```

APPENDIX B

R CODE FOR VESSEL DIAMETER DATA PROCESS AND PLOTTING

This code is used to generate plots that present in Chapter 3.

```
# read data
T0<-read.csv('T=0.csv',header = F)
T15<-read.csv('T=15.csv',header = F)
T30<-read.csv('T=30.csv',header = F)
T45<-read.csv('T=45.csv',header = F)

# rename column
colnames(T0)<-c('Frame','1','2','3','4','5')
colnames(T15)<-c('Frame','1','2','3','4','5')
colnames(T30)<-c('Frame','1','2','3','4','5')
colnames(T45)<-c('Frame','1','2','3','4','5')

# add label
T0$time<-'baseline'
T15$time<-'15 min after alcohol'
T30$time<-'30 min after alcohol'
T45$time<-'45 min after alcohol'

# plot
T0reshape<-melt(T0,id.vars = 'Frame')
T0reshape$variable<-NULL
T0reshape$Frame<-as.factor(as.character(T0reshape$Frame))
T0sum<-
  T0reshape%>%
  group_by(Frame)%>%
  summarise(mean=mean(value),sd=sd(value))
T0sum$Frame<-
  as.numeric(as.character(T0sum$Frame))
ggplot(T0sum,aes(x=Frame,y=mean))+
  geom_errorbar(aes(ymin=mean-sd,ymax=mean+sd),width=0.1)+
  geom_point()+
  geom_line(data = spline_int,aes(x=x,y=y))
spline_int<-as.data.frame(spline(T0sum$Frame, T0sum$mean))


plotfunction<-function(a){
  x1<-melt(a,id.vars = 'Frame')
  x1$variable<-NULL
  x1$Frame<-as.factor(as.character(x1$Frame))
  x2<-
    x1%>%
    group_by(Frame)%>%
    summarise(mean=mean(value),sd=sd(value))
  x2$Frame<-
    as.numeric(as.character(x2$Frame))
  spline_int<-as.data.frame(spline(x2$Frame, x2$mean))
  ggplot(x2,aes(x=Frame,y=mean))+
```

```
   geom_errorbar(aes(ymin=mean-sd,ymax=mean+sd),width=0.1)+
   geom_point()+
   geom_line(data = spline_int,aes(x=x,y=y))
}

plotfunction(T30)

T30<-T30[-12,]
T30
row.names(T30) <- 1:nrow(T30)
ggplot(data=T30,aes(x=Frame,y=mean))+geom_point()

# encoding time lapse

T15$Frame<-T15$Frame+40
T30$Frame<-T30$Frame+77
T45$Frame<-T45$Frame+116

combine<-rbind(T0,T15,T30,T45)
combine<-combine[-c(89,90),]
combine[combine$time=='30 min after alcohol','Frame']<-seq(78,114)
combine[combine$time=='45 min after alcohol','Frame']<-seq(115,191)

combine_reshape<-melt(combine,id.vars = c('Frame','time'))

combine_reshape$Frame<-as.factor(as.character(combine_reshape$Frame))

combine_reshape_sum<-
  combine_reshape%>%
  group_by(Frame)%>%
  summarise(mean=mean(value),sd=sd(value))
combine_reshape_sum$Frame<-
  as.numeric(as.character(combine_reshape_sum$Frame))

combine_reshape_sum$timelapse<-ifelse(combine_reshape_sum$Frame>=117,'45 min after alcohol',
                          ifelse(combine_reshape_sum$Frame<117&combine_reshape_sum$Frame>=78,'30
min after alcohol',

ifelse(combine_reshape_sum$Frame<78&combine_reshape_sum$Frame>=41,'15 min after
alcohol','baseline')))

combine_reshape_sum$timelapse<-as.factor(combine_reshape_sum$timelapse)
is.factor(combine_reshape_sum$timelapse)
combine_reshape_sum$label<-NULL

# Plot for the combine

spline_int<-as.data.frame(spline(x=combine_reshape_sum$Frame, y=combine_reshape_sum$mean))

p<-
  ggplot(combine_reshape_sum,aes(x=Frame,y=mean,color=timelapse))+
  geom_errorbar(aes(ymin=mean-sd,ymax=mean+sd),width=0.5)+geom_point()+
  geom_line(data = spline_int,aes(x=x,y=y),inherit.aes = FALSE)+
  scale_color_discrete(breaks=c('baseline','15 min after alcohol','30 min after alcohol','45 min after
alcohol'))+
  theme(legend.title=element_blank())
```

```
# add theme
p+xlab("Frame")+ylab("Diameter (um)")+
  ggtitle("Cerebral vessel diameter change under low dose alochol")+
  theme(axis.title.x = element_text(size=15),
        axis.title.y = element_text(size=15),
        axis.text.x=element_text(color="Black",size=10),
        axis.text.y = element_text(color="Black",size=10),
        plot.title = element_text(size=15,hjust=0.5),
        panel.background = element_rect(fill='White',color='Black'))
# plot
T0reshape<-melt(T0,id.vars = 'Frame')
T0reshape$variable<-NULL
T0reshape$Frame<-as.factor(as.character(T0reshape$Frame))
grouped<-group_by(T0reshape,Frame)
summarise(grouped,mean=mean(value),sd=sd(value))
T0sum<-
T0reshape%>%
group_by(Frame)%>%
summarise(mean=mean(value),sd=sd(value))
View(T0sum)
T0sum$Frame<-
as.numeric(as.character(T0sum$Frame))
View(T0sum)
geom_errorbar(aes(ymin=mean-sd, ymax=mean+sd), width=.1) +
library("ggplot2", lib.loc="~/R/win-library/3.4")
ggplot(T0sum, aes(x=Frame, y=mean) +
str(T0sum)
str(T0sum)
summary(T0sum)
geom_errorbar(aes(ymin=mean-sd, ymax=mean+sd), width=.1) +
geom_point()
geom_line() +
gplot(T0sum, aes(x=Frame, y=mean) +
geom_errorbar(aes(ymin=mean-sd, ymax=mean+sd), width=.1) +
geom_line() +
geom_point()
gplot(T0sum, aes(x=Frame, y=mean)
gplot(T0sum, aes(x=Frame, y=mean)+geom_errorbar(aes(ymin=mean-sd, ymax=mean+sd), width=.1) +
ggplot(T0sum,aes(x=Frame,y=mean))
ggplot(T0sum,aes(x=Frame,y=mean))
View(T0sum)
ggplot(T0sum,aes(x=Frame,y=mean))
ggplot(T0sum,aes(x=Frame,y=mean))+
geom_errorbar(aes(ymin=mean-sd,ymax=mean+sd),width=0.1)+
geom_point()
ggplot(T0sum,aes(x=Frame,y=mean))+
geom_errorbar(aes(ymin=mean-sd,ymax=mean+sd),width=0.1)+
geom_point()+geom_line()
ggplot(T0sum,aes(x=Frame,y=mean))+
geom_errorbar(aes(ymin=mean-sd,ymax=mean+sd),width=0.1)+
geom_point()+
stat_smooth(aes(x=Frame,y=mean),method = 'lm',
formula = y~ploy(x,39))
ggplot(T0sum,aes(x=Frame,y=mean))+
geom_errorbar(aes(ymin=mean-sd,ymax=mean+sd),width=0.1)+
```

```
geom_point()+
stat_smooth(aes(x=Frame,y=mean),method = 'lm',
formula = y~poly(x,39))
ggplot(T0sum,aes(x=Frame,y=mean))+
geom_errorbar(aes(ymin=mean-sd,ymax=mean+sd),width=0.1)+
geom_point()+
stat_smooth(aes(x=Frame,y=mean),method = 'lm',
formula = y~poly(x,10))
ggplot(T0sum,aes(x=Frame,y=mean))+
geom_errorbar(aes(ymin=mean-sd,ymax=mean+sd),width=0.1)+
geom_point()+
stat_smooth(aes(x=Frame,y=mean),method = 'lm',
formula = y~poly(x,38))
ggplot(T0sum,aes(x=Frame,y=mean))+
geom_errorbar(aes(ymin=mean-sd,ymax=mean+sd),width=0.1)+
geom_point()+
stat_smooth(aes(x=Frame,y=mean),method = 'lm',
formula = y~poly(x,30))
formula = y~poly(x,20)
ggplot(T0sum,aes(x=Frame,y=mean))+
geom_errorbar(aes(ymin=mean-sd,ymax=mean+sd),width=0.1)+
geom_point()+
stat_smooth(aes(x=Frame,y=mean),method = 'lm',
formula = y~poly(x,20))
ggplot(T0sum,aes(x=Frame,y=mean))+
geom_errorbar(aes(ymin=mean-sd,ymax=mean+sd),width=0.1)+
geom_point()
spline_int<-as.data.frame(spline(T0sum$Frame, T0sum$mean))
ggplot(T0sum,aes(x=Frame,y=mean))+
geom_errorbar(aes(ymin=mean-sd,ymax=mean+sd),width=0.1)+
geom_point()+
geom_line(data = spline_int,aes(x=x,y=y))
plotfunction<-function(a){
x1<-melt(a,id.vars = 'Frame')
x1$variable<-NULL
x1$Frame<-as.factor(as.character(x1$Frame))
x2<-
x%>%
group_by(Frame)%>%
summarise(mean=mean(value),sd=sd(value))
x2$Frame<-
as.numeric(as.character(x2$Frame))
spline_int<-as.data.frame(spline(x2$Frame, x2$mean))
ggplot(x2,aes(x=Frame,y=mean))+
geom_errorbar(aes(ymin=mean-sd,ymax=mean+sd),width=0.1)+
geom_point()+
geom_line(data = spline_int,aes(x=x,y=y))
}
plotfunction(T0)
plotfunction(T0)
T0reshape<-melt(T0,id.vars = 'Frame')
T0reshape$variable<-NULL
T0reshape$Frame<-as.factor(as.character(T0reshape$Frame))
T0sum<-
T0reshape%>%
group_by(Frame)%>%
```

```
summarise(mean=mean(value),sd=sd(value))
T0sum$Frame<-
as.numeric(as.character(T0sum$Frame))
ggplot(T0sum,aes(x=Frame,y=mean))+
geom_errorbar(aes(ymin=mean-sd,ymax=mean+sd),width=0.1)+
geom_point()+
geom_line(data = spline_int,aes(x=x,y=y))
spline_int<-as.data.frame(spline(T0sum$Frame, T0sum$mean))
plotfunction<-function(a){
x1<-melt(a,id.vars = 'Frame')
x1$variable<-NULL
x1$Frame<-as.factor(as.character(x1$Frame))
x2<-
x1%>%
group_by(Frame)%>%
summarise(mean=mean(value),sd=sd(value))
x2$Frame<-
as.numeric(as.character(x2$Frame))
spline_int<-as.data.frame(spline(x2$Frame, x2$mean))
ggplot(x2,aes(x=Frame,y=mean))+
geom_errorbar(aes(ymin=mean-sd,ymax=mean+sd),width=0.1)+
geom_point()+
geom_line(data = spline_int,aes(x=x,y=y))
}
plotfunction(T0)
plotfunction(T15)
plotfunction(T30)
plotfunction(T45)
View(T45)
View(T30)
T45<-read.csv('T=45.csv',header = F)
colnames(T45)<-c('Frame','1','2','3','4','5')
plotfunction(T45)
View(T0)
View(T15)
View(T30)
View(T45)
# add label
T0$time<-'baseline'
T15$time<-'15 min after alcohol'
T30$time<-'30 min after alcohol'
T45$time<-'45 min after alcohol'
View(T0)
combine<-rbind(T0,T15,T30,T45)
View(combine)
View(T0)
View(T15)
T15$Frame<-T15$Frame+40
View(T15)
View(T15)
View(T30)
T30$Frame<-T30$Frame++77
View(T30)
T30$Frame<-T30$Frame+77
View(T30)
T30<-read.csv('T=30.csv',header = F)
```

```
colnames(T30)<-c('Frame','1','2','3','4','5')
T30$time<-'30 min after alcohol'
View(T30)
T30$Frame<-T30$Frame+77
T45$Frame<-T45$Frame+116
combine<-rbind(T0,T15,T30,T45)
View(combine)
combine_reshape<-melt(combine,id.vars = 'Frame')
View(combine_reshape)
combine<-rbind(T0,T15,T30,T45)
combine_reshape<-melt(combine,id.vars = c('Frame','time'))
View(combine_reshape)
combine$Frame<-as.factor(as.character(combine$Frame))
combine<-rbind(T0,T15,T30,T45)
combine_reshape$Frame<-as.factor(as.character(combine_reshape$Frame))
combine_reshape_sum<-
combine_reshape%>%
group_by(Frame)%>%
summarise(mean=mean(value),sd=sd(value))
combine_reshape_sum$Frame<-
as.numeric(as.character(combine_reshape_sum$Frame))
View(combine_reshape_sum)
View(combine_reshape_sum)
View(combine_reshape)
combine_reshape_sum<-
combine_reshape%>%
group_by(Frame)%>%
summarise(time=time,mean=mean(value),sd=sd(value))
combine_reshape_sum$Frame<-
as.numeric(as.character(combine_reshape_sum$Frame))
View(combine_reshape_sum)
View(combine_reshape_sum)
View(T0)
View(T15)
View(T30)
View(T45)
combine_reshape_sum$label<-ifelse(combine_reshape_sum$Frame>=117,'45min after alcohol',
ifelse(combine_reshape_sum$Frame<117&combine_reshape_sum$Frame>=78,'30 min after alcohol',
ifelse(combine_reshape_sum$Frame<78&combine_reshape_sum$Frame>=41,'15 min after
alcohol','baseline')))
View(combine_reshape_sum)
is.numeric(combine_reshape_sum$Frame)
# Plot for the combine
spline_int<-as.data.frame(spline(combine_reshape_sum$Frame, combine_reshape_sum$mean))
ggplot(combine_reshape_sum,aes(x=Frame,y=mean,color=label))+
geom_errorbar(aes(ymin=mean-sd,ymax=mean+sd),width=0.1)+
geom_point()+
geom_line(data = spline_int,aes(x=x,y=y))
ggplot(combine_reshape_sum,aes(x=Frame,y=mean))+
geom_errorbar(aes(ymin=mean-sd,ymax=mean+sd),width=0.1)+
geom_point()+
geom_line(data = spline_int,aes(x=x,y=y,color=label))
View(combine_reshape_sum)
ggplot(combine_reshape_sum,aes(x=Frame,y=mean))+
geom_errorbar(aes(ymin=mean-sd,ymax=mean+sd),width=0.1)+
geom_point()+
```

```
geom_line(data = spline_int,aes(x=x,y=y))
ggplot(combine_reshape_sum,aes(x=Frame,y=mean,color=label))+
geom_errorbar(aes(ymin=mean-sd,ymax=mean+sd),width=0.1)+
geom_point()+
geom_line(data = spline_int,aes(x=x,y=y))
ggplot(combine_reshape_sum,aes(x=Frame,y=mean,color=label),inherit.aes = FALSE)+
geom_errorbar(aes(ymin=mean-sd,ymax=mean+sd),width=0.1)+
geom_point()+
geom_line(data = spline_int,aes(x=x,y=y))
combine_reshape_sum$timelapse<-ifelse(combine_reshape_sum$Frame>=117,'45min after alcohol',
ifelse(combine_reshape_sum$Frame<117&combine_reshape_sum$Frame>=78,'30 min after alcohol',
ifelse(combine_reshape_sum$Frame<78&combine_reshape_sum$Frame>=41,'15 min after
alcohol','baseline')))
View(combine_reshape_sum)
ggplot(combine_reshape_sum,aes(x=Frame,y=mean,color=timelapse)+
ggplot(combine_reshape_sum,aes(x=Frame,y=mean,color=timelapse)+
geom_errorbar(aes(ymin=mean-sd,ymax=mean+sd),width=0.1)+
geom_point()+
geom_line(data = spline_int,aes(x=x,y=y))
combine_reshape_sum$label<-NULL
combine_reshape_sum$label<-NULL
View(combine_reshape_sum)
# Plot for the combine
spline_int<-as.data.frame(spline(combine_reshape_sum$Frame, combine_reshape_sum$mean))
ggplot(combine_reshape_sum,aes(x=Frame,y=mean,color=timelapse)+
geom_point()+
head(combine_reshape_sum)
head(combine_reshape_sum)
head(combine_reshape_sum)
ggplot(combine_reshape_sum,aes(x=Frame,y=mean,color=timelapse)+
geom_point()+
head(combine_reshape_sum)
head(combine_reshape_sum)
ggplot(combine_reshape_sum,aes(x=Frame,y=mean,color=timelapse)+
geom_errorbar(aes(ymin=mean-sd,ymax=mean+sd),width=0.1)+
geom_point()+
geom_line(data = spline_int,aes(x=x,y=y))
ggplot(combine_reshape_sum,aes(x=Frame,y=mean,color=timelapse)+
geom_errorbar(aes(ymin=mean-sd,ymax=mean+sd),width=0.1)+
geom_point()+
geom_line(data = spline_int,aes(x=x,y=y))
# Plot for the combine
spline_int<-as.data.frame(spline(combine_reshape_sum$Frame, combine_reshape_sum$mean))
geom_point()+geom_line(data = spline_int,aes(x=x,y=y))
ggplot(combine_reshape_sum,aes(x=Frame,y=mean,color=timelapse)+
geom_point()+geom_line(data = spline_int,aes(x=x,y=y))
head(combine_reshape_sum)
p<-ggplot(combine_reshape_sum,aes(x=Frame,y=mean,color=timelapse)
geom_errorbar(aes(ymin=mean-sd,ymax=mean+sd),width=0.1)+
geom_point()+geom_line(data = spline_int,aes(x=x,y=y))
p<-ggplot(combine_reshape_sum,aes(x=Frame,y=mean,color=timelapse))
geom_errorbar(aes(ymin=mean-sd,ymax=mean+sd),width=0.1)+geom_point()+geom_line(data =
spline_int,aes(x=x,y=y))
p<-ggplot(combine_reshape_sum,aes(x=Frame,y=mean,color=timelapse))+
geom_errorbar(aes(ymin=mean-sd,ymax=mean+sd),width=0.1)+geom_point()+geom_line(data =
spline_int,aes(x=x,y=y))
```

```
p
View(combine_reshape_sum)
is.factor(combine_reshape_sum$timelapse)
is.character(combine_reshape_sum$timelapse)
as.factor(combine_reshape_sum$timelapse)
is.factor(combine_reshape_sum$timelapse)
combine_reshape_sum$timelapse<-as.factor(combine_reshape_sum$timelapse)
is.factor(combine_reshape_sum$timelapse)
spline_int<-as.data.frame(spline(combine_reshape_sum$Frame, combine_reshape_sum$mean))
ggplot(data=combine_reshape_sum,
aes(x=Frame,y=mean,color=timelapse))+
geom_errorbar(aes(ymin=mean-sd,ymax=mean+sd),width=0.1)+geom_point()+geom_line(data =
spline_int,aes(x=x,y=y))
ggplot(data=combine_reshape_sum,
aes(x=Frame,y=mean))+
geom_errorbar(aes(ymin=mean-sd,ymax=mean+sd),width=0.1)+geom_point()+geom_line(data =
spline_int,aes(x=x,y=y,color=timelapse))
ggplot(data=combine_reshape_sum,
aes(x=Frame,y=mean))+
geom_errorbar(aes(ymin=mean-sd,ymax=mean+sd),width=0.1)+geom_point()+geom_line(data =
spline_int,aes(x=x,y=y))
ggplot(data=combine_reshape_sum,
aes(x=Frame,y=mean,colour=timelapse))+
geom_errorbar(aes(ymin=mean-sd,ymax=mean+sd),width=0.1)+geom_point()+geom_line(data =
spline_int,aes(x=x,y=y))
ggplot(data=combine_reshape_sum,
aes(x=Frame,y=mean,fill=timelapse))+
geom_errorbar(aes(ymin=mean-sd,ymax=mean+sd),width=0.1)+geom_point()+geom_line(data =
spline_int,aes(x=x,y=y))
ggplot(data=combine_reshape_sum,
aes(x=Frame,y=mean,fill=timelapse))+geom_point()+geom_line(data = spline_int,aes(x=x,y=y))
ggplot(data=combine_reshape_sum,
aes(x=Frame,y=mean,color=timelapse))+geom_point()+geom_line(data = spline_int,aes(x=x,y=y))
summary(combine_reshape_sum)
ggplot(data=combine_reshape_sum,
aes(x=Frame,y=mean,color=timelapse))+
geom_errorbar(aes(ymin=mean-sd,ymax=mean+sd),width=0.1)+geom_point()+geom_line(data =
spline_int,aes(x=x,y=y))
ggplot(combine_reshape_sum)
ggplot(combine_reshape_sum,aes(x=Frame,y=mean))
ggplot(combine_reshape_sum,aes(x=Frame,y=mean,color=timelapse))
ggplot(combine_reshape_sum,aes(x=Frame,y=mean,color=timelapse))+
geom_errorbar(aes(ymin=mean-sd,ymax=mean+sd),width=0.1)
ggplot(combine_reshape_sum,aes(x=Frame,y=mean,color=timelapse))+
geom_errorbar(aes(ymin=mean-sd,ymax=mean+sd),width=0.5)
ggplot(combine_reshape_sum,aes(x=Frame,y=mean,color=timelapse))+
geom_errorbar(aes(ymin=mean-sd,ymax=mean+sd),width=0.5)+geom_point()
ggplot(combine_reshape_sum,aes(x=Frame,y=mean,color=timelapse))+
geom_errorbar(aes(ymin=mean-sd,ymax=mean+sd),width=0.5)+geom_point()+
geom_linegeom_line(data = spline_int,aes(x=x,y=y))
ggplot(combine_reshape_sum,aes(x=Frame,y=mean,color=timelapse))+
geom_errorbar(aes(ymin=mean-sd,ymax=mean+sd),width=0.5)+geom_point()+
geom_line(data = spline_int,aes(x=x,y=y))
ggplot(combine_reshape_sum,aes(x=Frame,y=mean,color=timelapse))+
geom_errorbar(aes(ymin=mean-sd,ymax=mean+sd),width=0.5)+geom_point()+
geom_line(data = spline_int,aes(x=x,y=y),inherit.aes = FALSE)
```

```
spline_int<-as.data.frame(spline(x=combine_reshape_sum$Frame, y=combine_reshape_sum$mean))
spline_int<-as.data.frame(spline(x=combine_reshape_sum$Frame,
y=combine_reshape_sum$mean,color=combine_reshape_sum$timelapse))
ggplot(combine_reshape_sum,aes(x=Frame,y=mean,color=timelapse))+
geom_errorbar(aes(ymin=mean-sd,ymax=mean+sd),width=0.5)+geom_point()+
geom_line(data = spline_int,aes(x=x,y=y),inherit.aes = FALSE)+
scale_fill_discrete(breaks=c('baseline','15 min after alcohol','30 min after alcohol','45 min after
alcohol'))+
theme(legend.title=element_blank())
ggplot(combine_reshape_sum,aes(x=Frame,y=mean,color=timelapse))+
geom_errorbar(aes(ymin=mean-sd,ymax=mean+sd),width=0.5)+geom_point()+
geom_line(data = spline_int,aes(x=x,y=y),inherit.aes = FALSE)+
scale_color_discrete(breaks=c('baseline','15 min after alcohol','30 min after alcohol','45 min after
alcohol'))+
theme(legend.title=element_blank())
ggplot(combine_reshape_sum,aes(x=Frame,y=mean,color=timelapse))+
geom_errorbar(aes(ymin=mean-sd,ymax=mean+sd),width=0.5)+geom_point()+
geom_line(data = spline_int,aes(x=x,y=y),inherit.aes = FALSE)+
scale_color_discrete(breaks=c('baseline','15 min after alcohol','30 min after alcohol','45 min after
alcohol'))+
theme(legend.title=element_blank())
combine_reshape_sum$timelapse<-ifelse(combine_reshape_sum$Frame>=117,'45 min after alcohol',
ifelse(combine_reshape_sum$Frame<117&combine_reshape_sum$Frame>=78,'30 min after alcohol',
ifelse(combine_reshape_sum$Frame<78&combine_reshape_sum$Frame>=41,'15 min after
alcohol','baseline')))
combine_reshape_sum$timelapse<-as.factor(combine_reshape_sum$timelapse)
spline_int<-as.data.frame(spline(x=combine_reshape_sum$Frame, y=combine_reshape_sum$mean))
ggplot(combine_reshape_sum,aes(x=Frame,y=mean,color=timelapse))+
geom_errorbar(aes(ymin=mean-sd,ymax=mean+sd),width=0.5)+geom_point()+
geom_line(data = spline_int,aes(x=x,y=y),inherit.aes = FALSE)+
scale_color_discrete(breaks=c('baseline','15 min after alcohol','30 min after alcohol','45 min after
alcohol'))+
theme(legend.title=element_blank())
combine_reshape_sum[,combine_reshape_sum$mean<10]
combine_reshape_sum[combine_reshape_sum$mean<10,]
backup<-combine_reshape_sum
backup[backup$mean<10,]<-NULL
backup[66,]
backup[89,]
backup[89,]
View(combine_reshape_sum)
View(combine_reshape_sum)
backup[182,]
backup<-backup[-182,]
View(backup)
ggplot(backup,aes(x=Frame,y=mean,color=timelapse))+
geom_errorbar(aes(ymin=mean-sd,ymax=mean+sd),width=0.5)+geom_point()+
geom_line(data = spline_int,aes(x=x,y=y),inherit.aes = FALSE)+
scale_color_discrete(breaks=c('baseline','15 min after alcohol','30 min after alcohol','45 min after
alcohol'))+
theme(legend.title=element_blank())
T30
T30[-12,]
T30<-T30[-12,]
T30
plotfunction(T30)
```

```
plotfunction<-function(a){
x1<-melt(a,id.vars = 'Frame')
x1$variable<-NULL
x1$Frame<-as.factor(as.character(x1$Frame))
x2<-
x1%>%
group_by(Frame)%>%
summarise(mean=mean(value),sd=sd(value))
x2$Frame<-
as.numeric(as.character(x2$Frame))
spline_int<-as.data.frame(spline(x2$Frame, x2$mean))
ggplot(x2,aes(x=Frame,y=mean))+
geom_errorbar(aes(ymin=mean-sd,ymax=mean+sd),width=0.1)+
geom_point()+
geom_line(data = spline_int,aes(x=x,y=y))
}
plotfunction(T30)
ggplot(data=T30,aes(x=Frame,y=mean))+geom_line
ggplot(data=T30,aes(x=Frame,y=mean))+geom_line()
ggplot(data=T30,aes(x=Frame,y=mean))+geom_point()
row.names(T30) <- 1:nrow(T30)
ggplot(data=T30,aes(x=Frame,y=mean))+geom_point()
View(T30)
T30
View(T0)
View(T15)
View(T30)
T30$Frame<-T30$Frame+77
T30<-read.csv('T=30.csv',header = F)
colnames(T30)<-c('Frame','1','2','3','4','5')
T30$time<-'30 min after alcohol'
T30$Frame<-T30$Frame+77
View(T30)
View(T45)
combine<-rbind(T0,T15,T30,T45)
combine_reshape<-melt(combine,id.vars = c('Frame','time'))
combine_reshape$Frame<-as.factor(as.character(combine_reshape$Frame))
combine_reshape_sum<-
combine_reshape%>%
group_by(Frame)%>%
summarise(mean=mean(value),sd=sd(value))
combine_reshape_sum$Frame<-
as.numeric(as.character(combine_reshape_sum$Frame))
combine_reshape_sum$timelapse<-ifelse(combine_reshape_sum$Frame>=117,'45 min after alcohol',
ifelse(combine_reshape_sum$Frame<117&combine_reshape_sum$Frame>=78,'30 min after alcohol',
ifelse(combine_reshape_sum$Frame<78&combine_reshape_sum$Frame>=41,'15 min after
alcohol','baseline')))
combine_reshape_sum$timelapse<-as.factor(combine_reshape_sum$timelapse)
is.factor(combine_reshape_sum$timelapse)
combine_reshape_sum$label<-NULL
spline_int<-as.data.frame(spline(x=combine_reshape_sum$Frame, y=combine_reshape_sum$mean))
ggplot(combine_reshape_sum,aes(x=Frame,y=mean,color=timelapse))+
geom_errorbar(aes(ymin=mean-sd,ymax=mean+sd),width=0.5)+geom_point()+
geom_line(data = spline_int,aes(x=x,y=y),inherit.aes = FALSE)+
scale_color_discrete(breaks=c('baseline','15 min after alcohol','30 min after alcohol','45 min after
alcohol'))+
```

```
theme(legend.title=element_blank())
View(combine_reshape_sum)
View(combine)
View(combine_reshape)
View(combine)
combine<-combine[-89,]
View(combine)
combine<-combine[-c(89,90),]
combine[combine$time=='30 min after alcohol',]
combine[combine$time=='30 min after alcohol','Frame']
combine[combine$time=='30 min after alcohol','Frame']<-seq(78,114)
seq(78,114)
combine<-rbind(T0,T15,T30,T45)
combine<-combine[-c(89,90),]
combine[combine$time=='30 min after alcohol','Frame']
combine[combine$time=='30 min after alcohol','Frame']<-seq(78,114)
combine[combine$time=='45 min after alcohol','Frame']
combine[combine$time=='45 min after alcohol','Frame']<-seq(115,191)
combine_reshape<-melt(combine,id.vars = c('Frame','time'))
combine_reshape$Frame<-as.factor(as.character(combine_reshape$Frame))
combine_reshape_sum<-
combine_reshape%>%
group_by(Frame)%>%
summarise(mean=mean(value),sd=sd(value))
combine_reshape_sum$Frame<-
as.numeric(as.character(combine_reshape_sum$Frame))
combine_reshape_sum$timelapse<-ifelse(combine_reshape_sum$Frame>=117,'45 min after alcohol',
ifelse(combine_reshape_sum$Frame<117&combine_reshape_sum$Frame>=78,'30 min after alcohol',
ifelse(combine_reshape_sum$Frame<78&combine_reshape_sum$Frame>=41,'15 min after
alcohol','baseline')))
combine_reshape_sum$timelapse<-as.factor(combine_reshape_sum$timelapse)
is.factor(combine_reshape_sum$timelapse)
combine_reshape_sum$label<-NULL
spline_int<-as.data.frame(spline(x=combine_reshape_sum$Frame, y=combine_reshape_sum$mean))
ggplot(combine_reshape_sum,aes(x=Frame,y=mean,color=timelapse))+
geom_errorbar(aes(ymin=mean-sd,ymax=mean+sd),width=0.5)+geom_point()+
geom_line(data = spline_int,aes(x=x,y=y),inherit.aes = FALSE)+
scale_color_discrete(breaks=c('baseline','15 min after alcohol','30 min after alcohol','45 min after
alcohol'))+
theme(legend.title=element_blank())
P<-
ggplot(combine_reshape_sum,aes(x=Frame,y=mean,color=timelapse))+
geom_errorbar(aes(ymin=mean-sd,ymax=mean+sd),width=0.5)+geom_point()+
geom_line(data = spline_int,aes(x=x,y=y),inherit.aes = FALSE)+
scale_color_discrete(breaks=c('baseline','15 min after alcohol','30 min after alcohol','45 min after
alcohol'))+
theme(legend.title=element_blank())
p<-
ggplot(combine_reshape_sum,aes(x=Frame,y=mean,color=timelapse))+
geom_errorbar(aes(ymin=mean-sd,ymax=mean+sd),width=0.5)+geom_point()+
geom_line(data = spline_int,aes(x=x,y=y),inherit.aes = FALSE)+
scale_color_discrete(breaks=c('baseline','15 min after alcohol','30 min after alcohol','45 min after
alcohol'))+
theme(legend.title=element_blank())
p
# add theme
```

```
p+xlab("Frame")+ylab("Diameter (um)")+
ggtitle("Cerebral vessel diameter change under low dose alochol")+
theme(axis.title.x = element_text(size=20),
axis.title.y = element_text(size=20),
axis.text.x=element_text(color="Black",size=15),
axis.text.y = element_text(color="Black",size=15),
plot.title = element_text(size=20,hjust=0.5))
# add theme
p+xlab("Frame")+ylab("Diameter (um)")+
ggtitle("Cerebral vessel diameter change under low dose alochol")+
theme(axis.title.x = element_text(size=10),
axis.title.y = element_text(size=10),
axis.text.x=element_text(color="Black",size=5),
axis.text.y = element_text(color="Black",size=5),
plot.title = element_text(size=10,hjust=0.5))
# add theme
p+xlab("Frame")+ylab("Diameter (um)")+
ggtitle("Cerebral vessel diameter change under low dose alochol")+
theme(axis.title.x = element_text(size=15),
axis.title.y = element_text(size=15),
axis.text.x=element_text(color="Black",size=10),
axis.text.y = element_text(color="Black",size=10),
plot.title = element_text(size=15,hjust=0.5))
# add theme
p+xlab("Frame")+ylab("Diameter (um)")+
ggtitle("Cerebral vessel diameter change under low dose alochol")+
theme(axis.title.x = element_text(size=15),
axis.title.y = element_text(size=15),
axis.text.x=element_text(color="Black",size=10),
axis.text.y = element_text(color="Black",size=10),
plot.title = element_text(size=15,hjust=0.5),
panel.background = element_rect(fill='White'))
# add theme
p+xlab("Frame")+ylab("Diameter (um)")+
ggtitle("Cerebral vessel diameter change under low dose alochol")+
theme(axis.title.x = element_text(size=15),
axis.title.y = element_text(size=15),
axis.text.x=element_text(color="Black",size=10),
axis.text.y = element_text(color="Black",size=10),
plot.title = element_text(size=15,hjust=0.5),
panel.background = element_rect(fill='White',color='Black'))
```

APPENDIX C

TIME COURSE VESSEL DIAMETER CHANGE PLOT

The plots that are presented here are used to support Chapter 3.

Figure C.1 Time course vessel diameter change

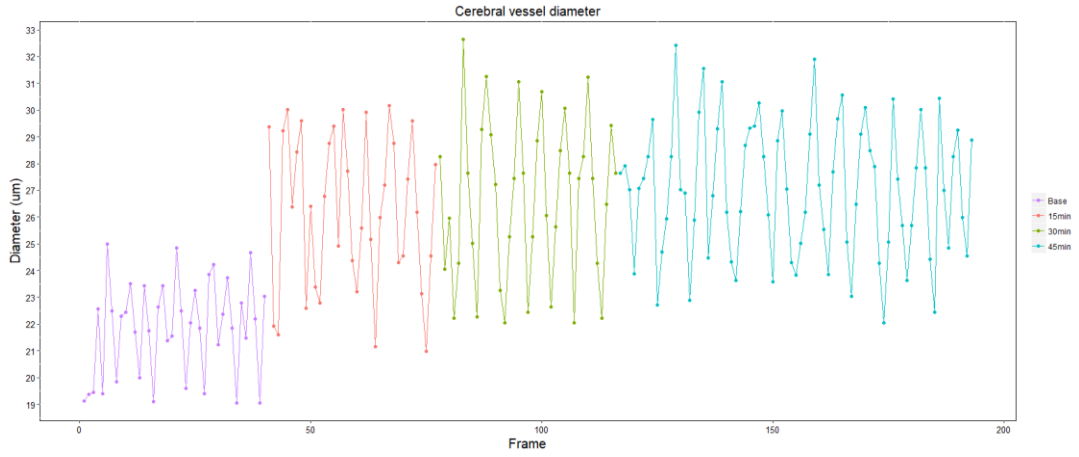

Figure C.2 Vessel diameter amplitude change at different time point

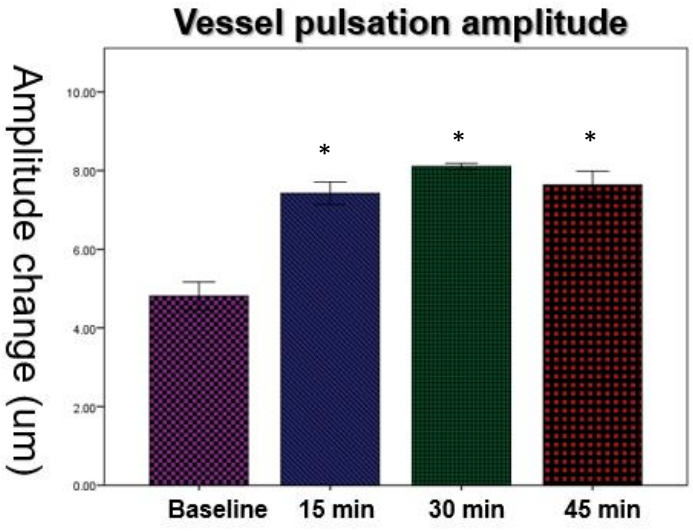

APPENDIX D

VALIDATION OF USING FITC-D2000 TRACERS AS MIMIC OF LARGE SIZE WASTE METABOLITES

The figures serve to validate the tracers that are used in experiments.

Figure D.1 Bio-distribution comparison of A-beta and FITC-d2000 tracers following intra-cranial injection (scale bar: whole brain: top: 500 μm, bottom: 1 mm; magnified vessels: 30 μm)

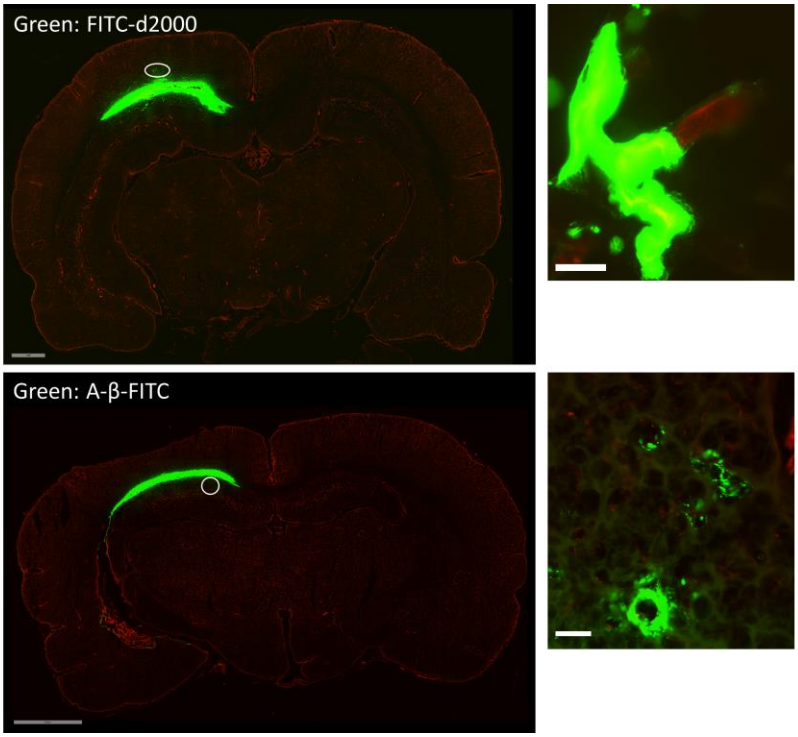

Figure D.2 Bio-distribution comparison of A-beta and FITC-d2000 tracers following CSF injection (scale bar: whole brain: 1 mm; magnified vasculatures: 50 μm)

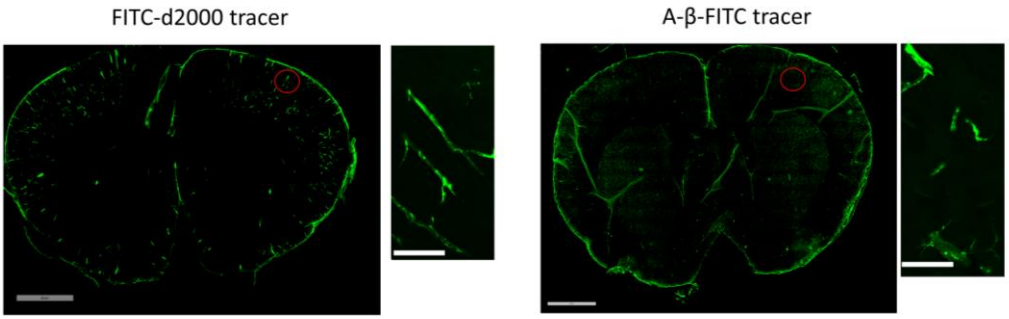

APPENDIX E

NO DOSE AND TIME DEPENDENT EFFECT IN LOW DOSE ALCOHOL TREATMENT

The figures examine dose- and time- dependent effects of low dose alcohol.

Figure E.1 No dose dependent effect on bio-distribution was found in low dose alcohol treatment (2.5 mM – 20 mM; 2 hours post-dose; scale bar: 1 mm)

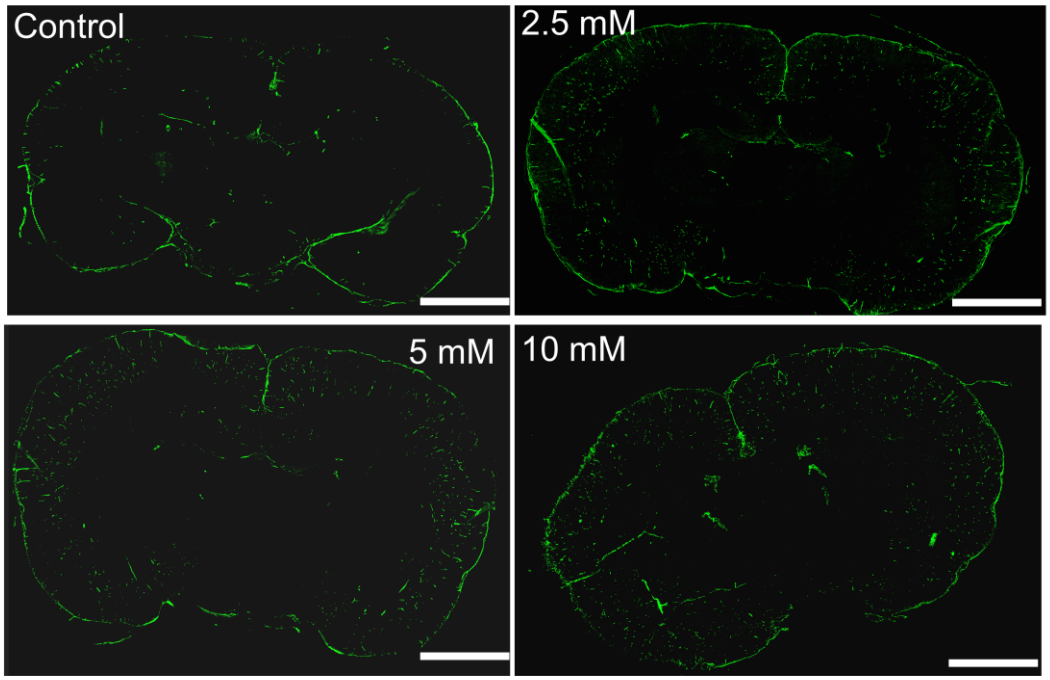

Figure E.2 No dose dependent effect on NO production and eNOS expression was found in low dose alcohol treatment (2.5 mM – 20 mM; 2 hours post-dose)

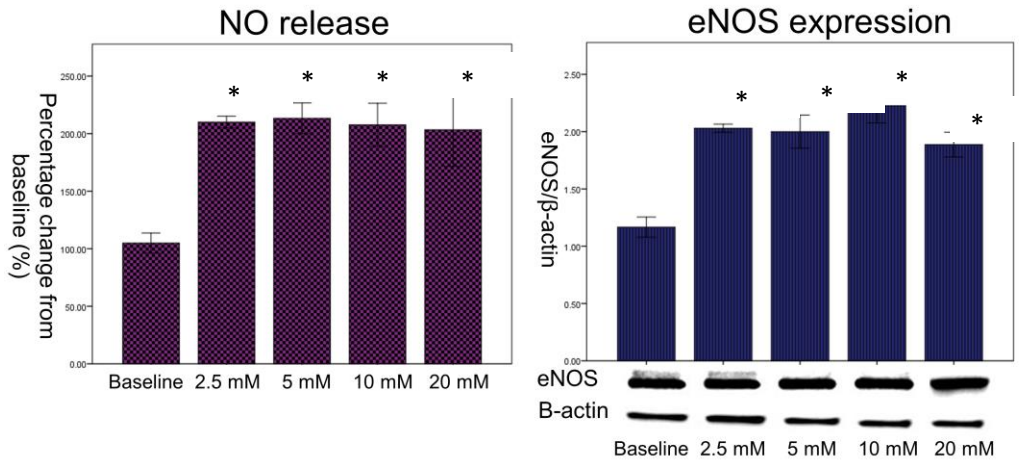

Figure E.3 No time dependent (2 hours, 5 days, 15 days and 20 days) effect on bio-distribution was found in low dose alcohol treatment (5 mM; 2 hours post-dose; scale bar: 1 mm)

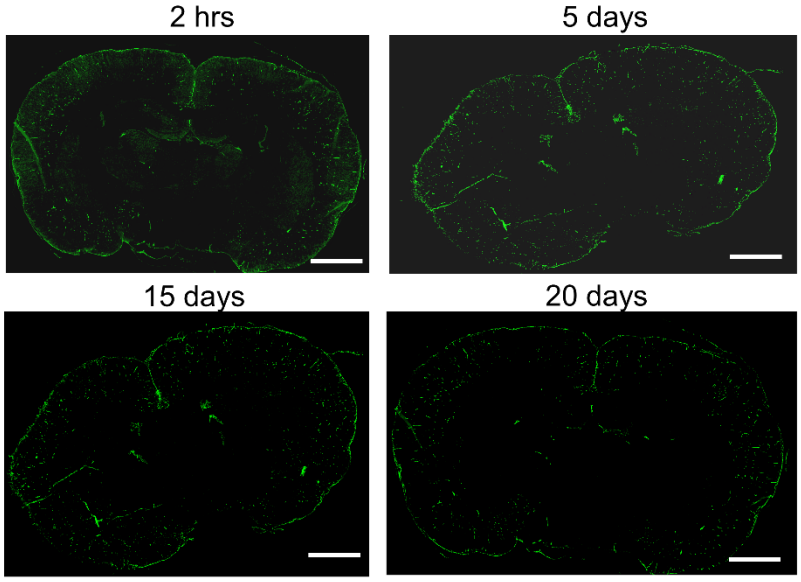

APPENDIX F

POSTIVE CONTROL OF TRACER BIODISTRIBUTION COMPARED WITH EFFECT OF ALCOHOL

The figure is positive control comparing with effects of low dose alcohol.

Figure F.1 Effect of Nitric Oxide (NO) donor S-Nitroso-N-acetylpenicillamine (SNAP: 100 μM, equivalent to 0.02 mg/mL through i.v injection) on tracer biodistribution (scale bar: 1 mm)

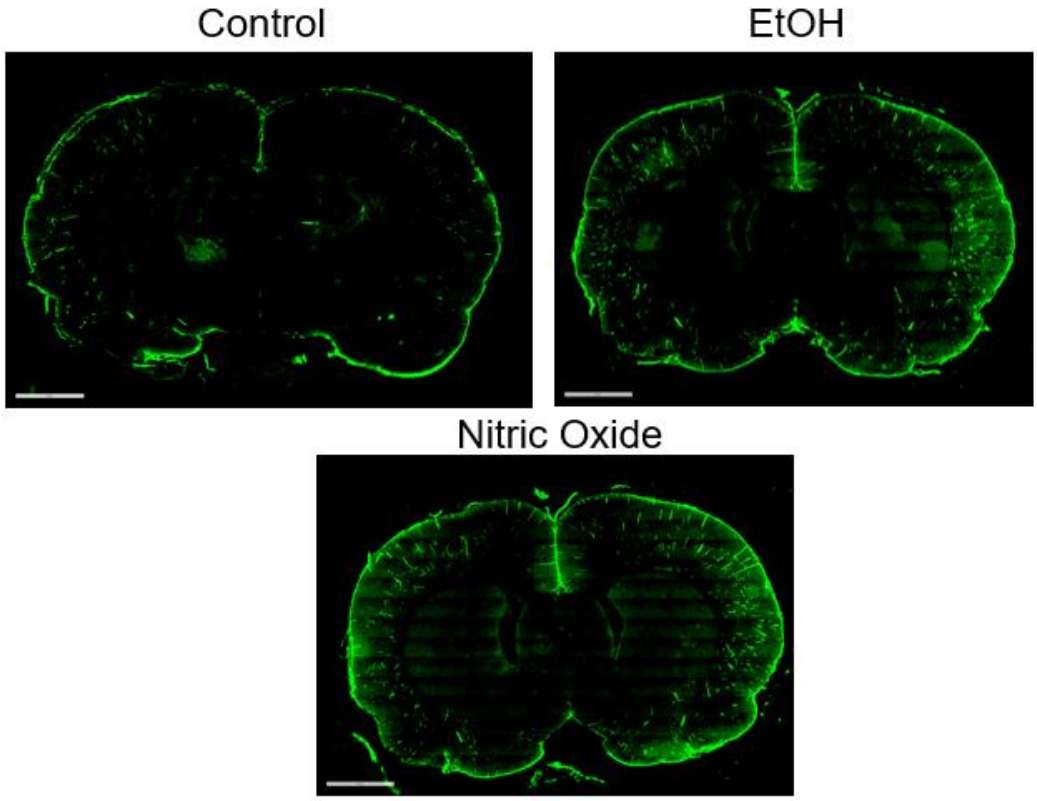

REFERENCES

1. Merlini, M., D. Wanner, and R.M. Nitsch, *Tau pathology-dependent remodelling of cerebral arteries precedes Alzheimer's disease-related microvascular cerebral amyloid angiopathy.* Acta Neuropathol, 2016. **131**(5): p. 737-52.

2. Rangel, A., et al., *Distinct patterns of spread of prion infection in brains of mice expressing anchorless or anchored forms of prion protein.* Acta Neuropathol Commun, 2014. **2**: p. 8.

3. Rennels, M.L., et al., *Evidence for a 'paravascular' fluid circulation in the mammalian central nervous system, provided by the rapid distribution of tracer protein throughout the brain from the subarachnoid space.* Brain Res, 1985. **326**(1): p. 47-63.

4. Greenberg, S.S., et al., *Ethanol relaxes pulmonary artery by release of prostaglandin and nitric oxide.* Alcohol, 1993. **10**(1): p. 21-9.

5. Rehm, J., et al., *Alcohol use and dementia: a systematic scoping review.* Alzheimers Res Ther, 2019. **11**(1): p. 1.

6. Zlokovic, B.V., *The blood-brain barrier in health and chronic neurodegenerative disorders.* Neuron, 2008. **57**(2): p. 178-201.

7. Strazielle, N. and J.F. Ghersi-Egea, *Physiology of blood-brain interfaces in relation to brain disposition of small compounds and macromolecules.* Mol Pharm, 2013. **10**(5): p. 1473-91.

8. Segal, M.B., Zlokovic, B.V, *The Blood–brain Barrier, Amino Acids and Peptides*. 1990: Kluwer Academic Publishers, Dordrecht, Boston and London.

9. Zlokovic, B.V., et al., *Circulating neuroactive peptides and the blood-brain and blood-cerebrospinal fluid barriers.* Endocrinol Exp, 1990. **24**(1-2): p. 9-17.

10. Kivisakk, P., et al., *Human cerebrospinal fluid central memory CD4+ T cells: evidence for trafficking through choroid plexus and meninges via P-selectin.* Proc Natl Acad Sci U S A, 2003. **100**(14): p. 8389-94.

11. Daum, R.S., et al., *Ventricular involvement in experimental Hemophilus influenzae meningitis.* J Pediatr, 1978. **93**(6): p. 927-30.

12. Schwerk, C., et al., *The choroid plexus-a multi-role player during infectious diseases of the CNS.* Front Cell Neurosci, 2015. **9**: p. 80.

13. Kaur, C., G. Rathnasamy, and E.A. Ling, *The Choroid Plexus in Healthy and Diseased Brain.* J Neuropathol Exp Neurol, 2016. **75**(3): p. 198-213.

14. Uchida, Y., et al., *Involvement of Claudin-11 in Disruption of Blood-Brain, -Spinal Cord, and -Arachnoid Barriers in Multiple Sclerosis.* Mol Neurobiol, 2019. **56**(3): p. 2039-2056.

15. Lun, M.P., E.S. Monuki, and M.K. Lehtinen, *Development and functions of the choroid plexus-cerebrospinal fluid system.* Nat Rev Neurosci, 2015. **16**(8): p. 445-57.

16. Praetorius, J. and H.H. Damkier, *Transport across the choroid plexus epithelium.* Am J Physiol Cell Physiol, 2017. **312**(6): p. C673-c686.

17. Yamashima, T., *Functional ultrastructure of cerebrospinal fluid drainage channels in human arachnoid villi.* Neurosurgery, 1988. **22**(4): p. 633-41.

18. Abbott, N.J., *Evidence for bulk flow of brain interstitial fluid: significance for physiology and pathology.* Neurochem Int, 2004. **45**(4): p. 545-52.

19. Brinker, T., et al., *A new look at cerebrospinal fluid circulation.* Fluids Barriers CNS, 2014. **11**: p. 10.

20. Cserr, H.F., D.N. Cooper, and T.H. Milhorat, *Flow of cerebral interstitial fluid as indicated by the removal of extracellular markers from rat caudate nucleus.* Exp Eye Res, 1977. **25 Suppl**: p. 461-73.

21. Cserr, H.F., et al., *Efflux of radiolabeled polyethylene glycols and albumin from rat brain.* Am J Physiol, 1981. **240**(4): p. F319-28.

22. Szentistvanyi, I., et al., *Drainage of interstitial fluid from different regions of rat brain.* Am J Physiol, 1984. **246**(6 Pt 2): p. F835-44.

23. Bakker, E.N., et al., *Lymphatic Clearance of the Brain: Perivascular, Paravascular and Significance for Neurodegenerative Diseases.* Cell Mol Neurobiol, 2016. **36**(2): p. 181-94.

24. Sykova, E. and C. Nicholson, *Diffusion in brain extracellular space.* Physiol Rev, 2008. **88**(4): p. 1277-340.

25. Keep, R.F. and H.C. Jones, *A morphometric study on the development of the lateral ventricle choroid plexus, choroid plexus capillaries and ventricular ependyma in the rat.* Brain Res Dev Brain Res, 1990. **56**(1): p. 47-53.

26. Bradley, W.G., Jr., K.E. Kortman, and B. Burgoyne, *Flowing cerebrospinal fluid in normal and hydrocephalic states: appearance on MR images.* Radiology, 1986. **159**(3): p. 611-6.

27. Feinberg, D.A. and A.S. Mark, *Human brain motion and cerebrospinal fluid circulation demonstrated with MR velocity imaging.* Radiology, 1987. **163**(3): p. 793-9.

28. Carare, R.O., et al., *Solutes, but not cells, drain from the brain parenchyma along basement membranes of capillaries and arteries: significance for cerebral amyloid angiopathy and neuroimmunology.* Neuropathol Appl Neurobiol, 2008. **34**(2): p. 131-44.

29. Iliff, J.J., et al., *A paravascular pathway facilitates CSF flow through the brain parenchyma and the clearance of interstitial solutes, including amyloid beta.* Sci Transl Med, 2012. **4**(147): p. 147ra111.

30. Weed, L.H., *Studies on Cerebro-Spinal Fluid. No. II : The Theories of Drainage of Cerebro-Spinal Fluid with an Analysis of the Methods of Investigation.* J Med Res, 1914. **31**(1): p. 21-49.

31. Weed, L.H., *Studies on Cerebro-Spinal Fluid. No. IV : The dual Source of Cerebro-Spinal Fluid.* J Med Res, 1914. **31**(1): p. 93-118.11.

32. Levine, J.E., J.T. Povlishock, and D.P. Becker, *The morphological correlates of primate cerebrospinal fluid absorption.* Brain Res, 1982. **241**(1): p. 31-41.

33. Nagra, G., et al., *Quantification of cerebrospinal fluid transport across the cribriform plate into lymphatics in rats.* Am J Physiol Regul Integr Comp Physiol, 2006. **291**(5): p. R1383-9.

34. Kida, S., A. Pantazis, and R.O. Weller, *CSF drains directly from the subarachnoid space into nasal lymphatics in the rat. Anatomy, histology and immunological significance.* Neuropathol Appl Neurobiol, 1993. **19**(6): p. 480-8.

35. Johnston, M., et al., *Evidence of connections between cerebrospinal fluid and nasal lymphatic vessels in humans, non-human primates and other mammalian species.* Cerebrospinal Fluid Res, 2004. **1**(1): p. 2.

36. Aspelund, A., et al., *A dural lymphatic vascular system that drains brain interstitial fluid and macromolecules.* J Exp Med, 2015. **212**(7): p. 991-9.

37. Louveau, A., et al., *Structural and functional features of central nervous system lymphatic vessels.* Nature, 2015. **523**(7560): p. 337-41.

38. Jessen, N.A., et al., *The Glymphatic System: A Beginner's Guide.* Neurochem Res, 2015. **40**(12): p. 2583-99.

39. Iliff, J.J., S.A. Goldman, and M. Nedergaard, *Implications of the discovery of brain lymphatic pathways.* Lancet Neurol, 2015. **14**(10): p. 977-9.

40. Iliff, J.J., et al., *Brain-wide pathway for waste clearance captured by contrast-enhanced MRI.* J Clin Invest, 2013. **123**(3): p. 1299-309.

41. Asgari, N., et al., *Cerebrospinal fluid aquaporin-4-immunoglobulin G disrupts blood brain barrier.* Ann Clin Transl Neurol, 2015. **2**(8): p. 857-63.

42. Holter, K.E., et al., *Interstitial solute transport in 3D reconstructed neuropil occurs by diffusion rather than bulk flow.* Proc Natl Acad Sci U S A, 2017. **114**(37): p. 9894-9899.

43. Smith, A.J., et al., *Test of the 'glymphatic' hypothesis demonstrates diffusive and aquaporin-4-independent solute transport in rodent brain parenchyma.* Elife, 2017. **6**.

44. Jin, B.J., A.J. Smith, and A.S. Verkman, *Spatial model of convective solute transport in brain extracellular space does not support a "glymphatic" mechanism.* J Gen Physiol, 2016. **148**(6): p. 489-501.

45. Asgari, M., D. de Zelicourt, and V. Kurtcuoglu, *Glymphatic solute transport does not require bulk flow.* Sci Rep, 2016. **6**: p. 38635.

46. Hladky, S.B. and M.A. Barrand, *Mechanisms of fluid movement into, through and out of the brain: evaluation of the evidence.* Fluids Barriers CNS, 2014. **11**(1): p. 26.

47. Spector, R., S. Robert Snodgrass, and C.E. Johanson, *A balanced view of the cerebrospinal fluid composition and functions: Focus on adult humans.* Exp Neurol, 2015. **273**: p. 57-68.

48. Hawkes, C.A., et al., *Failure of perivascular drainage of beta-amyloid in cerebral amyloid angiopathy.* Brain Pathol, 2014. **24**(4): p. 396-403.

49. Johnston, M., D. Armstrong, and L. Koh, *Possible role of the cavernous sinus veins in cerebrospinal fluid absorption.* Cerebrospinal Fluid Res, 2007. **4**: p. 3.

50. Squier, W., et al., *Demonstration of fluid channels in human dura and their relationship to age and intradural bleeding.* Childs Nerv Syst, 2009. **25**(8): p. 925-31.

51. Zenker, W., S. Bankoul, and J.S. Braun, *Morphological indications for considerable diffuse reabsorption of cerebrospinal fluid in spinal meninges particularly in the areas of meningeal funnels. An electronmicroscopical study including tracing experiments in rats.* Anat Embryol (Berl), 1994. **189**(3): p. 243-58.

52. Raper, D., A. Louveau, and J. Kipnis, *How Do Meningeal Lymphatic Vessels Drain the CNS?* Trends Neurosci, 2016. **39**(9): p. 581-586.

53. Krahn, V., *The pia mater at the site of the entry of blood vessels into the central nervous system.* Anat Embryol (Berl), 1982. **164**(2): p. 257-63.

54. Weller, R.O., *Microscopic morphology and histology of the human meninges.* Morphologie, 2005. **89**(284): p. 22-34.

55. Bechmann, I., I. Galea, and V.H. Perry, *What is the blood-brain barrier (not)?* Trends Immunol, 2007. **28**(1): p. 5-11.

56. Bechmann, I., et al., *Turnover of rat brain perivascular cells.* Exp Neurol, 2001. **168**(2): p. 242-9.

57. Bell, R.D., et al., *Transport pathways for clearance of human Alzheimer's amyloid beta-peptide and apolipoproteins E and J in the mouse central nervous system.* J Cereb Blood Flow Metab, 2007. **27**(5): p. 909-18.

58. Deane, R., et al., *apoE isoform-specific disruption of amyloid beta peptide clearance from mouse brain.* J Clin Invest, 2008. **118**(12): p. 4002-13.

59. Deane, R., et al., *LRP/amyloid beta-peptide interaction mediates differential brain efflux of Abeta isoforms.* Neuron, 2004. **43**(3): p. 333-44.

60. Shibata, M., et al., *Clearance of Alzheimer's amyloid-ss(1-40) peptide from brain by LDL receptor-related protein-1 at the blood-brain barrier*. J Clin Invest, 2000. **106**(12): p. 1489-99.

61. Zhao, Z., et al., *Central role for PICALM in amyloid-beta blood-brain barrier transcytosis and clearance.* Nat Neurosci, 2015. **18**(7): p. 978-87.

62. Cheng, Y., et al., *Alcohol promotes waste clearance in the CNS via brain vascular reactivity.* Free Radic Biol Med, 2019.

63. Hill, R.A., et al., *Regional Blood Flow in the Normal and Ischemic Brain Is Controlled by Arteriolar Smooth Muscle Cell Contractility and Not by Capillary Pericytes.* Neuron, 2015. **87**(1): p. 95-110.

64. Acevedo, C.G., et al., *Ethanol inhibits L-arginine uptake and enhances NO formation in human placenta.* Life Sci, 2001. **68**(26): p. 2893-903.

65. Venkov, C.D., et al., *Ethanol increases endothelial nitric oxide production through modulation of nitric oxide synthase expression.* Thromb Haemost, 1999. **81**(4): p. 638-42.

66. Tarasoff-Conway, J.M., et al., *Clearance systems in the brain-implications for Alzheimer disease.* Nat Rev Neurol, 2015. **11**(8): p. 457-70.

67. Alikunju, S., et al., *The inflammatory footprints of alcohol-induced oxidative damage in neurovascular components.* Brain Behav Immun, 2011. **25 Suppl 1**: p. S129-36.

68. Eyo, U.B. and J. Peng, *Regulation of Physical Microglia-Neuron Interactions by Fractalkine Signaling after Status Epilepticus.* 2016. **3**(6).

69. Yue, X., et al., *RGD-conjugated two-photon absorbing near-IR emitting fluorescent probes for tumor vasculature imaging.* eNeuro, 2015. **13**(43): p. 10716-25.

70. Haorah, J., et al., *Stabilization of superoxide dismutase by acetyl-l-carnitine in human brain endothelium during alcohol exposure: novel protective approach.* Free Radic Biol Med, 2011. **51**(8): p. 1601-9.

71. Boulay, A.C., et al., *Purification of Mouse Brain Vessels.* J Vis Exp, 2015(105): p. e53208.

72. Haorah, J., et al., *Mechanism of alcohol-induced oxidative stress and neuronal injury.* Free Radic Biol Med, 2008. **45**(11): p. 1542-50.

73. Iliff, J.J., et al., *Cerebral arterial pulsation drives paravascular CSF-interstitial fluid exchange in the murine brain.* J Neurosci, 2013. **33**(46): p. 18190-9.

74. Deng, X.S. and R.A. Deitrich, *Ethanol metabolism and effects: nitric oxide and its interaction.* Curr Clin Pharmacol, 2007. **2**(2): p. 145-53.

75. Utter, S., et al., *Cerebral small vessel disease-induced apolipoprotein E leakage is associated with Alzheimer disease and the accumulation of amyloid beta-protein in perivascular astrocytes.* J Neuropathol Exp Neurol, 2008. **67**(9): p. 842-56.

76. You, Y., et al., *Tau as a mediator of neurotoxicity associated to cerebral amyloid angiopathy.* Acta Neuropathol Commun, 2019. **7**(1): p. 26.

77. Anstey, K.J., H.A. Mack, and N. Cherbuin, *Alcohol consumption as a risk factor for dementia and cognitive decline: meta-analysis of prospective studies.* Am J Geriatr Psychiatry, 2009. **17**(7): p. 542-55.

78. Avellaneda-Gomez, C., et al., *Alcohol overuse and intracerebral hemorrhage: characteristics and long-term outcome.* 2018. **25**(11): p. 1358-1364.

79. Hasan, O.S.M., et al., *Alcohol intake and the risk of intracerebral hemorrhage in the elderly: The MUCH-Italy.* Alzheimers Res Ther, 2018. **91**(3): p. e227-e235.

80. Heymann, D., et al., *The Association Between Alcohol Use and the Progression of Alzheimer's Disease.* Curr Alzheimer Res, 2016. **13**(12): p. 1356-1362.

81. Miller, M., et al., *A retrospective, population-based cohort study of driving under the influence, Alzheimer's disease diagnosis, and survival.* Int Psychogeriatr, 2019. **31**(4): p. 571-577.

82. Rehm, J., *Alcohol use and dementia: a systematic scoping review.* Eur J Neurol, 2019. **11**(1): p. 1.

83. Schwarzinger, M., et al., *Contribution of alcohol use disorders to the burden of dementia in France 2008-13: a nationwide retrospective cohort study.* Lancet Public Health, 2018. **3**(3): p. e124-e132.

84. Xu, W., et al., *Alcohol consumption and dementia risk: a dose-response meta-analysis of prospective studies.* Eur J Epidemiol, 2017. **32**(1): p. 31-42.

85. Lundgaard, I., et al., *Beneficial effects of low alcohol exposure, but adverse effects of high alcohol intake on glymphatic function.* Sci Rep, 2018. **8**(1): p. 2246.

86. Mukamal, K.J., et al., *Roles of drinking pattern and type of alcohol consumed in coronary heart disease in men.* N Engl J Med, 2003. **348**(2): p. 109-18.

87. Ronksley, P.E., et al., *Association of alcohol consumption with selected cardiovascular disease outcomes: a systematic review and meta-analysis.* Bmj, 2011. **342**: p. d671.

88. Haorah, J., et al., *Ethanol-induced activation of myosin light chain kinase leads to dysfunction of tight junctions and blood-brain barrier compromise.* Alcohol Clin Exp Res, 2005. **29**(6): p. 999-1009.

89. Haorah, J., et al., *Alcohol-induced blood-brain barrier dysfunction is mediated via inositol 1,4,5-triphosphate receptor (IP3R)-gated intracellular calcium release.* J Neurochem, 2007. **100**(2): p. 324-36.

90. Lilly, B., *We have contact: endothelial cell-smooth muscle cell interactions.* Physiology (Bethesda), 2014. **29**(4): p. 234-41.

91. Truskey, G.A., *Endothelial Cell Vascular Smooth Muscle Cell Co-Culture Assay For High Throughput Screening Assays For Discovery of Anti-Angiogenesis Agents and Other Therapeutic Molecules.* Int J High Throughput Screen, 2010. **2010**(1): p. 171-181.

92. Brien, S.E., et al., *Effect of alcohol consumption on biological markers associated with risk of coronary heart disease: systematic review and meta-analysis of interventional studies.* Bmj, 2011. **342**: p. d636.

93. Cahill, P.A. and E.M. Redmond, *Alcohol and cardiovascular disease--modulation of vascular cell function.* Nutrients, 2012. **4**(4): p. 297-318.

94. Chiva-Blanch, G., et al., *Differential effects of polyphenols and alcohol of red wine on the expression of adhesion molecules and inflammatory cytokines related to atherosclerosis: a randomized clinical trial.* Am J Clin Nutr, 2012. **95**(2): p. 326-34.

95. Bonnefont-Rousselot, D., *Resveratrol and Cardiovascular Diseases.* Nutrients, 2016. **8**(5).

96. Renaud, S. and M. de Lorgeril, *Wine, alcohol, platelets, and the French paradox for coronary heart disease.* Lancet, 1992. **339**(8808): p. 1523-6.

97. Smoliga, J.M., J.A. Baur, and H.A. Hausenblas, *Resveratrol and health--a comprehensive review of human clinical trials.* Mol Nutr Food Res, 2011. **55**(8): p. 1129-41.

98. Bhatt, S.R., M.F. Lokhandwala, and A.A. Banday, *Resveratrol prevents endothelial nitric oxide synthase uncoupling and attenuates development of hypertension in spontaneously hypertensive rats.* Eur J Pharmacol, 2011. **667**(1-3): p. 258-64.

99. Crescente, M., et al., *Interactions of gallic acid, resveratrol, quercetin and aspirin at the platelet cyclooxygenase-1 level. Functional and modelling studies.* Thromb Haemost, 2009. **102**(2): p. 336-46.

100. Palmieri, D., et al., *Resveratrol counteracts systemic and local inflammation involved in early abdominal aortic aneurysm development.* J Surg Res, 2011. **171**(2): p. e237-46.

101. Vinson, J.A., et al., *Phenol antioxidant quantity and quality in foods: beers and the effect of two types of beer on an animal model of atherosclerosis.* J Agric Food Chem, 2003. **51**(18): p. 5528-33.

102. Serafini, M., G. Maiani, and A. Ferro-Luzzi, *Alcohol-free red wine enhances plasma antioxidant capacity in humans.* J Nutr, 1998. **128**(6): p. 1003-7.

103. Gaziano, J.M., et al., *Type of alcoholic beverage and risk of myocardial infarction.* Am J Cardiol, 1999. **83**(1): p. 52-7.

104. Kuhlmann, C.R., et al., *Dose-dependent activation of Ca2+-activated K+ channels by ethanol contributes to improved endothelial cell functions.* Alcohol Clin Exp Res, 2004. **28**(7): p. 1005-11.

105. Liu, J., et al., *Dose-dependent activation of antiapoptotic and proapoptotic pathways by ethanol treatment in human vascular endothelial cells: differential involvement of adenosine.* J Biol Chem, 2002. **277**(23): p. 20927-33.

106. Kleinhenz, D.J., et al., *Chronic ethanol ingestion increases aortic endothelial nitric oxide synthase expression and nitric oxide production in the rat.* Alcohol Clin Exp Res, 2008. **32**(1): p. 148-54.

107. Hatake, K., et al., *Increased endothelium-dependent vascular relaxation in ethanol-fed rats.* Alcohol Clin Exp Res, 1994. **18**(4): p. 1018-23.

108. Williams, S.P., R.D. Adams, and S.J. Mustafa, *The effects of chronic ethanol treatment on endothelium-dependent responses in rat thoracic aorta.* Alcohol, 1990. **7**(2): p. 121-7.

109. Suzuki, K., et al., *Moderate alcohol consumption is associated with better endothelial function: a cross sectional study.* BMC Cardiovasc Disord, 2009. **9**: p. 8.

110. Nakamura, K., et al., *cGMP-dependent relaxation of smooth muscle is coupled with the change in the phosphorylation of myosin phosphatase.* Circ Res, 2007. **101**(7): p. 712-22.

111. Haorah, J., et al., *Alcohol-induced oxidative stress in brain endothelial cells causes blood-brain barrier dysfunction.* J Leukoc Biol, 2005. **78**(6): p. 1223-32.

112. Ischiropoulos, H., et al., *Peroxynitrite-mediated tyrosine nitration catalyzed by superoxide dismutase.* Arch Biochem Biophys, 1992. **298**(2): p. 431-7.

113. Brozovich, F.V., et al., *Mechanisms of Vascular Smooth Muscle Contraction and the Basis for Pharmacologic Treatment of Smooth Muscle Disorders.* Pharmacol Rev, 2016. **68**(2): p. 476-532.

114. Stull, J.T., et al., *Phosphorylation of myosin light chain kinase: a cellular mechanism for Ca2+ desensitization.* Mol Cell Biochem, 1993. **127-128**: p. 229-37.

115. Etter, E.F., et al., *Activation of myosin light chain phosphatase in intact arterial smooth muscle during nitric oxide-induced relaxation.* J Biol Chem, 2001. **276**(37): p. 34681-5.

116. Lubomirov, L.T., et al., *The involvement of phosphorylation of myosin phosphatase targeting subunit 1 (MYPT1) and MYPT1 isoform expression in*

NO/cGMP mediated differential vasoregulation of cerebral arteries compared to systemic arteries. Acta Physiol (Oxf), 2018. **224**(1): p. e13079.

117. Lincoln, T.M., P. Komalavilas, and T.L. Cornwell, *Pleiotropic regulation of vascular smooth muscle tone by cyclic GMP-dependent protein kinase.* Hypertension, 1994. **23**(6 Pt 2): p. 1141-7.

118. Husain, K., *Vascular endothelial oxidative stress in alcohol-induced hypertension.* Cell Mol Biol (Noisy-le-grand), 2007. **53**(1): p. 70-7.

119. Sun, H. and W.G. Mayhan, *Superoxide dismutase ameliorates impaired nitric oxide synthase-dependent dilatation of the basilar artery during chronic alcohol consumption.* Brain Res, 2001. **891**(1-2): p. 116-22.

120. Sun, H., et al., *Role of NAD(P)H oxidase in alcohol-induced impairment of endothelial nitric oxide synthase-dependent dilation of cerebral arterioles.* Stroke, 2006. **37**(2): p. 495-500.

121. Haorah, J., T.J. Rump, and H. Xiong, *Reduction of brain mitochondrial beta-oxidation impairs complex I and V in chronic alcohol intake: the underlying mechanism for neurodegeneration.* PLoS One, 2013. **8**(8): p. e70833.

122. Rump, T.J., et al., *Acetyl-L-carnitine protects neuronal function from alcohol-induced oxidative damage in the brain.* Free Radic Biol Med, 2010. **49**(10): p. 1494-504.

123. Martinez, S.E., et al., *Distribution of alcohol dehydrogenase mRNA in the rat central nervous system. Consequences for brain ethanol and retinoid metabolism.* Eur J Biochem, 2001. **268**(19): p. 5045-56.

124. Zimatkin, S.M., et al., *Enzymatic mechanisms of ethanol oxidation in the brain.* Alcohol Clin Exp Res, 2006. **30**(9): p. 1500-5.

125. Avellaneda-Gomez, C., et al., *Alcohol overuse and intracerebral hemorrhage: characteristics and long-term outcome.* Eur J Neurol, 2018. **25**(11): p. 1358-1364.

126. Costa, P., et al., *Alcohol intake and the risk of intracerebral hemorrhage in the elderly: The MUCH-Italy.* Neurology, 2018. **91**(3): p. e227-e235.

127. Abdul Muneer, P.M., et al., *The mechanisms of cerebral vascular dysfunction and neuroinflammation by MMP-mediated degradation of VEGFR-2 in alcohol ingestion.* Arterioscler Thromb Vasc Biol, 2012. **32**(5): p. 1167-77.